Modeling and optimal operation for hydrogen-based power system with electric vehicle

Yuchen Pu

THÈSE DE DOCTORAT DE L'ETABLISSEMENT UNIVERSITÉ BOURGOGNE FRANCHE-COMTÉ

PRÉPARÉE A L'UNIVERSITÉ DE TECHNOLOGIE DE BELFORT-MONTBÉLIARD

École Doctorale n°37
Sciences Pour l'Ingénieur et Microtechniques

Doctorat de Génie Electrique

Par
Yuchen Pu

Modélisation et fonctionnement optimal d'un système d'alimentation à base d'hydrogène avec véhicule électrique

Thèse présentée et soutenue à Chengdu, le 05/12/2024

Composition du jury:

M. Zhenyuan Zhang	Professeur à l' Université des sciences et technologies électroniques de Chine	Président
M. Mohamed Benbouzid	Professeure à l' Université de Brest	Rapporteur
M. Yanbo Chen	Professeur à l' Université de l'énergie électrique de Chine du Nord	Rapporteur
M. Qi Li	Professeur à l'Université Jiaotong du Sud-ouest	Directeur de thèse
M. Fei Gao	Professeur à l'Université de Technologie de Belfort-Montbéliard	Directeur de thèse
Mme. Elena Breaz	Maitre de conférences à l'Université de Technologie de Belfort-Montbéliard	Codirecteur de thèse

PH.D. THESIS OF THE UNIVERSITY BOURGOGNE FRANCHE-COMTÉ

PREPARED AT THE UNIVERSITY OF TECHNOLOGY OF BELFORT-MONTBÉLIARD

Doctoral School n°37
Engineering Sciences and Microtechnologies

Doctor of Philosophy (Ph.D.) in Electrical Engineering

By
Yuchen Pu

Modeling and optimal operation for hydrogen-based power system with electric vehicle

Thesis presented and defended in Chengdu, le 05/12/2024

Composition of jury:

M. Zhenyuan Zhang	Professor at University of Electronic Science and Technology of China	President
M. Mohamed Benbouzid	Professor at University of Brest	Reviewer
M. Yanbo Chen	Professor at North China Electric Power University	Reviewer
M. Qi Li	Professor at Southwest Jiaotong University	Supervisor
M. Fei Gao	Professor at University of Technology of Belfort-Montbéliard	Supervisor
Mme. Elena Breaz	Associate professor at University of Technology of Belfort-Montbéliard	Co-supervisor

Titre: Modélisation et fonctionnement optimal d'un système d'alimentation à base d'hydrogène avec véhicule électrique

Mots-clés: Fonctionnement optimal, Véhicule électrique, Modélisation, Système d'énergie

Résumé: L'énergie hydrogène est respectueuse de l'environnement et durable par rapport à l'énergie traditionnelle. Elle ne produit de l'eau qu'après réaction chimique et présente les caractéristiques d'une pollution nulle, d'un rendement élevé et convient au transport sur de longues distances. Grâce aux piles à combustible, les électrolyseurs et autres équipements sont importants pour le fonctionnement des systèmes électriques et énergétiques. Par conséquent, cette thèse s'engage à étudier le fonctionnement, le contrôle et le commerce de l'énergie des systèmes électriques et énergétiques avec la participation de l'énergie hydrogène. Pour étudier la méthode de fonctionnement et de contrôle des micro-réseaux de stockage d'énergie à hydrogène, cette thèse propose une méthode de gestion hiérarchique de l'énergie basée sur la machine d'états et la minimisation des coûts de fonctionnement. Le fonctionnement économique et stable des micro-réseaux à hydrogène est obtenu. En outre, afin d'améliorer le taux d'utilisation de l'énergie des piles à combustible et des électrolyseurs pour le fonctionnement dans des systèmes énergétiques à plus grande échelle, cette thèse propose une méthode de planification d'optimisation en deux étapes pour les systèmes énergétiques intégrés prenant en compte la combinaison puissance-chaleur-hydrogène du système énergétique à hydrogène, et réalise le fonctionnement économique de systèmes énergétiques intégrés. Enfin, en considérant le partage de l'énergie électrique et de l'hydrogène entre les systèmes énergétiques régionaux, ce travail de thèse établit un marché régional de l'énergie de partage d'électricité et d'hydrogène et propose une méthode d'optimisation du marché régional de l'énergie prenant en compte l'implication des opérateurs de stockage d'énergie virtuels. La vérification a été réalisée sur la base d'un exemple de terrain pour analyser l'économie et l'utilisation de l'énergie du marché régional de l'énergie.

Title: Modeling and optimal operation for hydrogen-based power system with electric vehicle

Keywords: Optimal control, Electric vehicle, Modeling, Power system

Abstract: Hydrogen energy is environmentally friendly and sustainable compared with traditional energy. It only produces water after chemical reaction, and has the characteristics of zero pollution, high efficiency, and suitable for long-distance transportation. The production, transportation, storage and application of hydrogen energy through fuel cells, electrolyzers and other equipment are important to the operation of the power and energy systems. Therefore, this thesis is committed to studying the operation, control and energy trading of power systems and energy systems with the participation of hydrogen energy. In order to study the operation and control method of hydrogen energy storage microgrids, this thesis proposes a hierarchical energy management method based on state machine and operation cost minimization. The economic and stable operation of hydrogen microgrids is achieved. In addition, in order to improve the energy utilization rate of fuel cells and electrolyzers for the operation in larger-scale energy systems, this work proposes a two-stage optimization scheduling method for integrated energy systems considering the power-heat-hydrogen combining of hydrogen energy system, and realizes the economic operation of integrated energy systems. Finally, considering the sharing of electricity and hydrogen energy between regional energy systems, this thesis work establishes a regional electricity-hydrogen sharing energy market and proposes a regional energy market optimization method considering the involvement of virtual energy storage operators. Verification was carried out based on a field example to analyze the economics and energy utilization of the regional energy market.

Université Bourgogne Franche-Comté
32, avenue de l'Observatoire
25000 Besançon

Acknowledgement

The works of this thesis were done in FEMTO-ST Institute in the framework of FCLAB activities, Univ. Bourgogne Franche-Comté, UTBM, CNRS.

Firstly, I want to thank Prof. Zhenyuan Zhang, Prof. Mohamed Benbouzid, Prof. Yanbo Chen for their kind help in preparation for my thesis defense. I am very grateful to my supervisors Prof. Fei Gao, Prof. Qi Li, and Prof. Elana Breaz. Before I started my Ph.D. study, I knew very little about the hydrogen energy system and also didn't know how to deal with its modeling and operation. My supervisors provided me with the most meticulous guidance and encouraged me to conduct in-depth academic research. Prof. Qi Li and Prof. Fei Gao are always glad to give their suggestions and engineering experiences about the operation and control of hydrogen system. Their extensive professional knowledge and rigorous academic attitude will benefit me for the rest of my life. Prof. Elena Breaz helped me a lot in exploring the research contents and guiding my writing of papers. Also, they gave me comprehensive advice and spent a lot of time discussing my thesis, all my progress in research and publication of papers are inseparable from their enthusiastic guidance and help. It's really my great honor and luck to work with them over the past few years. In addition, I sincerely thank Prof. Weirong Chen from Southwest Jiaotong University for his guidance and suggestions for my future scientific career.

Secondly, I would like to convey my sincere appreciation to my dear colleagues at UTBM: Dr. Tianhong Wang, Dr. Zhiguang Hua, Dr. Liangzhen Yin, Dr. Qian Li, Dr. Xinyang Hao, Dr. Yuchen Liu, for they have helped me a lot no matter in the academic research and daily life. Also, I'd like to thank Dr. Yu Yan from Zhengzhou University for his suggestions on my research work, and Dr. Liang Guo from Aix-Marseille University for the frequent academic discussion. Mrs. Shuang Yu, Mr. Wenqiang Huang, Mr. Xukang Xiao, Ms. Shuyu Luo, Mr. Yongchang Tao, Mr. Bingxun Li, Ms. Shasha Huo, and Mr. Chunlin Li from Southwest Jiaotong University, for their company and help. Ms. Shuang Liu, Mr. Xiaotong Sun, Mr. Yiteng Hu, Mr. Dongfang Jin, Mr. Fangli Shi, Mrs. Qi An, Ms. Zhili Xiang, and Mr. Han Zhang, for our 11-year priceless friendship.

In particular, I would like to convey my sincere gratitude to my family. My parents Mr. Lixin Pu and Mrs. Liang Liu support me both financially and spiritually on the way to my dream. I hope they can keep fit during their work. My girlfriend Ms. Shuang Liu accompanies and supports me no matter what happens to me. I am so lucky to have met such a kind and pretty girl in my life. Her paintings are always eyeful and bring me peace after work. I hope she can do very well in her work, and I believe that we will fulfill each other's dreams in the following years.

Finally, I would like to express my heartfelt thanks to the China Scholarship Council (CSC) for funding during my Ph.D.

Table of contents

Abbreviations

ADN	Active distribution network
BAT	Battery
CHP	Combining heat and power
CPHH	Combining power heat and hydrogen
DC	Direct current
DR	Demand response
EB	Electric boiler
EHE	Electricity to hydrogen to electricity
EL	Electrolyzer
EMS	Energy management strategy
ESS	Energy storage system
EVs	Electrical vehicles
FC	Fuel cell
FCVs	Fuel cell vehicles
GWO	Grey wolf optimizer
H_2/Hy	Hydrogen
HVs	Hydrogen vehicles
IES	Integrated energy system
KKT	Karush-Kuhn-Tucker Conditions
LCC	Life cycle cost
LSTM	Long short-term memory
MILP	Mixed integer linear programming
MIQP	Mixed integer linear programming
MPC	Model predictive control
MPPT	Maximum Power Point Tracking
O&M	Operation and maintenance
P2HH	Power to hydrogen and heat
PEM	Proton exchange membrane
PEMFCPP	Proton exchange membrane fuel cell power plant
PI	Proportional integral controller
PV	Photovoltaic
RESs	Renewable energy sources
SES	Shared energy storage
SESO	Shared energy storage operator
SOC	State of charge
SOHC	State of hydrogen charge
TES	Thermal energy storage

WT	Wind turbine

General introduction

As energy crises and environmental problems become increasingly severe, the traditional energy utilization structure dominated by fossil energy is difficult to support the sustainable development of human society. In the process of seeking energy conservation, emission reduction, and green development, governments of various countries regard the distributed development and utilization of new energy as an important way. Therefore, as renewable energy is used more and more widely, energy production, transportation, and consumption issues based on renewable power generation systems have become the focus of solving energy problems [1-3]. In addition, a variety of energy storage systems are also added to the operation and control of the system to ensure the economic and stable operation of the system [4-6]. In this context, the widespread use of hydrogen energy has gradually added fuel cells, electrolyzers, and their energy storage systems to the renewable energy network [7-10].

As an important technical approach to global energy sustainable development and strategic transformation, hydrogen energy technology has been identified as an important support for global energy transportation [11]. In 2023, Europe proposed a multi-field green hydrogen replacement target, which strongly supported the demand for green hydrogen in the European market. In July of the same year, the European Council approved the release of the 'Alternative Fuels Infrastructure Regulation, AFIR' [12], requiring EU member states to build a 1,000 kg/day public hydrogen refueling station every 200 km along the core routes of the planned Trans-European Transport Network (TEN-T) by the end of 2030. The EU and its member states have worked hard to improve the policy system guarantees such as green hydrogen standards to lay a policy foundation for the large-scale development of green hydrogen. On February 13, 2023, the EU's 'Renewable Energy Directive' (RED II) [13] amendment was officially released, which proposed detailed rules to define the composition of EU renewable hydrogen. In addition, the governments of EU member states simultaneously introduced green hydrogen and electrolyzer subsidy policies. In 2023, France launched a 4 billion euros 'difference subsidy contract' plan to make up for the cost gap between clean hydrogen and grey hydrogen. The Italian Ministry of Infrastructure and Transport allocated 300 million euros to purchase hydrogen trains and build green hydrogen production, storage, and train hydrogen refueling

facilities in six regions across the country. At the same time, China has also included hydrogen energy in the scope of energy system management, clarified the energy attributes of hydrogen energy at the legal level, and vigorously promoted relevant policies such as large-scale green electricity hydrogen production and fuel cell vehicle applications. In June 2023, the U.S. Department of Energy released the National Hydrogen Energy Strategy, proposing that the production of clean hydrogen in the United States will increase to 10 million tons/year by 2030, and focus on the application in areas with limited decarbonization alternatives such as chemicals and heavy trucks. It also announced an investment of US$7 billion to build seven "clean hydrogen energy centers" across the United States in the form of project investment. The investment projects mainly include green hydrogen production from renewable energy, blue hydrogen production from natural gas, and nuclear power production of powdered hydrogen. Based on their own resource endowment characteristics, Japan and South Korea regard hydrogen energy as one of the main solutions for future energy transformation, and actively deploy practical application demonstrations of hydrogen energy in production, transportation, and other fields. For example, in 2023, Japan will try for the first time to use fuel cells retired from vehicles to power distributed data centers, launch a lunar rover research and development plan based on long-term hydrogen energy storage, and manufacture Japan's first domestically produced ammonia fuel ship; South Korea plans to build the world's first commercial ammonia cracking hydrogen production power plant. Japan and South Korea regard imported hydrogen and hydrogen-based energy as an important supplement to the future energy gap and have launched intensive international cooperation from the government to the enterprise end to open up international trade channels. In 2023, during the visit of the leaders of Japan and South Korea to the United States, they proposed to jointly build a hydrogen-ammonia decarbonization fuel supply chain. Major companies or consortiums in Japan and South Korea have signed a series of green hydrogen project development agreements in Australia, Southeast Asia, and other places, such as the hydrogen-ammonia project of South Korea's Samsung Group in Western Australia.

As a renewable energy source, hydrogen has the characteristics of large-scale storage and long-distance transportation. Therefore, integrating hydrogen energy into the power system for large-

scale renewable energy power consumption is one of the current development trends. Hydrogen-electricity synergy is expected to greatly improve the flexibility of high-proportion renewable energy power systems and provide new solutions for the construction of new power and energy systems [14, 15]. At present, 26 countries in the world have released hydrogen energy strategies. In 2022, global hydrogen energy demand will reach 95 million tons, a nearly 3% increase year-on-year. Under the influence of multiple factors such as high fossil fuel prices and energy supply shortages, the global hydrogen energy industry will accelerate in 2022. On the production side, the number of hydrogen production projects using renewable energy sources such as wind power and solar power has increased significantly. On the consumption side, hydrogen trains, green hydrogen ironmaking, and hydrogen-ammonia power generation projects have been put into operation at an accelerated pace. On the storage and transportation side, the world's first liquefied hydrogen transport ship completed its maiden voyage from Australia to Japan, marking a key step in the international hydrogen trade. According to the International Energy Agency (IEA)'s "Net Zero Emissions by 2050: A Global Energy Sector Roadmap"[16], the scale of global hydrogen production by water electrolysis will grow rapidly. By 2050, achieving global net zero emissions will require approximately 528 million tons of hydrogen, of which more than 320 million tons will be produced by water electrolysis [16].

For the power and energy systems in which hydrogen energy participates, the types of system energy are diverse [17-21]. Therefore, a variety of energy devices such as batteries, supercapacitors, superconducting energy storage, flywheel energy storage, and hydrogen energy storage can be connected to the power or energy system [22]. The choice of different energy storage methods also directly affects the operating characteristics of the system. Among them, hydrogen energy has unique advantages, and its levelized storage cost is better than other energy storage technologies [23]. The widespread use of hydrogen energy has prompted fuel cells, electrolyzers, and related hydrogen storage mechanisms to be gradually incorporated into power and energy systems. Generally speaking, the efficiency of the system is not high when only fuel cells are used to generate electricity or electrolyzers to produce hydrogen. The hydrogen energy utilization efficiency of fuel cells is usually 40-60%, while the hydrogen production efficiency of electrolyzers is usually 60-80%. Most of the remaining energy is

converted into heat and dissipated. Therefore, studying the electric-hydrogen-heat coupling characteristics of hydrogen energy systems, converting waste heat into usable heat energy, and improving the level of renewable energy consumption has important theoretical significance and practical engineering application value for improving the overall efficiency and economy of comprehensive energy systems [5, 24-29]. At the same time, under the background of the gradual integration of transportation and energy, the energy demand, transmission, and use of energy systems have become inextricably linked to the energy demand and energy transportation characteristics of the transportation system itself [30]. Therefore, in the face of the major challenges of building a green and low-carbon energy system and the actual situation of the close connection between transportation and energy, studying the operation control and commercial energy sharing of hydrogen energy systems has a high research value [31-35].

In summary, to realize the operation, control, and marketization of the hydrogen-based power system, it is of great academic significance and practical value to carry out the research on the modeling, control, operation, and trading of hydrogen-based power system for microgrid, integrated energy system (IES), and energy sharing suppliers. The research routes of this thesis are shown in Figure I. In addition, the research contents of each chapter are as follows:

Chapter 1 mainly introduces the structure of the hydrogen energy system, the operation and control of the hydrogen microgrid, the optimized operation of the hydrogen-based integrated energy system, and the energy sharing of multiple integrated energy systems under the background of energy marketization. According to the analysis in **Chapter 1**, the research progress and shortcomings of the current control, operation, and energy sharing of hydrogen-based microgrids, and energy systems are pointed out.

Chapter 2 studies the energy management and control methods of a hydrogen microgrid, which only considers the hydrogen system as an energy storage device. Taking the operation cost as the target of the microgrid, a two-layer energy management method is proposed, which effectively realizes the economic and stable operation of the microgrid, and semi-physical simulation analysis is carried out through RT-lab.

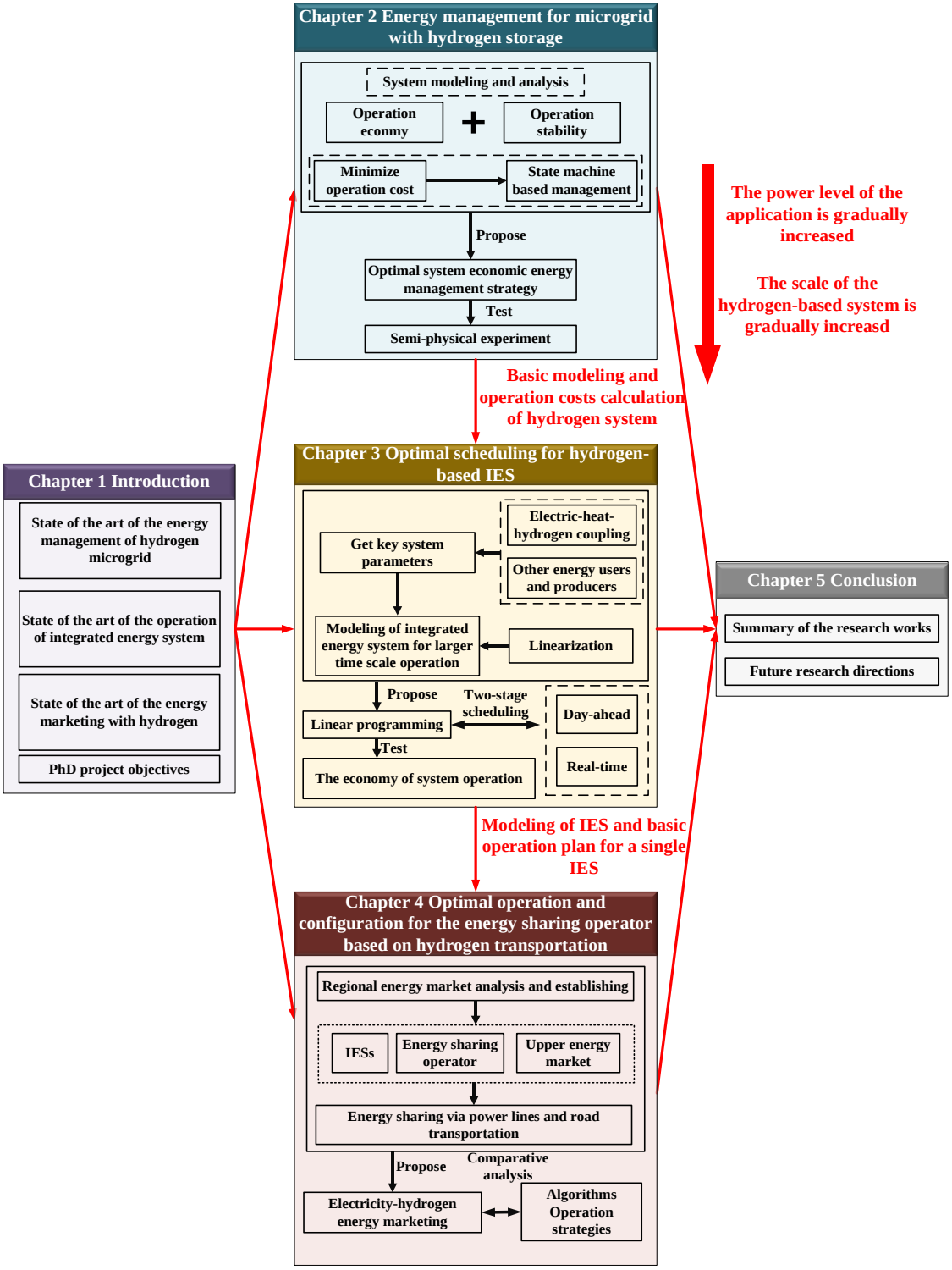

Figure I. The research route of this thesis.

Based on **Chapter 2**, **Chapter 3**, considers the application of hydrogen system in integrated energy system with higher power levels, and considers the waste heat recovery problem of fuel cells and electrolyzer. A two-stage optimization scheduling method for a residential integrated energy system under the access of multiple new energy vehicles is proposed. The optimization

strategy of day-ahead and real-time model predictive control is adopted to realize the optimized operation of integrated energy system and verify the economic advantages of waste heat recovery of fuel cell and electrolyzer.

Chapter 4, based on the modeling of the integrated energy system in **Chapter 3**, studies the energy-sharing problem between multiple integrated energy systems and shared energy storage operators in the region. A method of energy sharing based on hydrogen transportation is proposed and the optimal configuration of shared energy storage operators is realized, verifying the feasibility of hydrogen energy sharing based on road transportation. The operation of the regional energy market is analyzed, and the results show that regional energy sharing can greatly improve the efficiency and economy of the system operation.

Chapter 5 concludes the research contents of this PhD thesis, and also lists the future research works and directions.

Chapter 1. Introduction

To conduct in-depth research on hydrogen-based power systems, this thesis introduces the system structure and current research status first and addresses the main purpose of the work based on the problem raised by the current research. First, the structure and devices of the hydrogen system with fuel cell, electrolyzer, and hydrogen tank are introduced. Then the research status of the energy management of microgrids is studied, then, the literature review about the optimal operation of hydrogen-based integrated energy systems and the optimal energy and also energy storage sharing methods are discussed in detail. In the final section of this chapter, this chapter highlights the contributions of this PhD thesis in 3 aspects.

1.1. Hydrogen system and its application

1.1.1. Structure of the hydrogen system

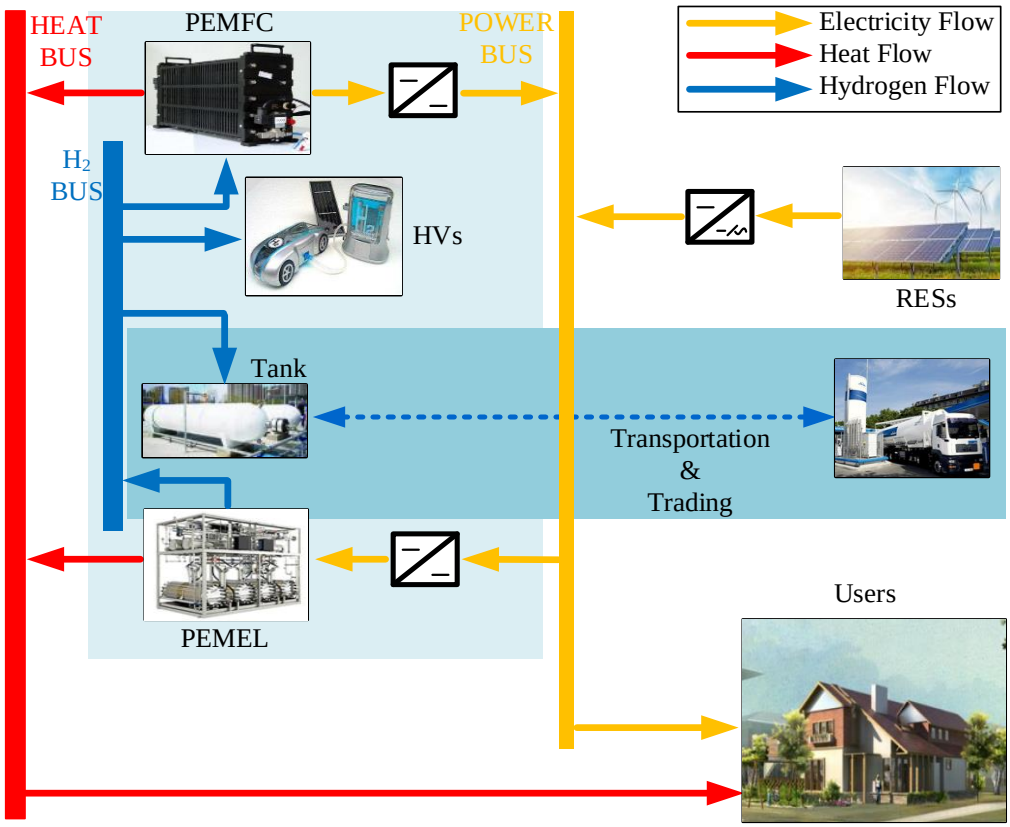

Figure 1- 1 Structure of hydrogen system

As an important petrochemical raw material, hydrogen has been widely used in the production of synthetic ammonia, methanol, and petroleum refining. At the same time, it is also an extremely important industrial raw material in the fields of electronics, food, metallurgy, fine

organic synthesis, aerospace, etc. [36-38]. With the rise and application of hydrogen fuel and fuel cells, the superiority of hydrogen energy has gradually emerged. Hydrogen energy represents a new way to combine with the power system and energy system. They can together form a future energy system with three main energy carriers (electricity, hydrogen energy, and heat) [39-41]. Because electricity and hydrogen energy are two complementary decarbonization energy carriers, they can be generated from the same main energy resource and can be converted into each other, as shown in Figure 1-1. Hydrogen energy storage technology has been developed by utilizing the mutual conversion of electricity and hydrogen energy. In renewable energy power generation systems, intermittent power generation and transmission are often limited. Using surplus, non-peak, or low-quality electricity to produce hydrogen on a large scale, converting electricity into hydrogen energy and storing it, on the one hand, hydrogen can be used to supplement power generation through fuel cells when power demand is high. At the same time, the hydrogen produced in this process can also be distributed to other industrial fields such as transportation and metallurgy for direct use, thereby improving economic efficiency.

1.1.2. Devices and their technology of the hydrogen system

At the technical level, hydrogen production by water electrolysis is mainly divided into alkaline water electrolysis (AWE), polymer electrolyte membrane (PEM) water electrolysis, solid polymer anion exchange membrane (AEM) water electrolysis, and solid oxide electrolysis (SOE) [42, 43]. Among them, AWE is the earliest industrialized water electrolysis technology, with decades of application experience, and the most mature; PEM water electrolysis technology has developed rapidly in recent years, SOE water electrolysis technology is in the initial demonstration stage, and AEM water electrolysis research has just started. From a time scale perspective, AWE technology is easy to deploy and apply quickly in solving the problem of renewable energy consumption in the near future [16]; but from a technical perspective, PEM water electrolysis technology has high current density, small electrolyzer volume, flexible operation, and is conducive to rapid load change, which is well matched with wind power and photovoltaic power (the volatility and randomness of power generation are relatively large). With the promotion and application of PEM electrolyzers, their cost is expected to drop rapidly, which is bound to be the development trend in the next 5 to 10 years [44, 45]. The development

of SOE and AEM water electrolysis depends on the breakthrough of related material technology. Therefore, this paper mainly takes the PEM electrolyzer as the main research object.

An important prerequisite for hydrogen utilization is to connect the green production of hydrogen with end users in a safe, reliable, economical, and convenient way, which requires solving the problem of hydrogen storage and transportation. Hydrogen storage and transportation methods include high-pressure hydrogen storage, liquid hydrogen, material hydrogen storage, organic compound hydrogen storage and transportation, and pipeline hydrogen transportation. Among them, high-pressure hydrogen storage, liquid hydrogen, and pipeline hydrogen transportation all require pressurized hydrogen. Therefore, PEM electrolysis with higher pressure has a natural advantage in matching hydrogen storage needs [46-49]. High-pressure hydrogen storage and transportation is a common method for small and medium-sized hydrogen use. Within a distance of 200 km, a single hydrogen trailer can transport 10 tons of hydrogen per day [50-52]. The material has good safety in hydrogen storage, but the hydrogen storage capacity is low (1%~2%), which is only suitable for on-site hydrogen storage; if used for transportation, the transportation cost is obviously too high. The storage capacity of organic compound hydrogen storage and transportation can reach 5%~6%, and the transportation requirements are similar to those of liquid fuels. After arriving at the destination, dehydrogenation equipment must be used for dehydrogenation treatment, and the dehydrogenation temperature is about 200 ℃. Japan plans to use the conversion process of toluene and methylcyclohexane for hydrogen storage and transportation, and transport hydrogen from Australia to the mainland. Using the existing natural gas pipeline, hydrogen is pressurized and input, so that hydrogen and natural gas are mixed and transported; at the hydrogen end, the natural gas/hydrogen mixture is extracted from the pipeline and reformed to produce hydrogen. This is a new direction for rapid hydrogen storage and transportation. The hydrogen production pressure of PEM water electrolysis is usually greater than 3.5 MPa, which can be easily increased to 4 MPa. Therefore, the hydrogen produced by PEM electrolysis can be directly injected into the natural gas pipeline network without additional pressurization process. Germany already has an engineering case of 20% hydrogen mixing in the natural gas pipeline network. The French GRHYD project began injecting natural gas containing hydrogen (with a blending rate of 6%)

into the natural gas pipeline network in 2018, and the hydrogen blending rate reached 20% in 2019. The UK implemented zero-carbon hydrogen production in the HyDeploy project and injected hydrogen (with a blending rate of 20%) into the natural gas pipeline network in 2020, verifying the technical feasibility of injecting hydrogen produced by electrolysis into the gas pipeline network. A more ideal situation is to build a new pure hydrogen pipeline. Many European countries have started the preliminary planning and demonstration of the pure hydrogen pipeline network, but it will take some time to start construction.

Like traditional fossil fuels, hydrogen can also be used for hydrogen internal combustion engines (ICE) to generate electricity. However, since fuel cells can directly convert the chemical energy of hydrogen into electrical energy, there is no energy form change through boilers, turbines, and generators like ordinary thermal power generators, which can avoid the loss of intermediate conversion, achieve a high power generation efficiency, and be more efficient and environmentally friendly, so it is more practical. According to their operating temperatures, alkaline fuel cells (AFC, 100 °C), solid polymer proton exchange membrane fuel cells (PEMFC, within 100 °C) and phosphoric acid fuel cells (PAFC, 200 °C) are called low-temperature fuel cells; molten carbonate fuel cells (MCFC, 650 °C) and solid oxide fuel cells (SOFC, 1000 °C) are called high-temperature fuel cells[53-56].

To achieve the application of hydrogen devices in power system, the control and optimal operation of those devices are the key to the problem. Therefore, the following section mainly focuses on the control and optimal operation of the hydrogen system.

1.2. Research status of the operation for microgrids and integrated energy system

1.2.1 Energy management of storage-based microgrid

With the continuous increase in global electricity demand and the increasingly serious environmental problems, the construction of a DC microgrid system containing multiple micro-sources has become one of the solutions to the problem. Various energy management optimization methods targeting micro-sources and load characteristics have emerged. In order to fully utilize renewable energy, its uncertainty must be taken into account. Therefore, DC

microgrids containing energy storage systems have been widely studied and play an important role in the intelligent process of power grids. Nowadays, microgrid systems containing multiple energy storage methods such as electric energy storage (batteries, supercapacitors) and power-to-gas energy storage (electrolyzers) have gradually entered the field of vision of scholars. The construction of a DC microgrid system containing multiple energy storage methods has become an attractive solution to increase power generation and reduce operating costs [57-59].

At present, there are many methods for effectively optimizing the capacity of microgrids containing energy storage systems [60, 61]. At the same time, there are also many energy management methods for power distribution and system stability control of microgrid systems containing different energy storage methods. Reference [62] proposed a DC microgrid control method based on the battery state of charge. This method constrains the battery operating state based on SOC (state of charge), thereby avoiding deep charging and discharging of the battery and optimizing the operating life of the energy storage system. Reference [63] analyzed the energy loss problem during the operation of the microgrid and optimized the operation of the microgrid system offline through the MINLP algorithm. In terms of hydrogen energy storage, the establishment of an active DC microgrid system with wind, light, and hydrogen energy storage can improve the utilization rate of wind and light renewable energy and achieve high penetration grid-connected operation [64, 65]. The energy management method based on the state machine can realize the effective operation of such systems according to the state of the hydrogen energy storage and electric energy storage systems [66]. Nasri S et al. proposed an energy management method for photovoltaic, fuel cells, and various energy storage systems based on the state machine [67]. This method introduced the typical working conditions of urban loads and made a strong demonstration of the feasibility of the management method. At the same time, based on the existing model, the battery was replaced with a supercapacitor, and further experimental verification was carried out [68]. In terms of the economic efficiency of microgrid operation, reference [69] used the actual situation of Lake Baikal to configure the capacity of a microgrid containing hydrogen energy storage and compared the economic efficiency with that of a system containing only electric energy storage facilities. Reference [70] first proposed a formula for calculating the cost of using an energy storage system and used a genetic algorithm

for offline optimization. However, most of the above articles use online energy management methods based on SOC, which makes it difficult to optimize the power distribution of various types of energy storage units in the system; in addition, most online energy management methods do not take into account the economic efficiency of the system. Offline optimization algorithms such as the genetic algorithm used in reference [70] can effectively achieve the optimization goal, but how to flexibly operate in real-time in a microgrid system with high uncertainty has not yet been solved. Although the electrical efficiency of an electric-hydrogen microgrid is lower than that of a microgrid containing only electric energy storage, generally speaking, electric energy storage systems are more suitable for short-term electric energy storage. When the time scale is large, the advantage of hydrogen energy storage systems in terms of cost of use is reflected because electric energy storage systems are limited by their scale and reliability [69].

1.2.2. Optimal scheduling for integrated energy system

With the increasing energy demand, the existing microgrid with various renewable energy devices is gradually expanding into an integrated energy system with multiple energy production and transmission equipment, aiming to provide multiple energy supplies for users. Therefore, the effective operation of integrated energy systems has become a hot research topic at present. For the scheduling of integrated energy systems, scholars have conducted in-depth research considering different objects and scenarios [71, 72]. Considering the impact of irradiance on the entry and exit of buildings and electric vehicles, a two-stage office building scheduling that combines day-ahead optimization and real-time optimization achieves economic operation [73]. Based on smart commercial buildings, an improved energy management method that considers building ambient temperature and thermal resistance is proposed to improve energy utilization and reduce operating costs [74]. Considering the economy, reliability, and demand under the liberalization of the electricity market, a scheduling method that combines day-ahead scheduling and real-time model predictive control is adopted to provide a general scheduling mode for integrated energy systems [75]. According to the required hot water and expected building temperature, it is recommended to adopt an integrated energy system building structure equipped with smart meters and controllable power loads; based on the information provided by such smart meters, an intelligent control method that considers load and temperature uncertainty is

applied to the architecture [76]. The uncertainty of the electricity market brings some difficulties to the scheduling of integrated energy systems. Therefore, a robust optimization scheduling method based on considering the degree of price deviation has emerged to avoid uneconomical operations under the influence of uncertainty [77]. Based on day-ahead scheduling, model predictive control can be dynamically adjusted according to the optimization results and real-time predictions to achieve real-time optimal control [78-80]. To minimize the negative impact of prediction errors, a hybrid model predictive control algorithm combining time series analysis and Kalman filtering is proposed [81], which can better compensate for prediction errors. By using an information-sharing model, a distributed model predictive control method based on dual decomposition and sub-gradient iteration uses real thermal and power demand patterns to establish and implement the expected control of an integrated energy system framework based on household-level embedded distributed generation [82]. For smart homes, a small predictive control method is used to combine predictions with the latest information, and a two-way communication infrastructure of a collaborative control scheme is used to achieve limited floor scheduling optimization of residential clusters [82].

At the same time, the wide application of hydrogen energy makes fuel cell and electrolyzer system become important parts of IES. In the study of hydrogen energy systems, due to the relatively low efficiency of fuel cells and electrolyzers, the possibility of waste heat recovery has become a new research focus [83-85]. Among them, most existing studies consider waste heat recovery in large-scale fuel cell application scenarios and use the obtained waste heat to supply the user's heat load. However, current research rarely involves waste heat recovery from electrolyzers. How to make full use of waste heat for local users under the access of hydrogen energy systems and meet the multi-energy needs of integrated energy systems is a key issue that needs to be solved urgently.

In summary, the existing research content mainly focuses on economic operations and pays attention to the integrated energy supply and information interaction of communities and residences. However, at different time scales, the coordinated operation of multiple energy sources such as hydrogen energy, and the scheduling issues under the intervention of new energy

vehicles have been ignored. Therefore, further exploration of the optimal scheduling of integrated energy systems is needed.

1.3 Current research on Energy sharing of integrated energy system

1.3.1 Energy sharing within integrated energy systems

In the process of energy transformation and the construction of new energy systems, electricity and hydrogen are both secondary energy sources and complementary energy carriers [86, 87]. Thus, by forming the renewable energy-based electricity-hydrogen IES, a zero-carbon energy network that fulfills the production, storage, transportation, and supply of multiple energies can be further established, which achieves the virtuous cycle of low-carbon energy production and supply and enhancing the consumption of renewable energy and also the flexibility of regional energy allocation. It is expected that by 2050, global hydrogen energy will bear 18% of the global energy demand, becoming the third largest energy source in the world after oil. Moreover, 40% of the raised electricity demand from 2035 to 2050 will be provided through green hydrogen [88]. Therefore, the IES with electricity and hydrogen production and supply is an important part of future energy systems [88].

At present, there have been some studies on the operation, planning, and marketization of IES. Among them, for the operation and planning of IES, the main focuses are on the system economy and renewable energy consumption [89, 90]. Meanwhile, more research mainly analyzes the energy sharing of multiple IESs within a region. To overcome the uncertainty of distributed energy generation, a day-ahead energy market design of IES is provided, and a consensus-based method is applied to form the electricity market [91]. A regional market transaction model for electric and natural gas systems is established, and the trading frame is analyzed in detail on the electricity trading. A day-ahead optimization for electric vehicles (EVs) charging park and hydrogen refueling stations (HRS) in an IES under the electricity market is proposed to improve the energy supply quality of the charging park and electric vehicles [92].

With the integration of new and renewable energy, the variety of energy trading increasingly grows, and many studies focus on the trading of multiple energy forms [93]. Also, heat transmission and trading are considered in some literature [91, 94]. The use of hydrogen gas in

IES is widely studied, which can be integrated along with electricity and heat supply [11, 92]. Thus, the hydrogen trading of IES is also analyzed [11, 95].

Given the hydrogen market, the European Commission released a hydrogen strategy that announced different policies and measures to support the construction of European hydrogen infrastructure in 2020. Based on this, the installed capacity of the electrolyzer in the EU will reach 40 GW by 2030, which will lead to huge power demands and thus strengthen the connection of hydrogen and the power market [96]. Similarly, other countries have begun to develop hydrogen technology and tried to establish a hydrogen market to achieve zero carbon emissions in the energy system, hence green hydrogen can play an important role in the future energy system and market [97]. Despite the current design or analysis showing that many regions can achieve independence of hydrogen energy supply, it is undeniable that the development of hydrogen energy requires a unified market environment, and trading within a hydrogen market is beneficial to reduce operation costs and hydrogen prices [98]. At present, the studies on the hydrogen energy market are mainly divided into two major categories. The first category is to study the macro international hydrogen market, and the second category is about the trading and scheduling of the regional hydrogen market with the supply chain. The research on the international hydrogen market focuses on the overall hydrogen energy production, demands, and policies of various countries, which analyzes the import and export of hydrogen based on the estimation of production of the overall hydrogen energy, thus the time and geographical scale are large [99]. The second category is to analyze the internal market within a region [100]. Since green hydrogen plays an important role in reaching a zero-carbon future, the green hydrogen supply chain gradually formed. The hydrogen supply chain in a region consists of three parts mainly, the hydrogen production and sales composed of renewable energy sources, electrolyzers, and storage, the transportation logistics formed by vehicles or pipelines, and the users composed of fuel cell vehicles, residential and industrial demands. In such regional markets, researchers usually discuss the interests of various producers and users in smaller time scales and geographical areas. Under these conditions, the trading mode of hydrogen can be similar to the trade of electricity. However, due to the problem caused by transport and the storage of hydrogen, many researchers simplify the model of hydrogen transportation by fixing the trading time and

delivery [101]. Still, the existing studies show the hydrogen market and electricity market will improve the stability of energy systems, reduce energy prices, and improve the flexibility and economy of energy systems. However, compared to the traditional electricity market, the hydrogen market is far more mature. With the gradual expansion of the scale of hydrogen energy production, transmission, and consumption, it can be foreseen that a large-scale market will be formed in the short term. Therefore, research on its market principles and supply needs to be carried out urgently.

1.3.2 Energy storage sharing in the regional energy market

As an important part of the energy system, the large-scale energy storage facility effectively improves the energy utilization rate of the energy system and reduces the operating costs [102]. In this context, the commercial development of user-side energy storage has received widespread attention to further facilitate the operation of energy systems. Among them, large-scale shared energy storage, as a form of improving resource utilization efficiency, can effectively provide flexible support for real-time energy balance and achieve coordination and complementarity of multiple energy sources, further reducing dependence on multiple energy suppliers [103, 104]. Studies have been widely carried out to analyze the electric shared energy storage among IESs [105, 106], and there are three main forms of electricity storage sharing structures: interconnected energy storage, common energy storage, and independent energy storage [104]. Also, more sharing mechanisms based on both hydrogen and electricity storage sharing are gradually developed. To relieve the burden of energy systems, a shared hydrogen storage structure is proposed, and the hydrogen storage is applied for electricity production and consumption [107]. Also, an evolution game is applied to realize energy storage and conversion with hydrogen storage [108]. A two-layered configuration method for hydrogen sharing is designed for multi-energy systems and also hydrogen vehicle charging [109].

To sum up, in the optimal operation and energy transaction of IESs with shared energy storage, batteries or hydrogen storage systems with fuel cells, electrolyzers, and hydrogen tanks are commonly applied for shared energy storage. However, the energy sharing between shared energy operators and IESs is still by the transactions of electricity by power lines [105], and the hydrogen stored in the tank should be transformed to electricity by fuel cells to accomplish the

energy transaction [108]. With the increasing demand for hydrogen energy and the energy utilization rate of fuel cells and electrolyzers by coupling the electricity, hydrogen, and heat supply, the scale of the hydrogen system within the IES is gradually increasing. Thus, it is essential to discuss the sharing of both hydrogen and electricity and study the economy of electric-hydrogen hybrid shared energy storage. In the current research on hydrogen energy storage sharing, however, hydrogen is still transported by pipelines, and the hydrogen demand of users can be met immediately on most occasions. It should be noted that hydrogen pipelines have a huge investment cost and are generally built for large-scale and long-distance transportation. For short and medium distances in which the transportation distance is less than 200km, gaseous hydrogen trailers are more suitable for transportation for their flexible, convenient, and efficient operation [110].

Therefore, for multi-IESs with hydrogen-shared energy storage, it is a realistic and economical scheme to achieve hydrogen transportation by trailers. For the existing works on hydrogen transportation by vehicles, most of them simplify the transportation links and mainly concern the fixed demand of hydrogen loads with fixed hydrogen price, thus ignoring the hydrogen energy transaction between the suppliers and the demanders, and the transportation quantity, transportation time, and the hydrogen energy transaction prices [101, 111, 112]. Still, some studies have been carried out to model hydrogen transportation and consider the transport time of hydrogen energy [112, 113]. However, the relevant research is still mainly applied to the potential of hydrogen energy transport vehicles as an emergency power supply for power system emergency power supply under a fault state [113].

1.4. PhD project objectives

This thesis takes the operation, control, and energy sharing of microgrids and integrated energy systems with hydrogen energy system (fuel cell, electrolyzer, hydrogen tank, and auxiliary devices) as the research object. The main research contents include 1) establishing a hydrogen energy model for small scaled microgrid and a hydrogen energy system model for large integrated energy systems; 2) energy management and control strategy of electric-hydrogen hybrid energy storage island DC microgrid; 3) a two-stage optimization method for integrated energy systems taking into account the combined power, heat and hydrogen of hydrogen energy

system; 4) optimal operation and configuration method of shared energy storage taking into account hydrogen energy transportation under the framework of regional energy sharing.

1) Propose a hierarchical energy management control for the island DC microgrid with electric-hydrogen hybrid storage system

Different from the traditional state machine control method based on the SOC of the battery, this thesis proposed an energy management method for hydrogen-based DC microgrid, which considers the utilization cost of the hybrid energy storage system. A control system with two layers is proposed, the top layer is mainly responsible for providing reference output for each micro source according to the working state and load requirement of each micro source by optimization algorithm, while the bottom layer controls the micro sources specifically according to the reference power output transmitted by top layer. By controlling the working state of each energy storage system, the cost of the energy storage equipment is minimized, and the reserves of energy storage system are kept at a reasonable level. Through the RTLAB semi-physical real-time simulation platform, the results are obtained, and the traditional energy management method based on the state of charge and the energy management methods that contain only electric energy storage system are compared.

2) Propose a two-stage scheduling method for IES with renewable energy vehicles and hydrogen system with power-heat-hydrogen coupling

Considering the advantages of thermal-electric coupling of fuel cell and electrolyzer, an island IES combined power-heat -hydrogen (CPHH) supply is built, and the power-heat-hydrogen relationship of CPHH is analyzed. The optimal power scheduling and real-time operation of IES in small island residential areas with EVs and hydrogen vehicles (HVs) is studied. A two-stage scheduling method is provided. After the prediction of the output power of RESs and temperature, mixed integer linear programming (MILP) is used to achieve optimal scheduling. As for real-time operation, model predictive control (MPC) is carried out by using mixed integer quadratic programming (MIQP). Also, as demand response (DR) loads, EVs help to improve the system economy and flexibility in the optimization,

Finally, the economy and efficiency of IES without the CPHH system are discussed and analyzed.

3) Propose a sizing and operation method for a transportation-based electric-hydrogen hybrid shared energy storage system and its operator in a regional electricity-hydrogen energy market

A transportation-based electric-hydrogen hybrid shared energy storage system and its operator are presented. A two-level configuration method is developed for shared energy storage operator (SESO) configuration and the transactions between SESO and IESs. For the upper level, an improved grey wolf method is proposed for optimal configuration, for the bottom level, a Stackelberg-based game is established, and a bisection method is provided for fast solving of the optimal trading and operation scheme. Finally, a case study is implemented to analyze the economy of the proposed SESO and the performance of the proposed method.

1.5. Publication list

This PhD thesis has contributed to 4 publications, which are listed below:

Papers have been published in international journals:

1. **Yuchen Pu**, Qi Li, Shuyu Luo, Weirong Chen, Elena Breaz, and Fei Gao. Peer-to-Peer Electricity-Hydrogen Trading Among Integrated Energy Systems Considering Hydrogen Delivery and Transportation. ***IEEE Transactions on Power Systems***, 2024, 39(2): 3895-3911. **(Q1, IF = 6.5)**
2. **Yuchen Pu,** Qi Li, Xueli Zou, Ruirui Li, Luoyi, Li, Weirong Chen, Hong Liu. Optimal sizing for an integrated energy system considering degradation and seasonal hydrogen storage. ***Applied Energy***, 2021, 302: 117542. **(Q1, IF = 10.1)**
3. **Yuchen Pu**, Qi Li, Yibin Qiu, Xueli Zou, Weirong Chen. Two-stage scheduling for island CPHH IES considering plateau climate. ***CSEE Journal of Power and Energy Systems***, 2024,10(4): 1775 - 1786. **(Q1, IF = 6.9)**
4. Qi Li, Xukang Xiao, **Yuchen Pu**, Shuyu Luo, Weirong Chen. Hierarchical optimal scheduling method for regional integrated energy systems considering electricity-hydrogen shared energy. ***Applied Energy***, 2023, 349: 121670. **(Q1, IF = 10.1)**

References

[1] W. Shen, X. Chen, J. Qiu, J. A. Hayward, S. Sayeef, P. Osman, K. Meng, and Z. Y. Dong, "A comprehensive review of variable renewable energy levelized cost of electricity," Renewable and Sustainable Energy Reviews, 133, p. 110301, (2020).

[2] M. A. Bagherian and K. Mehranzamir, "A comprehensive review on renewable energy integration for combined heat and power production," Energy Conv. Manag., 224, p. 113454, (2020).

[3] A. Israr, Q. Yang, W. Li, and A. Y. Zomaya, "Renewable energy powered sustainable 5G network infrastructure: Opportunities, challenges and perspectives," J. Netw. Comput. Appl., 175, p. 102910, (2021).

[4] A. Chauhan and R. P. Saini, "A review on Integrated Renewable Energy System based power generation for stand-alone applications: Configurations, storage options, sizing methodologies and control," Renewable and Sustainable Energy Reviews, 38, pp. 99-120, (2014).

[5] T. Özgür and A. C. Yakaryılmaz, "A review: Exergy analysis of PEM and PEM fuel cell based CHP systems," Int. J. Hydrog. Energy, 43, pp. 17993-18000, (2018).

[6] J. O. Abe, A. P. I. Popoola, E. Ajenifuja, and O. M. Popoola, "Hydrogen energy, economy and storage: Review and recommendation," Int. J. Hydrog. Energy, 44, pp. 15072-15086, (2019).

[7] F. J. Vivas, A. De Las Heras, F. Segura, and J. M. Andújar, "A review of energy management strategies for renewable hybrid energy systems with hydrogen backup," Renewable and Sustainable Energy Reviews, 82, pp. 126-155, (2018).

[8] M. Farrokhifar, Y. Nie and D. Pozo, "Energy systems planning: A survey on models for integrated power and natural gas networks coordination," Appl. Energy, 262, p. 114567, (2020).

[9] E. L. V. Eriksson and E. M. Gray, "Optimization and integration of hybrid renewable energy hydrogen fuel cell energy systems – A critical review," Appl. Energy, 202, pp. 348-364, (2017).

[10] A. Z. Arsad, M. A. Hannan, A. Q. Al-Shetwi, M. Mansur, K. M. Muttaqi, Z. Y. Dong, and F. Blaabjerg, "Hydrogen energy storage integrated hybrid renewable energy systems:

A review analysis for future research directions," Int. J. Hydrog. Energy, 47, pp. 17285-17312, (2022).

[11] T. Khan, M. Yu and M. Waseem, "Review on recent optimization strategies for hybrid renewable energy system with hydrogen technologies: State of the art, trends and future directions," Int. J. Hydrog. Energy, 47, pp. 25155-25201, (2022).

[12] E. Union, "REGULATION (EU) 2023/1804 OF THE EUROPEAN PARLIAMENT AND OF THE COUNCIL of 13 September 2023 on the deployment of alternative fuels infrastructure, and repealing Directive 2014/94/EU," 2023.

[13] E. Union, "Renewable Energy – Recast to 2030 (RED II)," 2023.

[14] D. Wang, L. Liu, H. Jia, W. Wang, Y. Zhi, Z. Meng, and B. Zhou, "Review of key problems related to integrated energy distribution systems," CSEE J. Power Energy Syst., 4, pp. 130-145, (2018).

[15] Erdiwansyah, Mahidin, H. Husin, Nasaruddin, M. Zaki, and Muhibbuddin, "A critical review of the integration of renewable energy sources with various technologies," Prot. Control Mod. Power Syst., 6, pp. 1-18, (2021).

[16] I. E. Agency, "Net Zero Roadmap: A Global Pathway to Keep the 1.5℃ Goal in Reach,", 2023.

[17] M. A. Hannan, M. Faisal, P. Jern Ker, R. A. Begum, Z. Y. Dong, and C. Zhang, "Review of optimal methods and algorithms for sizing energy storage systems to achieve decarbonization in microgrid applications," Renewable and Sustainable Energy Reviews, 131, p. 110022, (2020).

[18] A. Chauhan and R. P. Saini, "A review on Integrated Renewable Energy System based power generation for stand-alone applications: Configurations, storage options, sizing methodologies and control," Renewable and Sustainable Energy Reviews, 38, pp. 99-120, (2014).

[19] R. Amirante, E. Cassone, E. Distaso, and P. Tamburrano, "Overview on recent developments in energy storage: Mechanical, electrochemical and hydrogen technologies," Energy Conv. Manag., 132, pp. 372-387, (2017).

[20] O. Schmidt, S. Melchior, A. Hawkes, and I. Staffell, "Projecting the Future Levelized Cost of Electricity Storage Technologies," Joule, 3, pp. 81-100, (2019).

[21] H. Beltran, J. Cardo-Miota, J. Segarra-Tamarit, and E. Pérez, "Battery size determination for photovoltaic capacity firming using deep learning irradiance forecasts," J. Energy Storage, 33, p. 102036, (2021).

[22] M. A. Hannan, M. Faisal, P. Jern Ker, R. A. Begum, Z. Y. Dong, and C. Zhang, "Review of optimal methods and algorithms for sizing energy storage systems to achieve decarbonization in microgrid applications," Renewable and Sustainable Energy Reviews, 131, p. 110022, (2020).

[23] W. Shen, X. Chen, J. Qiu, J. A. Hayward, S. Sayeef, P. Osman, K. Meng, and Z. Y. Dong, "A comprehensive review of variable renewable energy levelized cost of electricity," Renewable and Sustainable Energy Reviews, 133, p. 110301, (2020).

[24] G. F. and B. C., "Optimal Economical Schedule of Hydrogen-Based Microgrids With Hybrid Storage Using Model Predictive Control," IEEE Trans. Ind. Electron., 62, pp. 5195-5207, (2015).

[25] J. Li, J. Lin, Y. Song, X. Xing, and C. Fu, "Operation Optimization of Power to Hydrogen and Heat (P2HH) in ADN Coordinated With the District Heating Network," IEEE Trans. Sustain. Energy, 10, pp. 1672-1683, (2019).

[26] T. Özgür and A. C. Yakaryılmaz, "A review: Exergy analysis of PEM and PEM fuel cell based CHP systems," Int. J. Hydrog. Energy, 43, pp. 17993-18000, (2018).

[27] A. Herrmann, A. Mädlow and H. Krause, "Key performance indicators evaluation of a domestic hydrogen fuel cell CHP," Int. J. Hydrog. Energy, 44, pp. 19061-19066, (2019).

[28] H. Pashaei-Didani, S. Nojavan, R. Nourollahi, and K. Zare, "Optimal economic-emission performance of fuel cell/CHP/storage based microgrid," Int. J. Hydrog. Energy, 44, pp. 6896-6908, (2019).

[29] M. A. Bagherian and K. Mehranzamir, "A comprehensive review on renewable energy integration for combined heat and power production," Energy Conv. Manag., 224, p. 113454, (2020).

[30] H. Liu and J. Ma, "A review of models and methods for hydrogen supply chain system planning," CSEE J. Power Energy Syst., (2020).

[31] S. Y., Z. J., L. Z., T. W., and S. M., "Stochastic Scheduling of Battery-Based Energy Storage Transportation System With the Penetration of Wind Power," IEEE Trans. Sustain. Energy, 8, pp. 135-144, (2017).

[32] E. L. V. Eriksson and E. M. Gray, "Optimization and integration of hybrid renewable energy hydrogen fuel cell energy systems – A critical review," Appl. Energy, 202, pp. 348-364, (2017).

[33] S. Zhang, Y. Li, E. Du, C. Fan, Z. Wu, Y. Yao, L. Liu, and N. Zhang, "A review and outlook on cloud energy storage: An aggregated and shared utilizing method of energy storage system," Renewable and Sustainable Energy Reviews, 185, p. 113606, (2023).

[34] A. Chauhan and R. P. Saini, "A review on Integrated Renewable Energy System based power generation for stand-alone applications: Configurations, storage options, sizing methodologies and control," Renewable and Sustainable Energy Reviews, 38, pp. 99-120, (2014).

[35] T. Capper, A. Gorbatcheva, M. A. Mustafa, M. Bahloul, J. M. Schwidtal, R. Chitchyan, M. Andoni, V. Robu, M. Montakhabi, I. J. Scott, C. Francis, T. Mbavarira, J. M. Espana, and L. Kiesling, "Peer-to-peer, community self-consumption, and transactive energy: A systematic literature review of local energy market models," Renewable and Sustainable Energy Reviews, 162, p. 112403, (2022).

[36] M. Kamran and M. Turzyński, "Exploring hydrogen energy systems: A comprehensive review of technologies, applications, prevailing trends, and associated challenges," J. Energy Storage, 96, p. 112601, (2024).

[37] G. Soyturk, S. A. Cetinkaya, M. Aslani Yekta, M. M. Kheiri Joghan, H. Mohebi, O. Kizilkan, A. M. Ghandehariun, C. O. Colpan, C. Acar, and S. Ghandehariun, "Dynamic analysis and multi-objective optimization of solar and hydrogen energy-based systems for residential applications: A review," Int. J. Hydrog. Energy, 75, pp. 662-689, (2024).

[38] M. Yue, H. Lambert, E. Pahon, R. Roche, S. Jemei, and D. Hissel, "Hydrogen energy systems: A critical review of technologies, applications, trends and challenges," Renewable and Sustainable Energy Reviews, 146, p. 111180, (2021).

[39] G. Cipriani, V. Di Dio, F. Genduso, D. La Cascia, R. Liga, R. Miceli, and G. Ricco Galluzzo, "Perspective on hydrogen energy carrier and its automotive applications," Int. J. Hydrog. Energy, 39, pp. 8482-8494, (2014).

[40] N. K. Obiora, C. O. Ujah, C. O. Asadu, F. O. Kolawole, and B. N. Ekwueme, "Production of hydrogen energy from biomass: Prospects and challenges," Green Technologies and Sustainability, 2, p. 100100, (2024).

[41] E. I. Zoulias, R. Glockner, N. Lymberopoulos, T. Tsoutsos, I. Vosseler, O. Gavalda, H. J. Mydske, and P. Taylor, "Integration of hydrogen energy technologies in stand-alone power systems analysis of the current potential for applications," Renewable and Sustainable Energy Reviews, 10, pp. 432-462, (2006).

[42] G. Xu, Y. Wu, S. Tang, Y. Wang, X. Yu, and M. Ma, "Optimal design of hydrogen production processing coupling alkaline and proton exchange membrane electrolyzers," Energy, 302, p. 131827, (2024).

[43] B. Xu, Y. Yang, J. Li, D. Ye, Y. Wang, L. Zhang, X. Zhu, and Q. Liao, "A comprehensive study of parameters distribution in a short PEM water electrolyzer stack utilizing a full-scale multi-physics model," Energy, 300, p. 131565, (2024).

[44] H. Sayed-Ahmed, Á. I. Toldy and A. Santasalo-Aarnio, "Dynamic operation of proton exchange membrane electrolyzers—Critical review," Renewable and Sustainable Energy Reviews, 189, p. 113883, (2024).

[45] T. Liu, Y. Tao, Y. Wang, M. Hu, Z. Zhang, and J. Shao, "Towards cost-effective and durable bipolar plates for proton exchange membrane electrolyzers: A review," Fuel, 368, p. 131610, (2024).

[46] X. Yang, J. Su, X. Lu, J. Kong, D. Huo, Y. Pan, and W. Li, "Application and development of LiBH4 hydrogen storage materials," J. Alloy. Compd., 1001, p. 175174, (2024).

[47] M. J. Adams, M. D. Wadge, D. Sheppard, A. Stuart, and D. M. Grant, "Review on onshore and offshore large-scale seasonal hydrogen storage for electricity generation: Focusing on improving compression, storage, and roundtrip efficiency," Int. J. Hydrog. Energy, 73, pp. 95-111, (2024).

[48] A. Ali and M. N. Shaikh, "Recent developments in catalyst design for liquid organic hydrogen carriers: Bridging the gap to affordable hydrogen storage," Int. J. Hydrog. Energy, 78, pp. 1-21, (2024).

[49] A. S. Mehr, A. D. Phillips, M. P. Brandon, M. T. Pryce, and J. G. Carton, "Recent challenges and development of technical and technoeconomic aspects for hydrogen storage, insights at different scales; A state of art review," Int. J. Hydrog. Energy, 70, pp. 786-815, (2024).

[50] N. S. Muhammed, A. O. Gbadamosi, E. I. Epelle, A. A. Abdulrasheed, B. Haq, S. Patil, D. Al-Shehri, and M. S. Kamal, "Hydrogen production, transportation, utilization, and storage: Recent advances towards sustainable energy," J. Energy Storage, 73, p. 109207, (2023).

[51] G. Jia, M. Lei, M. Li, W. Xu, R. Li, Y. Lu, and M. Cai, "Hydrogen embrittlement in hydrogen-blended natural gas transportation systems: A review," Int. J. Hydrog. Energy, 48, pp. 32137-32157, (2023).

[52] B. L. Salvi and K. A. Subramanian, "Sustainable development of road transportation sector using hydrogen energy system," Renewable and Sustainable Energy Reviews, 51, pp. 1132-1155, (2015).

[53] X. Zhang, L. Xu, L. Zou, Z. Jiang, J. Liao, P. Gao, S. Li, and Q. Shen, "Modeling and simulation of a residential-based PEMFC-CHP system," Int. J. Electrochem. Sci., 19, p. 100638, (2024).

[54] T. Raza, J. Yang, R. Wang, C. Xia, R. Raza, B. Zhu, and S. Yun, "Recent advance in physical description and material development for single component SOFC: A mini-review," Chem. Eng. J., 444, p. 136533, (2022).

[55] J. Zuo, N. Y. Steiner, Z. Li, and D. Hissel, "Health management review for fuel cells: Focus on action phase," Renewable and Sustainable Energy Reviews, 201, p. 114613, (2024).

[56] H. Kahraman and Y. Akın, "Recent studies on proton exchange membrane fuel cell components, review of the literature," Energy Conv. Manag., 304, p. 118244, (2024).

[57] S. Tajjour and S. Singh Chandel, "A comprehensive review on sustainable energy management systems for optimal operation of future-generation of solar microgrids," Sustain. Energy Technol. Assess., 58, p. 103377, (2023).

[58] L. P. Van, K. D. Chi and T. N. Duc, "Review of hydrogen technologies based microgrid: Energy management systems, challenges and future recommendations," Int. J. Hydrog. Energy, 48, pp. 14127-14148, (2023).

[59] H. M. Yassim, M. N. Abdullah, C. K. Gan, and A. Ahmed, "A review of hierarchical energy management system in networked microgrids for optimal inter-microgrid power exchange," Electr. Power Syst. Res., 231, p. 110329, (2024).

[60] M. S. Alam, M. A. Hossain, M. Shafiullah, A. Islam, M. S. H. Choudhury, M. O. Faruque, and M. A. Abido, "Renewable energy integration with DC microgrids: Challenges and opportunities," Electr. Power Syst. Res., 234, p. 110548, (2024).

[61] N. F. P. Dinata, M. A. M. Ramli, M. I. Jambak, M. A. B. Sidik, and M. M. Alqahtani, "Designing an optimal microgrid control system using deep reinforcement learning: A systematic review," Engineering Science and Technology, an International Journal, 51, p. 101651, (2024).

[62] X. Liu, M. Zhang, X. Xie, L. Zhao, and Q. Sun, "Consensus-based energy management of multi-microgrid: An improved SoC-based power coordinated control method," Appl. Math. Comput., 425, p. 127086, (2022).

[63] B. Cortés-Caicedo, J. Ocampo-Toro, R. I. Bolaños, O. D. Montoya, and L. F. Grisales-Noreña, "A multi-objective PSO for DC microgrids: Efficient battery management to minimize energy losses and operating costs," J. Energy Storage, 96, p. 112550, (2024).

[64] S. S. Zehra, A. Ur Rahman and I. Ahmad, "Fuzzy-barrier sliding mode control of electric-hydrogen hybrid energy storage system in DC microgrid: Modelling, management and experimental investigation," Energy, 239, p. 122260, (2022).

[65] Y. Han, H. Yang, Q. Li, W. Chen, F. Zare, and J. M. Guerrero, "Mode-triggered droop method for the decentralized energy management of an islanded hybrid PV/hydrogen/battery DC microgrid," Energy, 199, p. 117441, (2020).

[66] Y. Han, G. Zhang, Q. Li, Z. You, W. Chen, and H. Liu, "Hierarchical energy management for PV/hydrogen/battery island DC microgrid," Int. J. Hydrog. Energy, 44, pp. 5507-5516, (2019).

[67] S. Nasri, B. S. Sami and A. Cherif, "Power management strategy for hybrid autonomous power system using hydrogen storage," Int. J. Hydrog. Energy, 41, pp. 857-865, (2016).

[68] S. Nasri, S. Ben Slama, I. Yahyaoui, B. Zafar, and A. Cherif, "Autonomous hybrid system and coordinated intelligent management approach in power system operation and control using hydrogen storage," Int. J. Hydrog. Energy, 42, pp. 9511-9523, (2017).

[69] O. V. Marchenko and S. V. Solomin, "Modeling of hydrogen and electrical energy storages in wind/PV energy system on the Lake Baikal coast," Int. J. Hydrog. Energy, 42, pp. 9361-9370, (2017).

[70] R. Dufo-López, J. L. Bernal-Agustín and J. Contreras, "Optimization of control strategies for stand-alone renewable energy systems with hydrogen storage," Renew. Energy, 32, pp. 1102-1126, (2007).

[71] W. Lin, X. Jin, Y. Mu, H. Jia, X. Xu, X. Yu, and B. Zhao, "A two-stage multi-objective scheduling method for integrated community energy system," Appl. Energy, 216, pp. 428-441, (2018).

[72] T. Y., W. Z., L. Y., M. Q., H. Q., and L. S., "Multi-energy storage system model based on electricity heat and hydrogen coordinated optimization for power grid flexibility," CSEE J. Power Energy Syst., 5, pp. 266-274, (2019).

[73] X. Jin, J. Wu, Y. Mu, M. Wang, X. Xu, and H. Jia, "Hierarchical microgrid energy management in an office building," Appl. Energy, 208, pp. 480-494, (2017).

[74] A. H. M., C. W., Z. M., and D. L., "Economic Dispatch of Grid-Connected Microgrid for Smart Building Considering the Impact of Air Temperature," IEEE Access, 7, pp. 70332-70342, (2019).

[75] V. J., G. S., J. D., and Z. M., "Day-Ahead Scheduling and Real-Time Economic MPC of CHP Unit in Microgrid With Smart Buildings," IEEE Trans. Smart Grid, 10, pp. 1992-2001, (2019).

[76] T. M., G. H. and R. A., "Residential Microgrid Scheduling Based on Smart Meters Data and Temperature Dependent Thermal Load Modeling," IEEE Trans. Smart Grid, 5, pp. 349-357, (2014).

[77] N. M., M. B., B. G. G., and S. M., "Robust Short-Term Scheduling of Integrated Heat and Power Microgrids," IEEE Syst. J., 13, pp. 3295-3303, (2019).

[78] G. F. and B. C., "Optimal Economical Schedule of Hydrogen-Based Microgrids With Hybrid Storage Using Model Predictive Control," IEEE Trans. Ind. Electron., 62, pp. 5195-5207, (2015).

[79] G. F., B. C. and A. R. M., "Optimal Economic Schedule for a Network of Microgrids With Hybrid Energy Storage System Using Distributed Model Predictive Control," IEEE Trans. Ind. Electron., 66, pp. 1919-1929, (2019).

[80] A. V. M., B. J., Q. N., I. C. A., and S. M., "Intra-Hour Microgrid Economic Dispatch Based on Model Predictive Control," IEEE Trans. Smart Grid, 11, pp. 1968-1979, (2020).

[81] Y. L., Z. C., T. Y., Z. W., Z. Y., L. P., Z. B., L. H., and L. Z., "Hierarchical Model Predictive Control Strategy Based on Dynamic Active Power Dispatch for Wind Power Cluster Integration," IEEE Trans. Power Syst., 34, pp. 4617-4629, (2019).

[82] G. W., W. Z., W. Z., L. Z., T. Y., and W. J., "An Online Optimal Dispatch Schedule for CCHP Microgrids Based on Model Predictive Control," IEEE Trans. Smart Grid, 8, pp. 2332-2342, (2017).

[83] J. Kim, C. Han, S. Lee, D. Lee, and Y. Kim, "Performance analysis of PEMFC-assisted renewable energy source heat pumps as a novel active system for plus energy buildings," Energy Build., p. 114477, (2024).

[84] M. A. Sabbaghi, M. Soltani, R. Fraser, and M. B. Dusseault, "Emergy-based exergoeconomic and exergoenvironmental assessment of a novel CCHP system integrated with PEME and PEMFC for a residential building," Energy, p. 132301, (2024).

[85] T. Zhang, M. Li, J. Ni, and C. Qian, "Study of dynamic performance of PEMFC-based CCHP system in a data center based on real-time load and a novel synergistic control method with variable working conditions," Energy, 300, p. 131637, (2024).

[86] N. S. Muhammed, A. O. Gbadamosi, E. I. Epelle, A. A. Abdulrasheed, B. Haq, S. Patil, D. Al-Shehri, and M. S. Kamal, "Hydrogen production, transportation, utilization, and storage: Recent advances towards sustainable energy," J. Energy Storage, 73, p. 109207, (2023).

[87] Y. Pu, Q. Li, X. Zou, R. Li, L. Li, W. Chen, and H. Liu, "Optimal sizing for an integrated energy system considering degradation and seasonal hydrogen storage," Appl. Energy, 302, p. 117542, (2021).

[88] Q. Hassan, A. Z. Sameen, H. M. Salman, M. Jaszczur, and A. K. Al-Jiboory, "Hydrogen energy future: Advancements in storage technologies and implications for sustainability," J. Energy Storage, 72, p. 108404, (2023).

[89] A. M. O. Haruni, M. Negnevitsky, M. E. Haque, and A. Gargoom, "A Novel Operation and Control Strategy for a Standalone Hybrid Renewable Power System," IEEE Trans. Sustain. Energy, 4, pp. 402-413, (2013).

[90] J. Qi, C. Lai, B. Xu, Y. Sun, and K. Leung, "Collaborative Energy Management Optimization Toward a Green Energy Local Area Network," IEEE Trans. Ind. Inform., 14, pp. 5410-5418, (2018).

[91] Y. Chen, J. Wang, Y. Zhang, and X. Wang, "Consensus-based approach to day-ahead joint local energy-reserve market design considering uncertainties of renewable energy," CSEE J. Power Energy Syst., (2021).

[92] Z. M. Shoja, M. A. Mirzaei, H. Seyedi, and K. Zare, "Sustainable energy supply of electric vehicle charging parks and hydrogen refueling stations integrated in local energy systems under a risk-averse optimization strategy," J. Energy Storage, 55, p. 105633, (2022).

[93] Z. Wu, J. Wang, H. Zhong, F. Gao, T. Pu, C. Tan, X. Chen, G. Li, H. Zhao, M. Zhou, and Q. Xia, "Sharing Economy in Local Energy Markets," J. Mod. Power Syst. Clean Energy, 11, pp. 714-726, (2023).

[94] G. Sun, J. Sun, S. Chen, Z. Wei, and H. Zang, "Market-based coordination of regional electric and natural gas systems: A peer-to-peer energy trading model," CSEE J. Power Energy Syst., (2022).

[95] K. Zhang, B. Zhou, C. Y. Chung, S. Bu, Q. Wang, and N. Voropai, "A Coordinated Multi-Energy Trading Framework for Strategic Hydrogen Provider in Electricity and Hydrogen Markets," IEEE Trans. Smart Grid, 14, pp. 1403-1417, (2023).

[96] P. Hesel, S. Braun, F. Zimmermann, and W. Fichtner, "Integrated modelling of European electricity and hydrogen markets," Appl. Energy, 328, (2022).

[97] L. Eicke and N. De Blasio, "Green hydrogen value chains in the industrial sector—Geopolitical and market implications," Energy Res. Soc. Sci., 93, p. 102847, (2022).

[98] A. Nuñez-Jimenez and N. De Blasio, "Competitive and secure renewable hydrogen markets: Three strategic scenarios for the European Union," Int. J. Hydrog. Energy, 47, pp. 35553-35570, (2022).

[99] E. M. Morton, T. A. Deetjen and S. Goodarzi, "Optimizing hydrogen production capacity and day ahead market bidding for a wind farm in Texas," Int. J. Hydrog. Energy, (2023).

[100] S. A. Ikonnikova, B. R. Scanlon and S. A. Berdysheva, "A global energy system perspective on hydrogen Trade: A framework for the market color and the size analysis," Appl. Energy, 330, p. 120267, (2023).

[101] Z. Guo, W. Wei, L. Chen, X. Zhang, and S. Mei, "Equilibrium model of a regional hydrogen market with renewable energy based suppliers and transportation costs," Energy, 220, p. 119608, (2021).

[102] W. Wang, B. Yuan, Q. Sun, and R. Wennersten, "Application of energy storage in integrated energy systems — A solution to fluctuation and uncertainty of renewable energy," J. Energy Storage, 52, p. 104812, (2022).

[103] S. Rasool, K. M. Muttaqi and D. Sutanto, "A Multi-Filter Based Dynamic Power Sharing Control for a Hybrid Energy Storage System Integrated to a Wave Energy Converter for Output Power Smoothing," IEEE Trans. Sustain. Energy, 13, pp. 1693-1706, (2022).

[104] R. Dai, R. Esmaeilbeigi and H. Charkhgard, "The Utilization of Shared Energy Storage in Energy Systems: A Comprehensive Review," IEEE Trans. Smart Grid, 12, pp. 3163-3174, (2021).

[105] C. Chen, Y. Zhu, T. Zhang, Q. Li, Z. Li, H. Liang, C. Liu, Y. Ma, Z. Lin, and L. Yang, "Two-stage multiple cooperative games-based joint planning for shared energy storage provider and local integrated energy systems," Energy, 284, p. 129114, (2023).

[106] C. Chen, Y. Li, W. Qiu, C. Liu, Q. Zhang, Z. Li, Z. Lin, and L. Yang, "Cooperative-Game-Based Day-Ahead Scheduling of Local Integrated Energy Systems With Shared Energy Storage," IEEE Trans. Sustain. Energy, 13, pp. 1994-2011, (2022).

[107] M. Shi, Y. Huang and H. Lin, "Research on power to hydrogen optimization and profit distribution of microgrid cluster considering shared hydrogen storage," Energy, 264, p. 126113, (2023).

[108] X. Li, L. Chen, Y. Hao, Z. Wang, Y. Changxing, and S. Mei, "Sharing hydrogen storage capacity planning for multi-microgrid investors with limited rationality: A differential evolution game approach," J. Clean. Prod., 417, p. 138100, (2023).

[109] H. Deng, J. Wang, Y. Shao, Y. Zhou, Y. Cao, X. Zhang, and W. Li, "Optimization of configurations and scheduling of shared hybrid electric-hydrogen energy storages supporting to multi-microgrid system," J. Energy Storage, 74, p. 109420, (2023).

[110] M. Reuß, T. Grube, M. Robinius, P. Preuster, P. Wasserscheid, and D. Stolten, "Seasonal storage and alternative carriers: A flexible hydrogen supply chain model," Appl. Energy, 200, pp. 290-302, (2017).

[111] Z. Y. Dong, J. Yang, L. Yu, R. Daiyan, and R. Amal, "A green hydrogen credit framework for international green hydrogen trading towards a carbon neutral future," Int. J. Hydrog. Energy, 47, pp. 728-734, (2022).

[112] C. Shao, C. Feng, M. Shahidehpour, Q. Zhou, X. Wang, and X. Wang, "Optimal Stochastic Operation of Integrated Electric Power and Renewable Energy With Vehicle-Based Hydrogen Energy System," IEEE Trans. Power Syst., 36, pp. 4310-4321, (2021).

[113] Y. Zhao, J. Lin, Y. Song, and Y. Xu, "A Hierarchical Strategy for Restorative Self-Healing of Hydrogen-Penetrated Distribution Systems Considering Energy Sharing via Mobile Resources," IEEE Trans. Power Syst., 38, pp. 1388-1404, (2023).

Chapter 2. Hierarchical Energy Management Control for Islanding DC Microgrid with Electric-hydrogen Hybrid Storage System

2.1. Introduction

With the increase in global power demand, power systems containing a variety of micro sources have become one of the solutions to the problem [1-3]. Thus, energy management methods for micro source and load characteristics emerge as the times require [4]. To make full use of renewable energy, one must consider its uncertainty and volatility, so the DC microgrid containing energy storage system has been widely used and plays an important role in the intelligent power grid [5-7]. Nowadays, the microgrid with an electric energy storage system (battery, super capacitor) and power to the gas energy storage system (electrolyzer) has gotten gradual attention [8,9], and the construction of a DC microgrid system with multiple energy storage systems has become an attractive solution to increase the power generation and reduce the cost of the power system.

At present, there are many ways to optimize the capacity of energy storage devices for microgrids [10,11]. At the same time, for microgrids with different energy storage systems, there are also a variety of energy management methods for power distribution and system stability control. Ref. [12] proposes a DC microgrid control method based on the SOC of the battery, which divides the battery running state into multiple segments, thus avoiding the depth charge and discharge of the battery and optimizing the operating life of the energy storage system. Ref. [13] proposes a power management method for a hydrogen-based microgrid, while the power level and state of charge of the battery are considered during the operation. Besides, Ref. [14] provides a state machine-based energy management method for PV, fuel cells, and multiple energy storage systems. This method introduced a typical load condition of Tunisia city and explained the feasibility of the management method. Ref. [15] carries out an intelligent energy management method on the basis of the existing models, and the battery is replaced by super capacitor. In terms of economy, one of the common approaches is to use the droop control method based on cost [16]. Ref. [17] carries out the capacity configuration of a hydrogen storage microgrid based on the environmental condition in Lake Baikal and compares it with the system that contains only electrical energy storage facilities. Ref. [18] presents a calculation formula for the utilization cost of the energy storage system, and the genetic algorithm is used for offline optimization. However, most of these articles are based on the SOC-based online energy management method, which makes it difficult to

optimize the power allocation for various types of energy storage units in the system. In addition, the online energy management methods do not account for the cost of the system. The off-line optimization algorithm, such as Ref. [18], uses genetic algorithms to achieve the optimization goal effectively, but how to operate flexibly in the high uncertainty microgrid system has not been solved.

In this chapter, a hierarchical energy management control is proposed for the island DC microgrid with the electric-hydrogen hybrid storage system. Apart from the PV system, this microgrid is equipped with two different types of energy storage systems (electric and hydrogen). Different from the traditional state machine control method based on the SOC of the battery, the energy management method proposed in this chapter considers the utilization cost of the hybrid energy storage system. To achieve the management goals more flexible, this control system is divided into two layers, the top layer is mainly responsible for providing reference output for each micro source according to the working state and load requirement of each micro source by an optimization algorithm, while the bottom layer controls the micro sources specifically according to the reference power output transmitted by the top layer. By controlling the working state of each energy storage system, the cost of the energy storage equipment is minimized, and the reserves of the energy storage system are kept at a reasonable level. The 72-hour climate conditions recorded by the University of Queensland and a typical kind of load demand condition are used to verify the feasibility of the energy management method. Through the RTLAB semi-physical real-time simulation platform, the results are obtained, and the traditional energy management method based on the state of charge and the energy management methods that contain only electric energy storage systems are compared. The results show that the hierarchical management method based on minimum utilization cost is obviously superior to the state machine-only energy management method in the utilization cost and energy efficiency. Compared with the electric-storage-only method, the utilization cost is lower and the microgrid is more reliable.

2.2. Structure and modeling of island DC microgrid

2.2.1. System structure

As shown in Figure 2-1, the island DC microgrid based on an electric-hydrogen hybrid storage system is built in this chapter. The photovoltaic (PV) system, the electrolyzer, and the fuel cell are all connected to the DC bus by unidirectional DC/DC converters, and the battery is connected to the bus by a

bidirectional DC/DC converter. As the main distributed energy source, PV provides energy for the whole island grid. When the output power of a photovoltaic system is excessive, the energy storage system will consume redundant energy. Also, the hybrid energy storage system will provide energy when the output of the PV system cannot meet the needs of users.

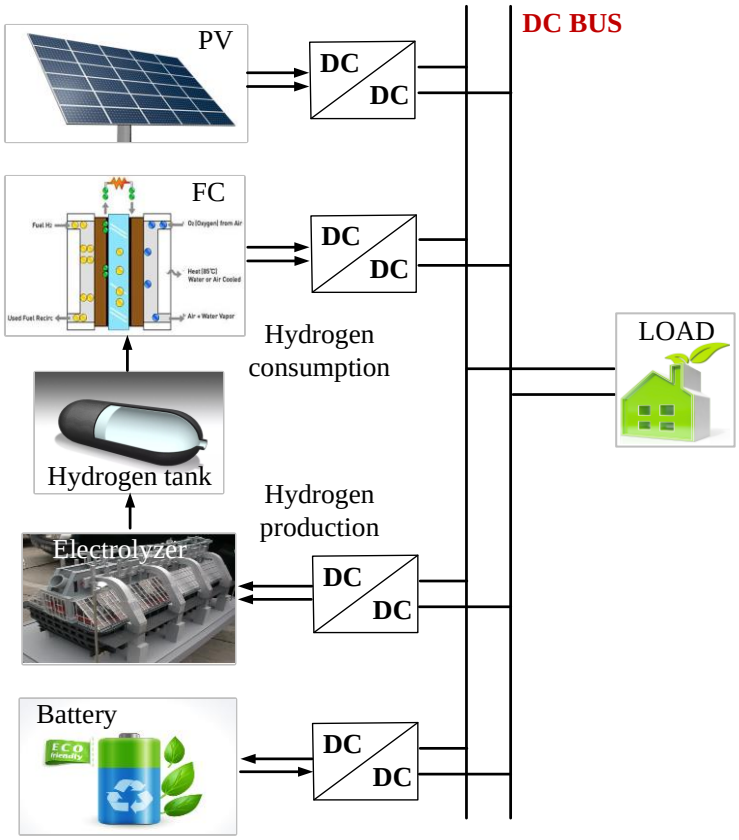

Figure 2- 1 Physical structure of DC microgrid.

2.2.2. Modeling of PV

The mathematical model of photovoltaic cells built in this chapter is a practical engineering model. The mathematical expression of the model is given by eq. (2.1)-eq.(2.9) [19]:

$$I = I_{sc}\left\{1 - C_1[\exp(\frac{U}{C_2 U_{oc}}) - 1]\right\} \tag{2.1}$$

$$C_1 = (1 - \frac{I_m}{I_{sc}})\exp(\frac{-U_m}{C_2 U_{oc}}) \tag{2.2}$$

$$C_2 = (\frac{U_m}{U_{oc}} - 1)[\ln(1 - \frac{I_m}{I_{sc}})]^{-1} \tag{2.3}$$

$$\Delta T = T - T_b \tag{2.4}$$

$$\Delta S = S / S_b - 1 \tag{2.5}$$

$$I_{sc}' = I_{sc}(S / S_b)(1 + a\Delta T) \tag{2.6}$$

$$I_m' = I_m(S / S_b)(1 + \Delta T) \tag{2.7}$$

$$U_{oc}' = U_{oc}\left\{[1 - c\Delta T]\ln(e + b\Delta S\right\} \tag{2.8}$$

$$U_m' = U_m\left\{[1 - c\Delta T]\ln(e + b\Delta S)\right\} \tag{2.9}$$

where I_{sc} is short circuit current, U_{oc} is open circuit voltage, I_m is peak current, U_m is peak voltage. When the above parameters are certain, the values of C_1 and C_2 are certain. When the solar radiation S and environmental temperature T change, it is necessary to recalculate the parameters. T_b and S_b are the standard values of temperature and solar radiation respectively. Coefficients a, b and c are the temperature coefficients, which are generally valued at 0.0025/℃, 0.5 and 0.00288/℃. I_{sc}', I_m', U_{oc}' and U_m' are updated values calculated by each parameter respectively.

2.2.3. Modeling of fuel cell

The fuel cell used in this chapter is proton exchange membrane fuel cell. The output voltage of a single cell is given by eq. (2.10) [20].

$$V_{cell} = E_{Nerst} - V_{act} - V_{ohmic} - V_{con} \tag{2.10}$$

where E_{Nernst} is the thermodynamic electromotive force, V_{act} is the activation overvoltage, V_{ohmic} is ohmic overvoltage, and V_{con} is the concentration difference overvoltage.

The voltage of the fuel cell stack is described by eq. (2.11):

$$V_{PEMFC} = n_c V_{cell} \tag{2.11}$$

where n_c is the number of cells.

2.2.4. Modeling of battery

The R_{INT} model is used as the mathematical model for the battery which simplifies the battery as an ideal voltage source with resistance[21]. Usually, the current and voltage of a battery can be expressed by eq. (2.12). The parameters of the R_{INT} model are affected by the state of charge and charge/discharge current as shown in eq. (2.13) and eq. (2.14).

$$U = U_t - R_{INT} I \tag{2.12}$$

$$R_{INT} = \begin{cases} R_{dis} = f_1(SOC, I), I \geq 0 \\ R_{chg} = f_2(SOC, I), I < 0 \end{cases} \tag{2.13}$$

$$SOC = SOC_0 - \int_0^t \eta I / Q dt \tag{2.14}$$

where U_t is open circuit voltage, R_{INT} is internal resistance, I is charge/discharge current, R_{chg} and R_{dis} are charged and discharge resistors respectively. SOC_0 is the state of charge at the last time. η is charge/discharge efficiency, Q is capacity.

2.2.5. Modeling of electrolyzer

The electrolyzer decomposes water into hydrogen and oxygen. The rate of hydrogen production is proportional to the current in the electrolytic circuit which is given by eq. (2.15)[13]:

$$n_h = \eta_F n_{c1} i_e / (2F) \tag{2.15}$$

The constant of Faraday efficiency is expressed by eq. (2.16).

$$\eta_F = 96.5 \exp(0.09 / i_e - 75.5 / i_e^2) \tag{2.16}$$

where n_h is the efficiency of hydrogen production, n_{c1} is the number of electrolyzer cells, i_e is the current of electrolyzer, F is Faraday constant.

2.2.6. Modeling of hydrogen tank

The hydrogen tank is a closed container which connects the fuel supply system of fuel cell and hydrogen output system of electrolyzer. According to Van der Waals equation, the expression of pressure in the hydrogen storage tank is given by eq. (2.17) [22]:

$$P_{sto} = \frac{(\int_{t_0}^{t_1}(n_{el} - n_{fc})dt + n_{sto})R_c K}{V_{sto} + n_{sto} b} - \frac{n^2 a}{V^2} \tag{2.17}$$

where n_{el} is the hydrogen production rate of electrolyzer, n_{fc} is the hydrogen consumption rate of fuel cell, R_c is Avogadro constant, K is Kopen temperature, V_{sto} is the volume of hydrogen tank, n is the amount of hydrogen in the hydrogen storage tank, usually in mol. a is a phenomenological parameter for measuring intermolecular gravity, b is the volume contained in a single molecule itself. As for hydrogen, a is 0.02476Pa·m^6/mol, b is 2.661×10^{5}m^3/mol.

In order to reflect the storage level of hydrogen tank directly, the equivalent state of charge *SOHC* of hydrogen tank is defined in this chapter by eq. (2.18).

$$SOHC = P_{sto} / P_N \tag{2.18}$$

where P_N is the maximum pressure of hydrogen tank.

2.3. Hierarchical energy management method for DC microgrid

To facilitate coordinated control, this chapter divides the DC microgrid system into two layers, the bottom layer is the physical layer, which is composed of various micro sources and DC converters. The top layer is the global control layer. Through the reception and analysis of the information collected by the bottom layer, the top layer sends the instructions to each converter according to the overall analysis of the microgrid system, and the bottom layer responds to instructions and controls the working state of each power source. The structure diagram of the system is shown in Figure 2-2.

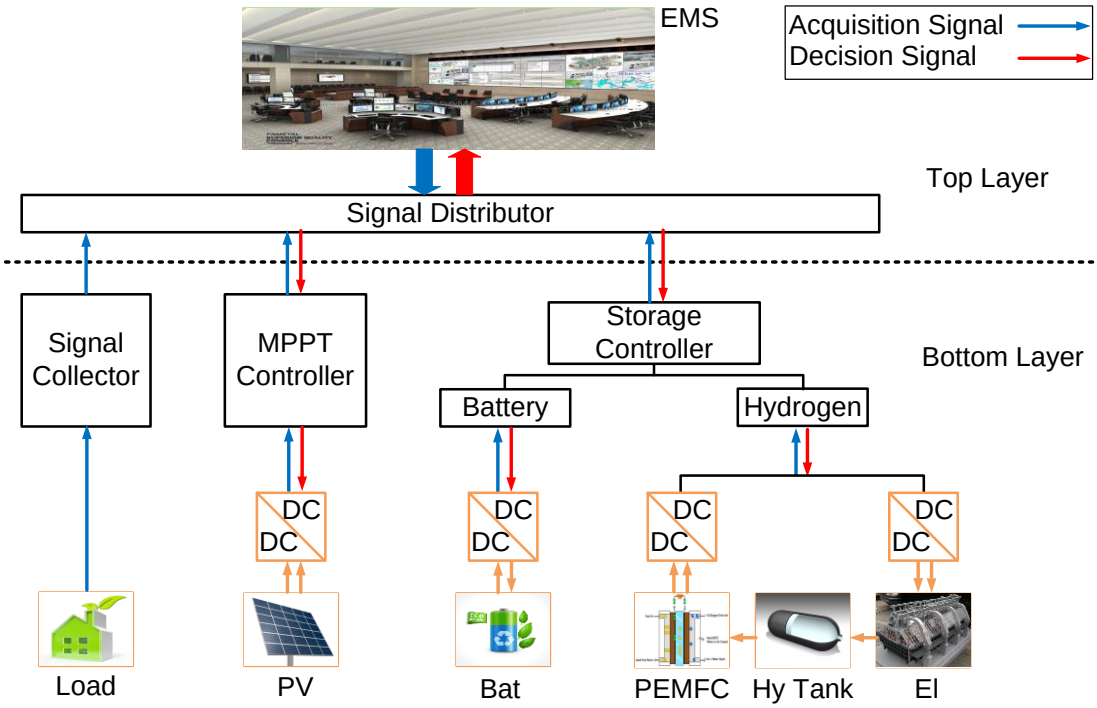

Figure 2- 2 Control structure of DC microgrid

2.3.1 Bottom layer control

The photovoltaic power generation system is composed of a photovoltaic array and a unidirectional DC/DC converter. In order to make the best use of solar energy, the maximum power point tracking control (MPPT) is used, and the control diagram of PV is shown in Figure 2-3. By the acquisition of the output voltage signal U_{pv} and the output current signal I_{pv}, the PV output power P_{pv} is calculated and compared with the power value at the last period of time. Finally, the comparison result is modulated as a duty cycle which will be input to the DC/DC converter as a control signal.

In the PEMFC generation system, the output power of the fuel cell is based on the power reference value Pfc given by the top layer. When the top layer calculates the value of reference power, this value will be transferred to the bottom layer. The reference current value I_{fcref} is the result of the elimination of P_{fc} which comes from the top layer and the U_{fc} which is collected from both ends of the fuel cell. Finally, the I_{fcref} and the measured current value I_{fc} will be sent to the PI controller, and the duty cycle produced by the PI controller will be transmitted to the DC/DC converter.

As for the electrolyzer system, the control is the same as the control of the fuel cell. The cell absorbs the bus power in the light of the power reference value P_{el} is given by the energy management system.

At the same time, considering the characteristics of PEMFC and electrolyzer, the change rate of power in the converter layer is limited. However, the battery generation system uses the droop control method to maintain the voltage stability of the DC bus. Therefore, the output power of the battery is controlled by a PI controller according to the reference value of the bus voltage and the reference voltage calculated by the droop controller.

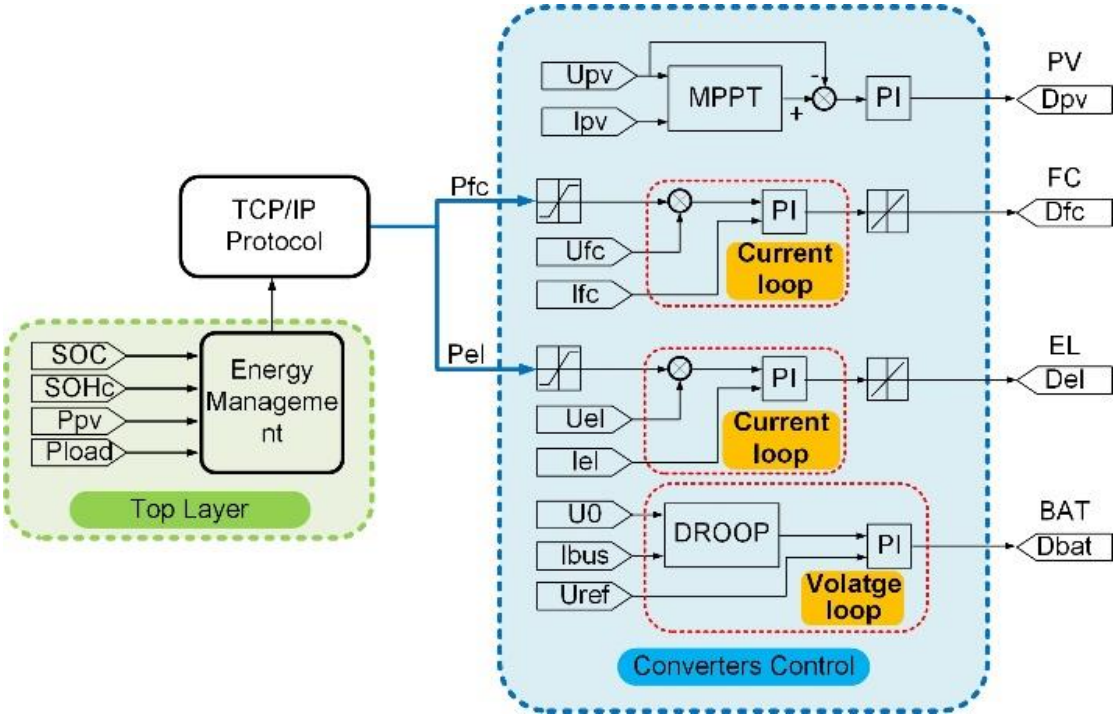

Figure 2- 3 Diagram of control system.

Figure 2-4 shows the validation results of the constructed model and the performance of upper-level control. As shown in Figure 2-4 (a), the photovoltaic control system can quickly achieve MPPT tracking control under changes in irradiance. For batteries, as shown in Figure 2-4 (b), the main objective of the battery is to maintain voltage stability in the system. When voltage fluctuates, it charges or discharges based on the current-voltage. For the fuel cell and electrolyzer, the power control is based on the PI controller after receiving the control signal from the upper-layer controller. Thus, the control strategy adopted has a good control effect on the lower layer, which can be used for further research on upper-layer control strategies.

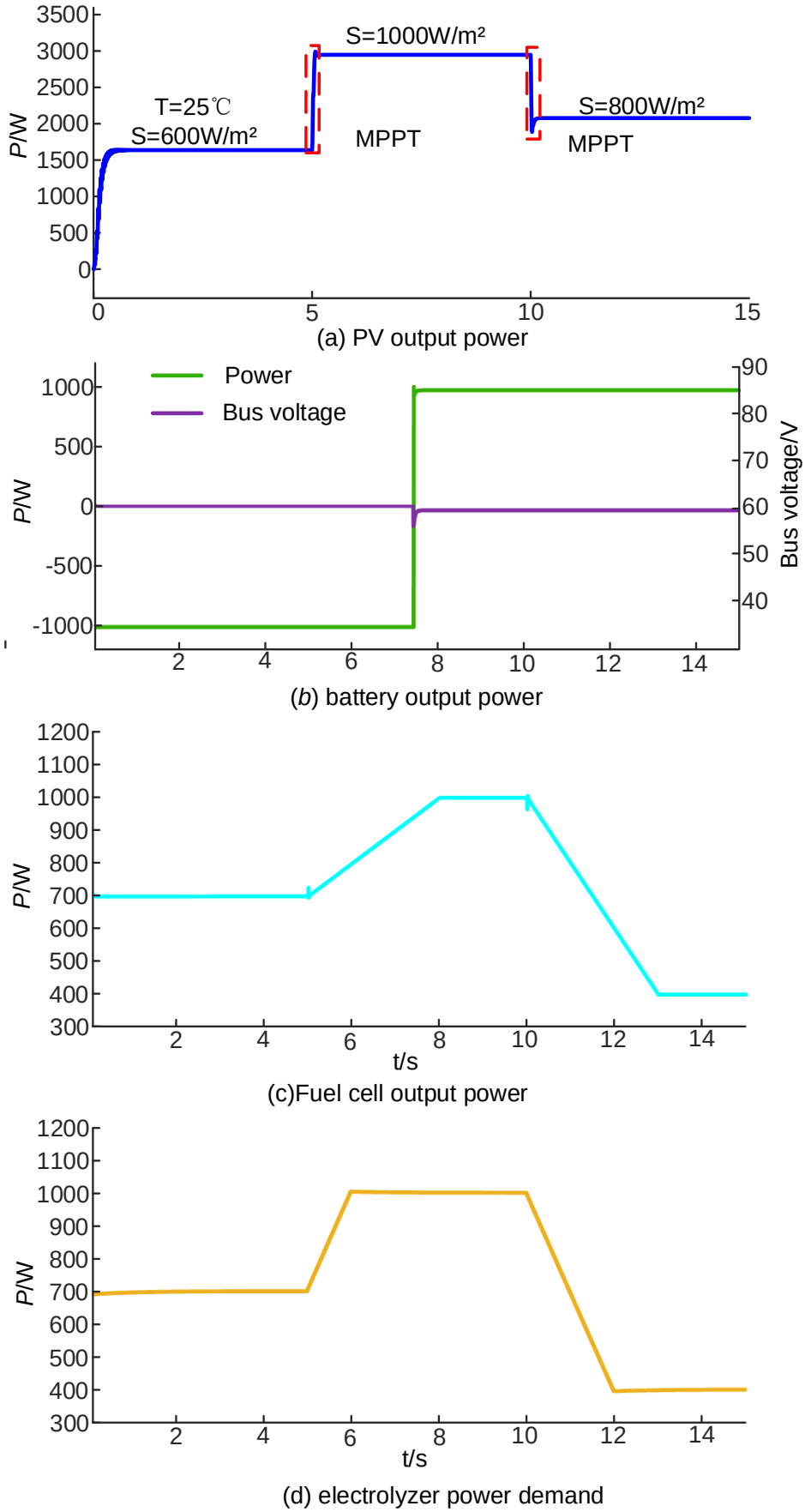

Figure 2- 4 Power curves of sources and load

2.3.2. Top layer control

1. Minimum utilization cost

In the island DC microgrid, PV always works in the maximum power point tracking mode. So, the hybrid energy storage system should assess the most convenient and lowest-cost way to store or release energy. More concretely, the energy management system will determine the output value and the working mode of each generation system separately when the energy storage system is needed to output or store the power. Since this model is an island microgrid, there is no hydrogen purchase cost, thus the utilization cost C of each storage device in eq. (2.19) is consist of the investment cost C_{inv} of each device and the operating and maintenance cost $C_{\text{o\&m}}$[18]:

$$C = \frac{1}{\eta}(C_{\text{inv}} / L + C_{\text{o\&m}}) \tag{2.19}$$

where L is the life of the storage device calculated by hours, η is the system efficiency.

Based on the eq. (2.19), the utilization cost of electric energy storage system can be expressed in eq. (2.20):

$$C_{\text{cycling\_bat}} = \frac{(C_{\text{B}} / L_{\text{bat}} + C_{\text{o\&m,b}})}{\eta_{\text{b,ch}}\eta_{\text{b,dis}}} \tag{2.20}$$

where $C_{\text{cycling\_bat}}$ is the cost during a single charging/discharging cycle, C_{B} is the investment cost of the battery, L_{bat} is the battery life, $\eta_{\text{b,ch}}$ is battery charging efficiency, $\eta_{\text{b,dis}}$ is battery discharging efficiency. $C_{\text{o\&m,b}}$ is the maintenance and operation cost of the battery.

As the battery life is usually given by the number of charge and discharge cycles than hours, so the number of charge and discharge cycles is converted into an hour unit life given by eq. (2.21).

$$L_{\text{bat}} = C_{\text{N}} N_{\text{bat,p}} U_{\text{DC}} N_{\text{cycles\_eq}} / P_{\text{bat}} \tag{2.21}$$

where U_{DC} is the voltage of the battery, $N_{\text{bat,p}}$ is the battery number, C_{N} is the rated capacity of the battery, $N_{\text{cycles\_eq}}$ is the charge and discharge cycle times, P_{bat} is the absolute value of the output power of the battery. By plugging eq. (2.21) into eq. (2.20), the eq. (2.22) shows the specific calculation method of the utilization cost of the battery.

$$C_{\text{cycling\_bat}} = \frac{1000PC_{\text{b}}}{C_{\text{N}} N_{\text{bat,p}} U_{\text{DC}} N_{\text{cycles\_eq}} \eta_{\text{b,ch}} \eta_{\text{b,dis}}} \tag{2.22}$$

For this island DC microgrid system, the main power source of the system is PV. In order to improve the overall energy utilization of the hybrid energy storage system, the charge and discharge efficiency should be taken into account when calculating the utilization cost of the battery, and because the battery has only two states (charge or discharge), then the upper formula can be divided into two parts. The first part calculates the cost during discharge mode, while the second part is responsible for the calculation during charge mode. By adding the two parts, the utilization cost of the battery can be calculated easily by eq. (2.23).

$$\begin{cases} C_{\text{cycling\_bat}} = C_{\text{dis\_bat}} + C_{\text{ch\_bat}} \\ C_{\text{dis\_bat}} = \dfrac{C_{\text{b}} / L_{\text{bat}} + C_{\text{o\&m,b}}}{\eta_{\text{b,ch}} \eta_{\text{b,dis}}} \\ C_{\text{ch\_bat}} = C_{\text{b}} / L_{\text{bat}} + C_{\text{o\&m,b}} \end{cases} \tag{2.23}$$

where $C_{\text{dis\_bat}}$ is the discharge cost, $C_{\text{ch\_bat}}$ is charging cost.

According to ref. [18], the cost of the hydrogen energy storage system is given by eq. (2.24).

$$C_{\text{cycling\_hy}} = \frac{C_{\text{el}} / L_{\text{el}} + C_{\text{o\&m,el}} + C_{\text{fc}} / L_{\text{fc}} + C_{\text{o\&m,fc}}}{\eta_{\text{el}} \eta_{\text{fc}}} \tag{2.24}$$

where C_{el} is the investment cost of the electrolyzer, C_{fc} is the investment cost of the fuel cell, $C_{\text{o\&m,el,}}$ and $C_{\text{o\&m,fc}}$ is the operation and maintenance cost of the electrolyzer and fuel cell respectively, η_{el} is the efficiency of the electrolyzer, η_{fc} is the efficiency of the fuel cell.

Because the fuel cell generation system and electrolyzer system are actually unrelated to each other, similarly, the cost of the hydrogen energy storage system can be simplified as follows:

$$\begin{cases} C_{\text{cycling\_hy}} = C_{\text{dis\_hy}} + C_{\text{ch\_hy}} \\ C_{\text{dis\_hy}} = \dfrac{C_{\text{fc}} / L_{\text{fc}} + C_{\text{o\&m,fc}}}{\eta_{\text{el}} \eta_{\text{fc}}} \\ C_{\text{ch\_hy}} = C_{\text{el}} / L_{\text{el}} + C_{\text{o\&m,el}} \end{cases} \tag{2.25}$$

where $C_{\text{dis\_hy}}$ is the utilization cost of the fuel cell, and the $C_{\text{ch\_hy}}$ is the cost of the electrolyzer.

The total cost of the hybrid storage system can be calculated by adding these four parts of the cost proposed above, which is given by eq. (2.26).

$$C_{sys} = \sum_{0}^{T} (C_{dis\_hy} + C_{ch\_hy} + C_{dis\_bat} + C_{ch\_bat}) \tag{2.26}$$

where C_{dis_hy}, C_{ch_hy}, C_{dis_bat}, and C_{ch_bat} are the utilization cost of each system under the time of t.

As shown in eq. (2.22), the cost of the battery is linearly related to its output power, while the cost of the hydrogen storage system is not changed within the rated power range in eq. (2.25). The relationship between the cost and power of the battery and the hydrogen energy system can be shown in the following diagram.

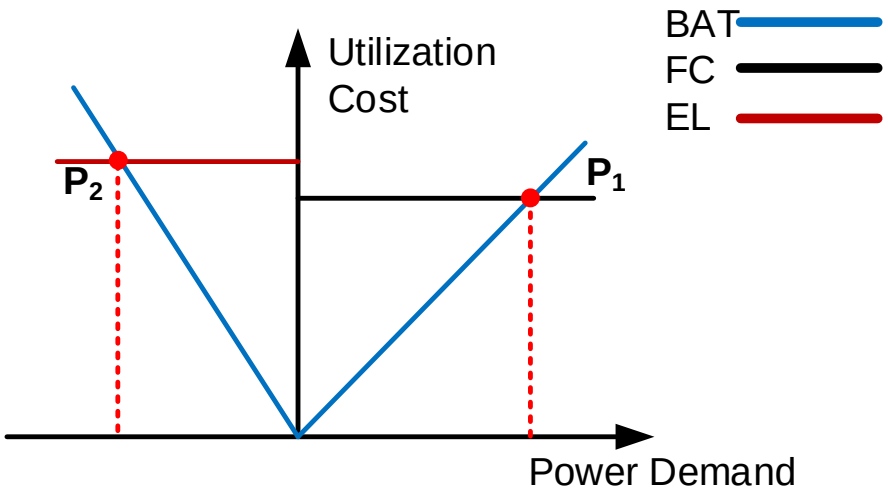

Figure 2- 5 Utilization cost of energy storage system.

Therefore, for a very small discrete time period σt, the overall demand power of the microgrid is determined. Under the condition of constant power, the power output and working mode of each energy storage system under this condition can be calculated according to Figure 2-5. Thus, the minimum utilization cost of the system can be obtained by adding the cost of the system work in each time period.

By calculating the difference value between the power demand of load and the power production of PV, the power reference value can be calculated. By comparing the reference value with the power value P1 and P2 at the intersection point as shown in Figure 2-5, the output power of each energy storage unit can be determined. The concrete calculation method is given by eq. (2.27).

$$\begin{cases} P_{\text{bat}} = P_{\text{ref}} & P_2 \le P_{\text{ref}} < P_1 \\ P_{\text{bat}} = 0 & P_1 \le P_{\text{ref}} < P_{\text{fcmax}} \\ P_{\text{bat}} = P_{\text{ref}} - P_{\text{hymax}} & P_{\text{ref}} \ge P_{\text{fcmax}} \\ P_{\text{bat}} = 0 & P_{\text{elmax}} \le P_{\text{ref}} \le P_2 \\ P_{\text{bat}} = P_{\text{ref}} - P_{\text{hymax}} & P_{\text{ref}} \le P_{\text{elmax}} \end{cases} \tag{2.27}$$

According to the calculated reference power of the battery, the reference power of the electrolyzer and fuel cell can be evaluated by the difference value between the total power demand and the reference power of the battery.

2. State Machine

Since the island DC microgrid is powered solely by renewable energy, PV should always operate at the maximum power point mode. Therefore, the output power of PV is a function of solar radiation and temperature. For a given load demand and photovoltaic output power, the purpose of the energy management system is to determine the best mode of operation of the storage devices (batteries, electrolyzer, fuel cells) so that the utilization cost of the energy storage system is the lowest. At the same time, in the island system, it is also essential to maintain the stability of *SOC* and *SOHC* which can ensure the stable operation of the system so that the energy storage system can not only provide enough storage capacity for the output power of the PV, but also prevent the shortage of energy effectively.

The state machine control method is a classical strategy for the energy management system [23,24]. In this chapter, a state machine control method is used to maintain the level of the energy storage system. However, because the typical state machine method based on *SOC* cannot effectively manage the island DC microgrid containing two kinds of energy storage systems, it is necessary to establish a multi-objective state machine based on the *SOC* and *SOHC*. Similarly, the working state of this state machine will be divided into 9 parts according to the level of *SOC* and *SOHC*. The working mode of the state machine is shown in Figure 2-6.

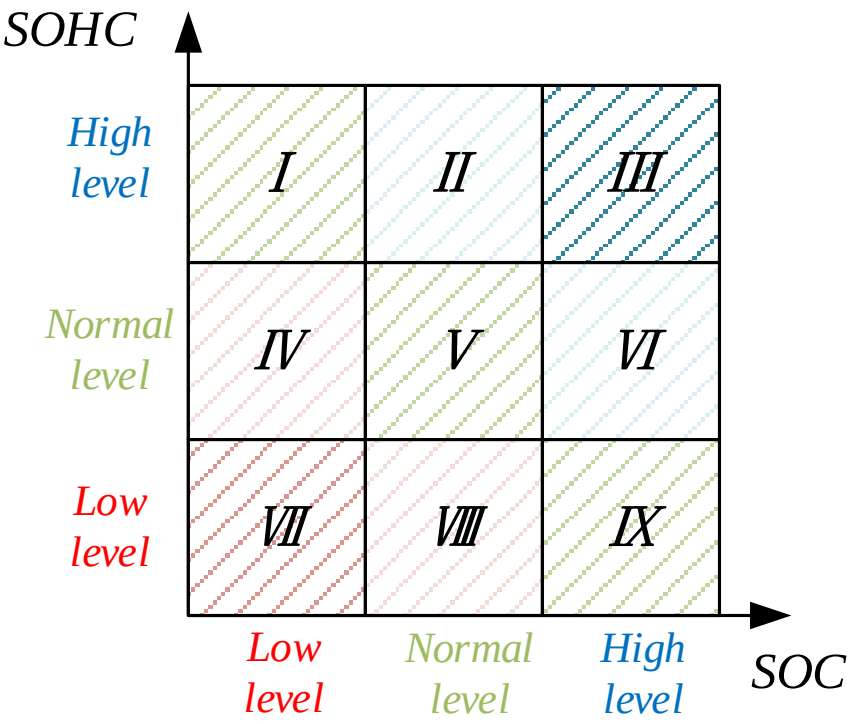

Figure 2- 6 Working state of the state machine.

Mode I: High *SOHC* level, low *SOC* level.

1. PV output is larger than the load demand.

In this case, the battery power is insufficient, so the excess power of the bus is transported to the battery.

PV output is less than the load demand.

In this case, as the *SOC* is lower than the normal limit, the fuel cell is responsible for the load demand power within the rated maximum output power.

Mode II: High *SOHC* level, normal *SOC* level.

PV output is greater than the load demand.

In this case, the battery can continue to charge, and the hydrogen storage tank is at a high level, so the excess power of the bus will be transported to the battery.

PV output is less than the load demand.

In this case, because the *SOHC* is at a high level, the fuel cell is responsible for the load demand power within the maximum output power.

Mode III: High level of *SOC* and *SOHC*.

The PV output is greater than the load demand.

In this case, both of the energy storage systems are at a high level, thus the battery and the electrolyzer continue to consume power. When the reserves are saturated, the PV is no longer working in MPPT mode, this situation should be avoided.

PV output is less than the load demand.

In this case, the battery takes all the electrical energy needs, and when it falls to the safety limit first, after the *SOC* is at normal level, the control mode will jump to other states.

Mode IV: Normal *SOHC* level, low *SOC* level.

In this mode, the working state is the same as the mode I

Mode V: Normal *SOHC* level, normal *SOC* level.

In this mode, the minimum utilization cost algorithm mentioned above is used to reduce the cost of the energy storage system.

Mode VI: Normal *SOHC* level, high *SOC* level.

PV output is greater than the load demand.

In this case, the battery stops working, and the electrolyzer begins to consume power from the DC bus.

PV output is less than the load demand.

In this case, because the *SOC* is higher, the battery provides power for the microgrid system.

Mode VII: Low *SOHC* and *SOC* level.

PV output is greater than the load demand.

In this case, the storage level of both devices is low, at this time the battery is charged to the normal level first.

PV output is less than the load demand.

In this case, the discharge of hydrogen under the low pressure of the hydrogen storage tank has a smaller impact on the system performance, so the fuel cell bears the power output first.

Mode VIII: Low *SOHC* level, normal *SOC* level.

PV output is greater than the load demand.

In this case, the level of *SOHC* is low, the battery will not work at this time, and the extra power will flow to the electrolyzer.

PV output is less than the load demand.

In this case, the battery will output all the power required by the system, and the fuel cell will not work.

Mode IX: Low *SOHC* level, high *SOC* level.

In this mode, the working state is the same as the mode VIII.

Combining the above two methods, the schematic diagram of the state machine energy management method based on the minimum utilization cost proposed in this chapter is as follows. Therefore, the flexible and coordinated control of the microgrid is achieved by the minimum utilization cost control system based on the state machine at the top layer and the control system of the devices at the bottom layer.

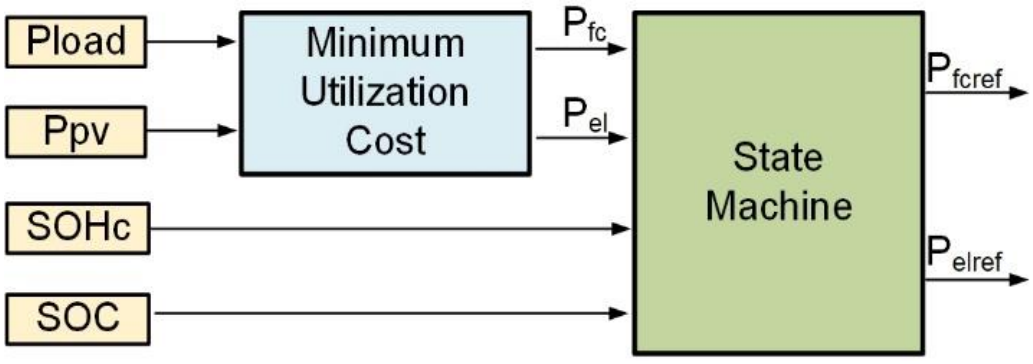

Fig. 2- 7 Top layer control.

2.4. Experimental validation and results

2.4.1. Experimental platform and parameter setting

In order to verify the effectiveness of the proposed energy management method, the simulation is carried out by using the RT-LAB hardware in the loop real-time simulation platform. The experimental platform is shown in the following diagram. The simulation platform is OP5600HIL Box with a running speed of 3.3GHz. In this experiment, the running step is 0.1 ms and the simulation time is 72 hours. The real-time simulation is given in Figure 2-8.

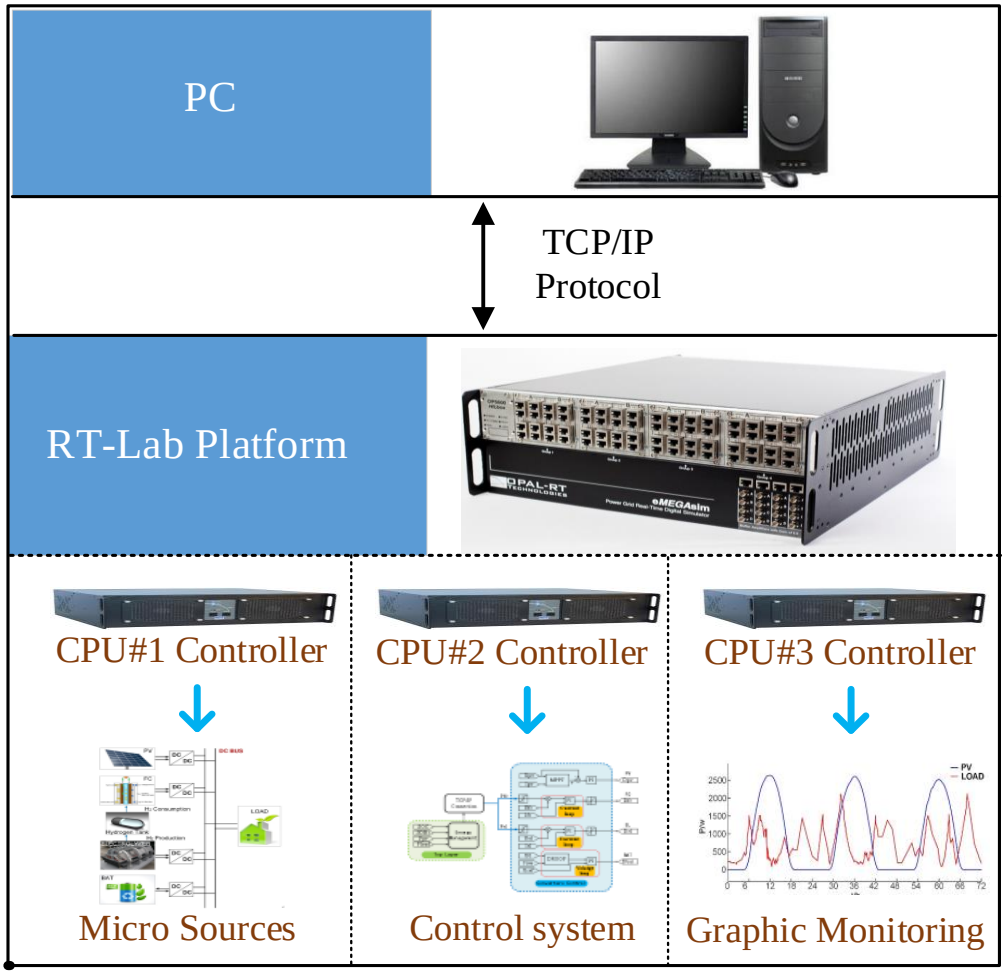

Figure 2- 8 RT-LAB real-time simulation platform for hardware in the loop.

The investment cost of the battery, fuel cell, and electrolyzer used in this chapter is shown in Table 2-1 according to ref [25]:

Table 2- 1 Cost and life time of storage devices.

Component	Cost($)	Life	CO&M
Battery	440$/kwh	1500cycles	0.5%

Fuel Cell	3721$/kw	30000h
Electrolyzer	4694$/kw	30000h

The specific parameters of the battery, fuel cell, hydrogen tank, and electrolyzer are given in Table 2-2:

Table 2- 2 Component parameters.

Subsystems	Descriptions	Values
Battery	capacity	600Ah
	rated voltage	35V
	initial SOC	60%
	number of cells	42
Fuel Cell	maximum power	1000W
	rated voltage	23-25V
	maximum pressure	35MPa
Hydrogen Tank	volume	24L
	initial SOHC	57%
Electrolyzer	maximum power	1000W
Bus	rated voltage	60V

The temperature and solar radiation parameters of the PV are derived from the measured data of the photovoltaic power station in the Saint Louis campus of the University of Queensland, Australia. The demand of load is obtained according to ref [15]. The output power of PV and load are given in Figure 2-9.

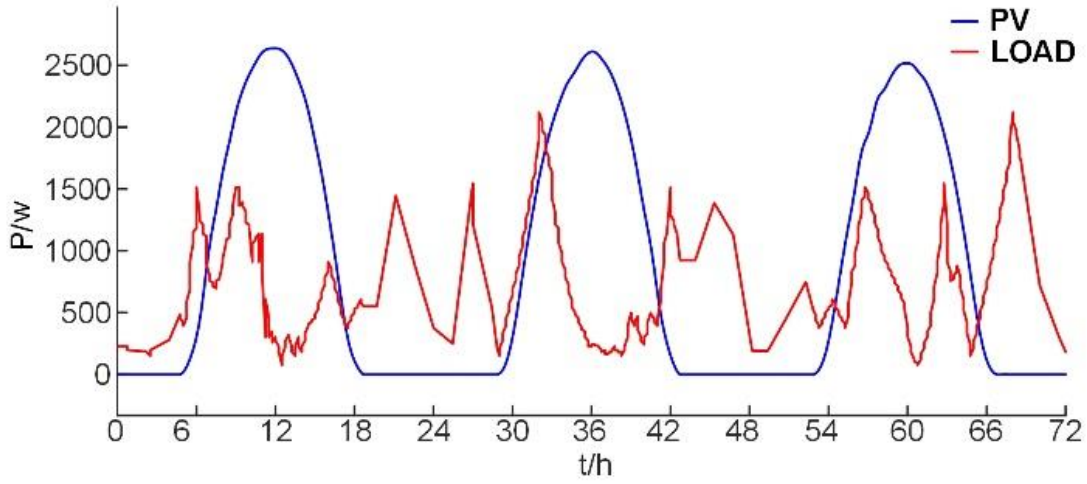

Figure 2- 9 Curve of load and photovoltaic power.

2.4.2 Comparative analysis

The simulation results are shown in Figure 2-10.

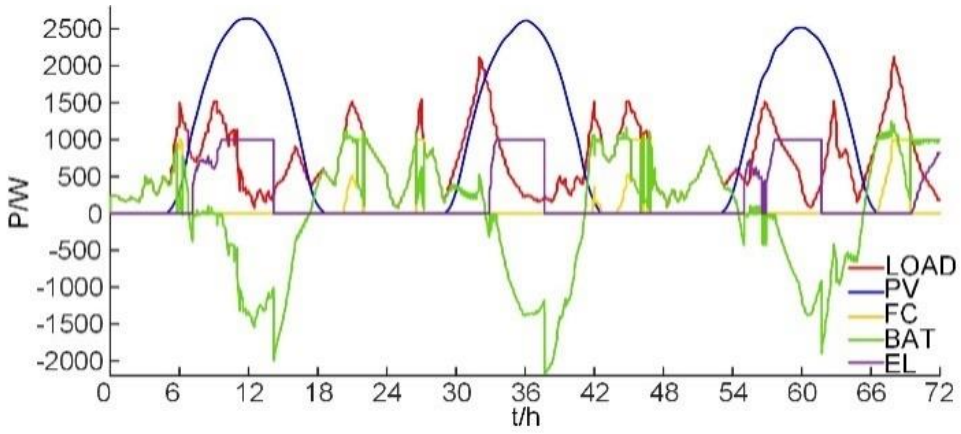

Figure. 2- 10 Power curve of system.

The change in SOC and SOHC is shown in Figure 2-11:

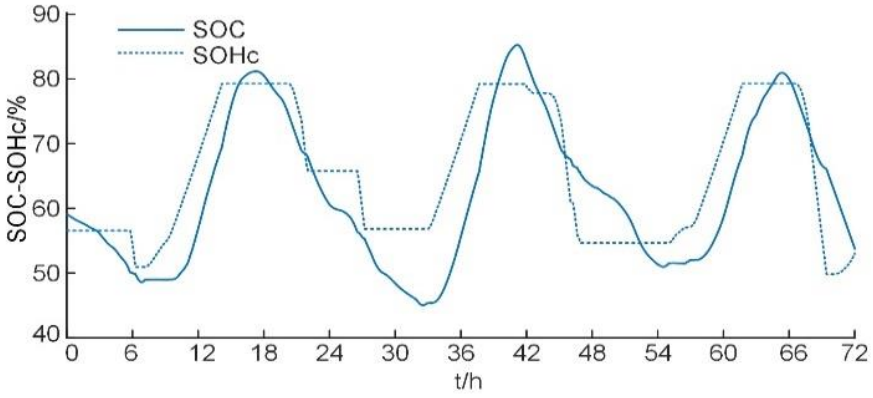

Figure 2- 11 State of the energy storage system.

The simulation results show that the energy management system can effectively allocate power for each energy storage system. When the output of the PV is larger than the load demand, the energy storage system starts to store energy, and the system distributes the redundant power based on the energy management method; when the output is not sufficient to maintain the load demand, the energy storage system output power on the basis of its own energy storage status and utilization cost. At the same time, the power output and input of the bottom layer are limited to the instantaneous change rate of the power of the fuel cell and the electrolyzer, and the output of the battery is more flexible, which accords with its operating characteristics.

In this chapter, the normal range of SOC and SOHC are both set between 50% to 80%. As shown in Figure 2-9, the island DC microgrid usually worked at mode V, which reduced the utilization cost of the energy storage system. However, at times, the level of the storage system is not at the normal level,

thus the state machine worked at the other 8 modes. At t=12h, 36h, and 70h, the SOHC is at a high level, so the state machine worked in mode II, when the SOC is at a high level, the energy management system jumped to mode III immediately. At t=69h, the SOHC is low, the battery provides extra energy for the hydrogen storage system until the SOHC is restored to normal level.

Although there is no unified assessment and comparison standard for each microgrid energy management method, some indicators can be introduced to show the advantages and disadvantages of each control method, which will help to evaluate the energy management method further. The definition of such indicators is closely related to energy, economic benefits, and the working conditions of the microgrid. The comparison of results based on each cycle can reflect the performance of the energy management system. In this chapter, the energy management strategies described above, more specifically minimum utilization cost and state machine methods are compared in terms of their utilization cost, SOC, SOHC, and the average efficiency of the hydrogen storage system. In the microgrid with only an electric energy storage system, in order to ensure the stability of the energy storage system, the capacity of the battery is adjusted to 1200Ah. The results are shown in Figure 2-12. The results of the specific index are shown in Table 2-3.

Table 2- 3 Comparison results of each method.

Method	Cost/$	SOC (Initial/Final)	SOHC (Initial/Final)	Efficiency of Hydrogen system
Minimum cost	21.58	60%/55.4%	57%/54.9%	53.55%
State Machine	23.81	60%/55.51	57%/37.8%	49.3%
Electric Storage	26.57	60%/64.83%	-	-

The experimental results show that the state machine method cannot maintain the energy storage level of the system normally. After the experiment, the SOHC becomes lower and cannot guarantee the operation of the microgrid. The state machine method will force the hydrogen energy storage system to provide extra power to maintain the value of SOC, thus reducing the efficiency of the hydrogen system and leading the value of SOHC to a lower level. More importantly, this strategy also produces a higher cost. As for the microgrid with only an electric energy storage system, the cost is the highest, but its SOC rises obviously. Compared with the state machine-only method and the battery-only method, the

cost of the proposed method is reduced by 10.3% and 23.2% respectively. The level of energy storage system is more stable, the final value of SOC is 55.4%, and the final value of SOHC is 54.9%, which is consistent with the initial value of the system. Furthermore, the utilization efficiency of the hydrogen storage system is the highest, which is 53.55%.

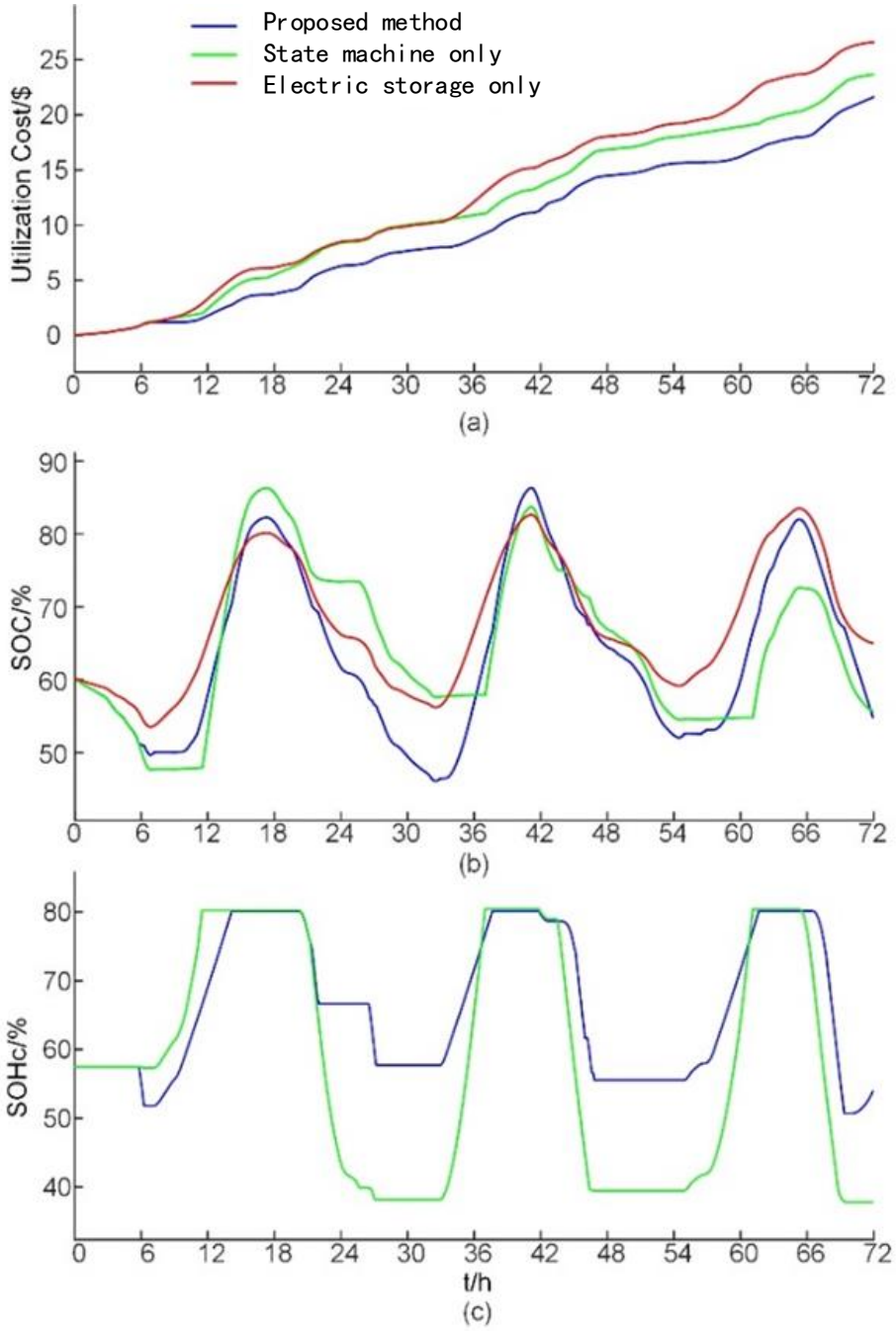

Fig. 2- 12 System index comparison curve.

Compared to the electric energy storage system, the energy efficiency of the microgrid is lower generally, but the coordination of the two energy storage systems greatly reduces the utilization cost. Moreover,

the microgrid that only contains an electric energy storage system cannot adjust the status of the energy storage system effectively. The change of SOC is fully constrained by the working condition of load and PV. In the long run, the SOC will be in a more extreme state, which affects the stable operation of the microgrid. Therefore, compared with the electric energy storage microgrid, the island microgrid with a hybrid energy storage system is more economical to operate, and also increases the reliability of the system.

2.5 Chapter summary

In this chapter, a DC microgrid with PV, fuel cell, battery, electrolyzer, and hydrogen tank is obtained, and a hierarchical state machine energy management control based on the minimum utilization cost is proposed. In this method, the cost of the energy storage system is reduced. At the same time, the energy storage level is maintained by adding the state machine control strategy.

The proposed control method is divided into two layers. At the bottom layer, the control of each device is realized separately, and the data from each power system is sent to the top layer which greatly assists the top layer control system. As for the top layer, by analyzing data collected by the bottom layer, this layer can obtain the best working mode for each power system. By the coordination work of two control layers, the power of the electric-hydrogen energy storage system is allocated reasonably in the case of the surplus and absence of the power of the microgrid, which realizes the optimal control of the cost and the energy storage level of the system. The energy management method proposed in this chapter is verified by the RT-LAB online real-time operation platform. The results show that the utilization cost of the system is much less than the traditional energy management method, and the level of the energy storage system is more stable. The reserves are always guaranteed at the expected level and the efficiency of the hydrogen storage system is high. It is of great significance to the economic and stable operation of the DC microgrid system.

References

[1] Rezaei M, Mohseni M. A predictive control based on neural network for dynamic model of proton exchange membrane fuel cell. Journal of Fuel Cell Science and Technology,2013,10(3):035001.

[2] Agbossou K, Kolhe M, Hamelin J, Bose TK. Performance of a stand-alone renewable energy system based on energy storage as hydrogen. IEEE Trans Energy Convers,2004, 19(3): 633-640

[3] Mehrpooya M. Dynamic modeling of a hybrid Photovoltaic system with hydrogen/air PEM fuel cell. Iranica Journal of Energy & Environment, 2013, 4(2):4-9.

[4] Katiraei F, Iravani MR. Power management strategies for a microgrid with multiple distributed generation units. IEEE Trans Power Syst 2006;21(4):1821-31.

[5] Uzunoglu M, Onar O, Alam M. Modeling, control and simulation of a PV/FC/UC based hybrid power generation system for standalone applications. Renew Energy,2009,34(3): 920.

[6] Nejabatkhah F, Li Y. Overview of power management strategies of hybrid AC/DC microgrid. IEEE Trans Power Electron 2014;30(12):7072-89.

[7] Azib T, Hemsas KE, Larouci C. Energy management and control strategy of hybrid energy storage system for fuel cell power sources. Int Rev Model Simulations (IREMOS) 2014;7(6):935. http://dx.doi.org/10.15866/iremos.v7i6.4620.

[8] Kraa O, Ghodbane H, Saadi R, Ayad M, Becherif M, Aboubou A. Energy management of fuel cell/ Supercapacitor hybrid source based on linear and sliding mode control. Energy Procedia,2015,74(12):58-64.

[9] Rekioua D, Bensmail S, Bettar N. Development of hybrid photovoltaic-fuel cell system for stand-alone application. International Journal of Hydrogen Energy,2014,39(3):4-11.

[10] Nelson DB, Nehrir MH, Wang C. Unit sizing and cost analysis of stand-alone hybrid wind/PV/fuel cell power generation systems. Renew Energy 2006; 31(10):1641-56.

[11] Beccali M, Brunone S, P Finocchiaro. Method for size optimization of large wind–hydrogen systems with high penetration on power grids. Applied Energy, 2013, 102(2): 534-544

[12] Han Y, Chen WR, Li Q. Energy management strategy based on multiple operating states for a photovoltaic/fuel cell/ energy storage DC microgrid. Energies 2017;10(1):136.

[13] Ipsakis D, Voutetakis S, Panos S, Stergiopoulos F, Elmasides C. Power management strategies for a stand-alone power system using renewable energy sources and hydrogen storage. International Journal of Hydrogen Energy,2009,34(16):7081–7095.

[14] Nasri S, Slama B S, Adnane C. Power management strategy for hybrid autonomous power system using hydrogen storage. International Journal of Hydrogen Energy,2016,41(2):857-865.

[15] Nasri S, Slama B, Yahyaoui I, Zafar B, Cherif A. Autonomous hybrid system and coordinated intelligent management approach in power system operation and control using hydrogen storage. International Journal of Hydrogen Energy,2017,42(15):9511-9523.

[16] Inam U, Wang P.Cost-based droop scheme for dc microgrid Energy Conversion Congress & Exposition , 2014 :765-769

[17] Marchenko O, Solomin S. Modeling of hydrogen and electrical energy storages in wind/PV energy system o237n the Lake Baikal coast. International Journal of Hydrogen Energy,2017,42(15):9361-9370.

[18] Rodolfo D L, Jose L, Bernal-Agustin, Javier C. Optimization of control strategies for stand-alone renewable energy systems with hydrogen storage. Renewable Energy, 2007,32(7):1102-11.

[19] Krismadinata, R, Ping H, Selvaraj J. Photovoltaic module modeling using Simulink/Matlab. Procedia Environ Sci 2013;17:537e46. http://dx.doi.org/10.1016/j.proenv.2013.02.069.

[20] HAN Y, LI Q, WANG T, CHEN W, MA L. Multisource coordination energy management strategy based on soc consensus for a PEMFC–Battery–Supercapacitor hybrid tramway. IEEE Transactions on Vehicular Technology, 2018, 67(1):296-305.

[21] Li X, Xu L, Hua J, Lin X, Li J, OuyangM. Power management strategy for vehicular-applied hybrid fuel cell/battery power system. Journal of Power Sources 2009,191(2):542-549.

[22] Lajnef T, Abid S, Ammous A. Modeling, control, and simulation of a solar hydrogen/fuel cell hybrid energy system for grid-connected applications. Advances in Power Electronics, 2013,(4):1-9.

[23] Wang J, ZHAO CH, Pratt A, Baggu M. Design of an advanced energy management system for microgrid control using a state machine. Applied Energy 2009,228(15):2407-21.

[24] Han Y et al. Two-level energy management strategy for PV-fuel cell-battery-based DC microgrid International Journal of Hydrogen Energy 2018, https://doi.org/10.1016/j.ijhydene.2018.04.013

[25] Zhang Yang, Anders L, Pietro E, Yan J. Comparative study of battery storage and hydrogen storage to increase photovoltaic self-sufficiency in a residential building of Sweden. Energy Procedia,2016, 103:268-273.

Chapter 3. Two-stage Scheduling for Island CPHH-IES

3.1. Introduction

With the continuous development of distributed energy technology, microgrids have gradually evolved into integrated energy systems that not only provide reliable power, but also can guarantee heat, travel, and other needs for users [1,2]. The emergence of IES further improves the utilization efficiency of various micro sources (MS) [3], and encourages scholars to work on the sizing, and scheduling of IES with heat, electricity, and gas supply [4]. IES includes various kinds of energy production, conversion, storage, and consumption devices, hence reasonable scheduling can reduce the operation cost and improve system efficiency.

The scheduling of IES mainly includes prediction, day-ahead optimal scheduling, and real-time optimization. Prediction is the basis of scheduling. For different optimization requirements, the long-term prediction method for day-ahead scheduling [5,6] and the short-term prediction method for dynamic real-time scheduling are used separately [7,8].

For the scheduling of IES, scholars have carried out in-depth research considering different objects and scenarios [9,10]. Considering the energy flow and access of EVs, two-stage scheduling realizes the economic operation of office buildings [11]. In view of the economy, reliability, and demand under the liberalization of the electricity market, a scheduling method combined with day-ahead scheduling and MPC is implemented to provide a general scheduling mode for IES [12]. Considering the waste of renewable energy, the construction of boiler and heat storage systems in wind power plants has become a solution. By establishing a multi-intelligent model, the difficulty of scheduling is reduced [13]. According to the required hot water and expected building temperature, the IES building architecture equipped with smart meters and controllable power load is proposed. Based on the information provided by such smart meters, intelligent control methods considering the uncertainty of load and temperature are applied to this architecture [14]. The uncertainty of the electricity market brings some difficulties to the economy dispatching of IES. Therefore, a robust optimization method considering the degree of price deviation is proposed, which avoids the higher cost under the influence of uncertainty [15].

After day-ahead scheduling, MPC can dynamically adjust according to the optimal results [11, 16, 17]. In order to minimize the negative impact caused by the prediction error, a hybrid MPC algorithm

combining time series analysis and Kalman filter is proposed [18]. By establishing the information sharing model and distributed model predictive control method based on double decomposition and sub-gradient iteration, the IES architecture embedded in distributed generation for home is built and the proposed control method is realized [19]. For the intelligent residence, the model predictive control method is used to combine the prediction with the latest information, and the two-way communication infrastructure in the intelligent residence is used to realize the limited layer scheduling optimization of the residential group [20].

At the same time, the wide application of hydrogen energy makes fuel cells and electrolyzer system become important parts of IES [21]. Scholars have studied the combining heat and power (CHP) model of fuel cell system [22]. By building the economic model, the influence of hydrogen production and heat recovery is discussed. A scheduling method that uses random scenarios to deal with system uncertainty is applied to the proton exchange membrane fuel cell power plant (PEMFCPP) [23]. For large-scale IES with fuel cell power generation system, an energy management model based on a stochastic MPC framework is proposed [24]. The energy management reduces the influences of uncertainty. Considering the minimization of cost and emission, the operation of a grid-connected CHP microgrid is realized by a multi-objective optimal thermal power scheduling method [25]. At the same time, by establishing an accurate model, the heat production of the electrolyzer is analyzed in detail, and the heat recovery system based on the electrolyzer is applied to the active distribution networks (ADN) and IES scheduling [26].

In addition, the intervention of DR and new energy vehicles makes the scheduling of IES more flexible and economic [11,25,27]. However, the scheduling of new energy vehicles mostly focuses on the scenario of a charging station or parking lot and ignores the overall situation of IES [28].

Up to now, the heat supply of fuel cell and electrolyzer has been studied separately. On the one hand, the research on the heat supply of fuel cell is mainly focused on large-scale applications such as fuel cell power plants. The flexibility of the system is low, and a natural gas supply is needed. On the other hand, the research on thermal-electric coupling of electrolyzer is rare, which aims to optimize the system node voltage as a large-scale load. However, it lacks the specific use of hydrogen production. In addition, most research focuses on the establishment of the thermal-electric coupling model and the optimization methods are relatively simple. Generally, only the day-ahead optimization is considered with a few kinds of energy devices.

For most of the area in France, renewable energy sources are rich, which can provide an adequate energy supply for renewable energy power generation devices such as photovoltaic and wind turbines. The temperature difference between day and night is large, hence the energy system should provide a lot of heat with a long supply time. Considering the energy supply and climate conditions of this kind of area, it is not suitable to use electrolyzers or fuel cell for heat energy supply alone. Moreover, the efficiency of traditional CHP devices such as gas turbines will be significantly reduced even if there is a reliable gas supply. Therefore, it is necessary to build a suitable IES to meet the demand of residents. Considering the advantages of thermal-electric coupling of fuel cell and electrolyzer, an island IES with CPHH is built in this chapter. The optimal power scheduling and real-time operation of IES in small island residential areas with EVs and hydrogen vehicles (HVs) is studied. In the day-ahead optimization, after the prediction of the output power of RESs and temperature, mixed integer linear programming (MILP) is used to achieve the optimal scheduling. As for real-time operation, MPC is carried out by using mixed integer quadratic programming (MIQP).

Compared with other methods mentioned above, the fuel cell and electrolyzer are integrated into IES as a CPHH system for the first time. The system enables IES to meet the needs of residents for electricity, heat, and hydrogen supply. Secondly, the EVs are added to the dispatching as special DR loads. Finally, the coordinated operation of IES is realized through the two-stage scheduling method. By establishing comparisons, the advantages of the method and IES structure in this chapter are verified.

In this chapter, an IES combined with a power-hydrogen-heat supply is established, and the electric-hydrogen-heat relations of the fuel cell and electrolyzer are considered in detail. Then, to solve the scheduling problem of the CPHH-IES with access to new energy vehicles, a two-stage scheduling method is provided. In this method, the upper stage is to solve the day-ahead operation problem of the IES, while the lower stage is to realize the intra-day operation of the system. Finally, the economy and efficiency of IES without CPHH system are discussed and analyzed by the case study.

3.2. Structure and modeling OF IES

3.2.1. Structure of IES

The IES proposed in this chapter includes a photovoltaic (PV) system, wind turbines (WT), electric boiler (EB), electric storage system (ESS), a thermal energy storage (TES) system, fuel cell, hydrogen

tank and electrolyzer. These power generation and consumption systems are connected to the power bus, and thermal devices are connected to the heat bus. Loads of IES are electric load, thermal load, EVs, and HVs. The structure of IES is shown in Figure 3-1.

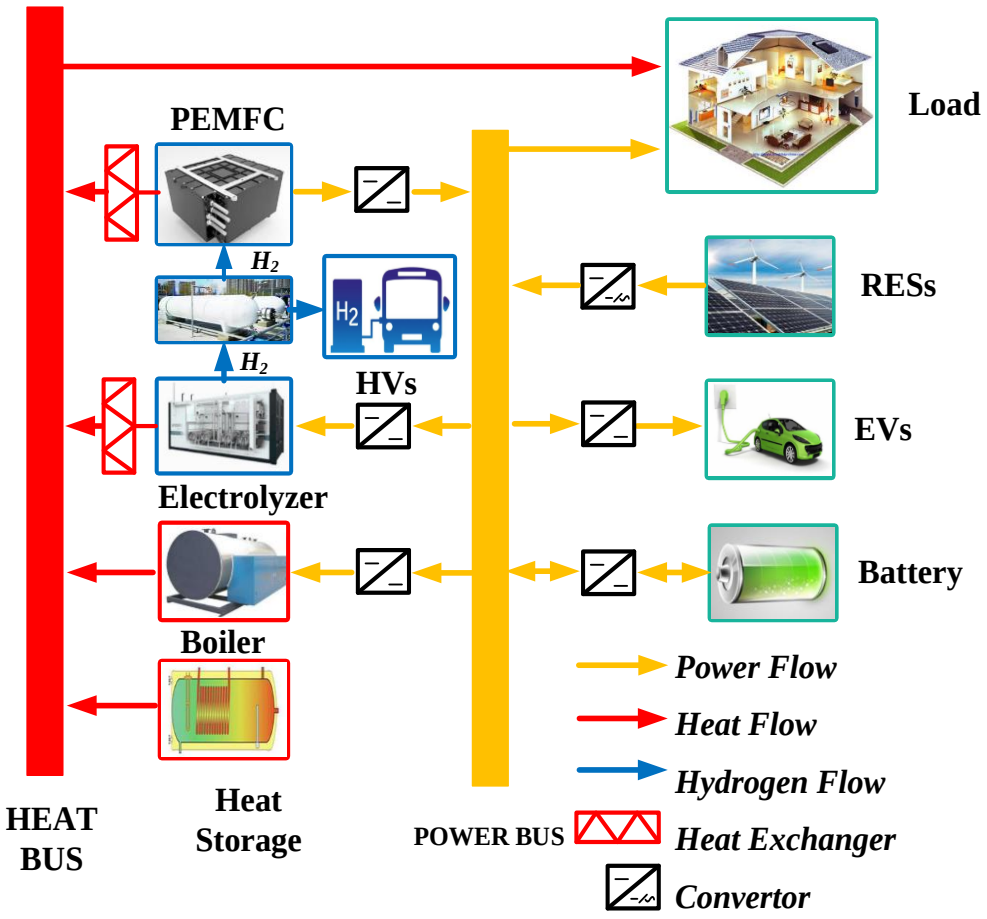

Figure 3- 1 Topology of IES

In Chapter 2, the detailed modeling of fuel cell, electrolyzer, PV and battery has been discussed by using Matlab/Simulink. However, those nonlinear models are applied for the accurate control of the system, which is not suitable for the optimal scheduling and operation of the IES on a larger time scale. Thus, the rest of the section is to provide suitable modeling methods for PV, WT, EB, ESS, TES, CHPP, and also the heat demands of residential areas.

3.2.2. CPHH

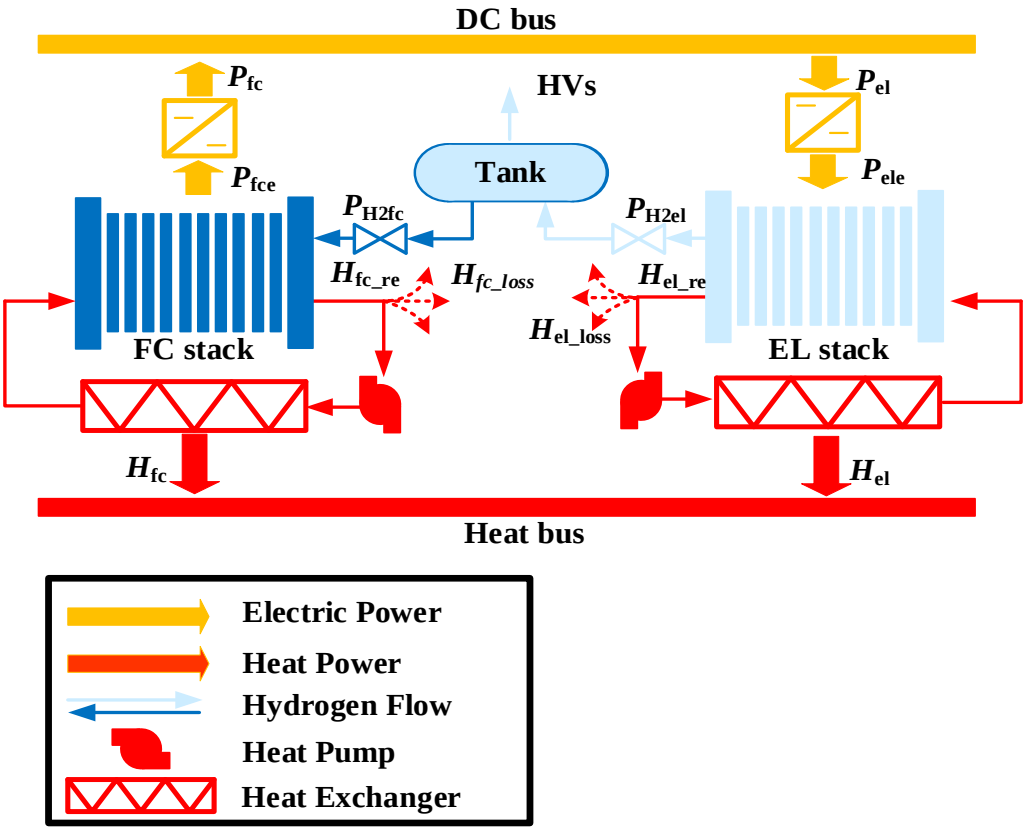

Figure 3- 2 CPHH system

Since hydrogen has been widely concerned as high efficiency and environment friendly fuel, the heat recovery technology has become an effective solution to improve the efficiency of hydrogen system. According to the CPHH system described above, hydrogen is produced directly by the electrolyzer, hence the heat of the CPHH system mainly comes from the electrolyzer and fuel cell stack. The structure of CPHH is shown in Figure 3-2.

The voltage and efficiency of the fuel cell are written as [23]:

$$\begin{cases} V_{\text{fc\_cell}} = E_{\text{Nernst}} - V_{\text{act\_fc}} - V_{\text{ohm\_fc}} - V_{\text{con\_fc}} \\ \eta_{\text{fc}} = \dfrac{\int_t P_{\text{cell}}}{E} \times 100\% \end{cases} \tag{3.1}$$

where $V_{\text{fc\_cell}}$ is the cell voltage of PEMFC, E_{Nerst} is the thermodynamic electromotive force, $V_{\text{act\_fc}}$ is the activation overvoltage, $V_{\text{ohm\_fc}}$ is the ohmic overvoltage and $V_{\text{con\_fc}}$ is the concentration overvoltage, η_{fc} is the efficiency of PEMFC, P_{cell} is the output power, E is the energy of the consumped hydrogen.

As shown in Figure 3-2, the power obtained from hydrogen is P_{H2fc}, and the power generated by PEMFC is P_{fce}. The energy flow of the fuel cell system can be expressed as follows:

$$P_{\mathrm{H2fc}} = P_{\mathrm{fce}} + H_{\mathrm{fc\_re}} \tag{3.2}$$

$$\begin{cases} P_{\mathrm{fce}} = \eta_{\mathrm{fc}} P_{\mathrm{H2fc}} \\ H_{\mathrm{fc\_re}} = (1-\eta_{\mathrm{fc}}) P_{\mathrm{H2fc}} = H_{\mathrm{loss}} + H_{\mathrm{fc}} / \eta_{\mathrm{fc\_h}} \end{cases} \tag{3.3}$$

where $H_{\mathrm{fc\_re}}$ is the heat released by the stack, $\eta_{\mathrm{fc\_h}}$ is the heat exchanger efficiency, H_{loss} is the heat loss of the stack. The thermal output from the fuel cell to the heat pipe can be simplified as follows:

$$H_{\mathrm{fc}} = k_{\mathrm{fc\text{-}h}} H_{\mathrm{fc\_re}} \tag{3.4}$$

where $k_{\mathrm{fc\text{-}h}}$ is the heat transfer coefficient.

By the above equations, the hydrogen consumption and heat-electric ratio of the fuel cell can by written as:

$$n_{\mathrm{fc}} = \frac{P_{\mathrm{fc}}}{\eta_{\mathrm{con}} \eta_{\mathrm{fc}} LHV_{\mathrm{H}}} \tag{3.5}$$

$$H_{\mathrm{fc}} = r_{\mathrm{te}} \eta_{\mathrm{fc\_h}} P_{\mathrm{fc}} / \eta_{\mathrm{con}} \tag{3.6}$$

where n_{fc} is the hydrogen production in mol/s, LHV_{h} is the lower heating value of hydrogen in J/kg, here the value is 1.20×10^{8} in J/kg, r_{te} is the fitting parameter of power to heat ratio.
r_{te} and η_{fc} can be calculated by:

$$r_{\mathrm{te}}(t) = f_{\mathrm{te}}(PLR) = \begin{cases} \gamma_0 & 0 \le PLR(t) \le 0.05 \\ \gamma_1 \cdot PLR^4 + \gamma_2 \cdot PLR^3 + \gamma_3 \cdot PLR^2 + \gamma_4 \cdot PLR + \gamma_5 & 0.05 < PLR(t) \le 1 \end{cases} \tag{3.7}$$

$$\eta_{\mathrm{fc}}(\mathrm{t}) = f_{\mathrm{fc}}(PLR) = \begin{cases} \zeta_0 & 0 \le PLR(t) \le 0.05 \\ \zeta_1 \cdot PLR^5 + \zeta_2 \cdot PLR^4 + \zeta_3 \cdot PLR^3 + \zeta_4 \cdot PLR^2 + \zeta_5 \cdot PLR + \zeta_6 & 0.05 < PLR(t) \le 1 \end{cases} \tag{3.8}$$

$$PLR = P_{\mathrm{fc}} / \mathrm{Cap}_{\mathrm{fc}} \tag{3.9}$$

where PLR is the ratio of the current output power and the capacity. γ_0-γ_5 and ζ_0-ζ_6 are constants, Cap_{fc} is the capacity of the fuel cell. And the recommended value of γ_0-γ_5 and ζ_0-ζ_6 are shown in the table below.

Table 3- 1 Value of constants

Constants	0	1	2	3	4	5	6
γ	0.6801	1.0758	-1.9739	1.5005	-0.2817	0.6838	
ζ	0.2716	0.9033	-2.9996	3.6503	-2.0704	0.4623	0.3747

The voltage and efficiency of a single electrolytic cell is [22]:

$$\begin{cases} V_{\text{el\_cell}} = V_{\text{rev}} + V_{\text{ohm\_el}} + V_{\text{act\_el}} \\ \eta_{\text{el}} = V_{\text{HHV}} / V_{\text{el\_cell}} \end{cases} \tag{3.10}$$

where $V_{\text{el\_cell}}$ is the cell voltage of the electrolyzer, V_{rev} is open circuit voltage, which can be expressed by Nernst expression, $V_{\text{ohm\_el}}$ is the ohmic overvoltage, $V_{\text{act\_el}}$ is the activation overvoltage, η_{el} is the efficiency of the electrolyzer, V_{HHV} is higher heating voltage.

According to [26], the heat release of the electrolyzer varies greatly with the temperature, while the hydrogen production rate hardly changes. Moreover, the higher the temperature, the more difficult to release heat. This chapter focuses on the scheduling of IES and the electrolyzer needs to provide heat, so the realization of temperature control is not discussed in detail, and this chapter sets the operating temperature to 70℃. Then, the relationship between electric demand, efficiency, and thermal output of the electrolyzer can be expressed as follows:

$$\begin{cases} P_{\text{ele}} = P_{\text{H2el}} / \eta_{\text{el}} \\ H_{\text{el\_re}} = (1-\eta_{\text{el}}) P_{\text{H2el}} \end{cases} \tag{3.11}$$

where the power flow into the electrolyzer is P_{ele}, the power used for hydrogen production is P_{H2el}, and the released heat is $H_{\text{el\_re}}$.

Finally, the heat flows to the heat bus are:

$$H_{\text{el}} = k_{\text{el-h}} H_{\text{el\_re}} \tag{3.12}$$

where $k_{\text{el-h}}$ is the heat transfer coefficient.

By the above equations, the hydrogen production and heat-electric ratio of the electrolyzer can by written as:

$$n_{\text{el}} = \frac{\eta_{\text{con}} \eta_{\text{el}} P_{\text{el}}}{HHV_H} \tag{3.13}$$

$$H_{\text{el}} = r_{\text{tel}} \eta_{\text{el\_h}} \eta_{\text{con}} P_{\text{el}} \tag{3.14}$$

where n_{el} is the hydrogen production in mol/s, HHV_{h} is the higher heating value of hydrogen in J/kg, here the value is 1.43×10^8 in J/kg, r_{tel} is the fitting parameter of power to heat ratio.
r_{tel} and η_{el} can be calculated by:

$$r_{\text{tel}} = f_{\text{tel}}(LF) = \iota_1 \cdot LF^3 + \iota_2 \cdot LF^2 + \iota_3 \cdot LF + \iota_4 \tag{3.15}$$

$$\eta_{\text{el}} = f_{\text{el}}(LF) = \xi_1 \cdot LF^3 + \xi_2 \cdot LF^2 + \xi_3 \cdot LF + \xi_4 \tag{3.16}$$

$$LF = P_{el} / Cap_{el} \tag{3.17}$$

where LF is the ratio of the current output power and the capacity. ι_0-ι_4 and ξ_0-ξ_4 are constants, Cap_{el} is the capacity of the fuel cell. The recommended value of ι_0-ι_4 and ξ_0-ξ_4 are shown in the table below.

Table 3- 2 Value of constants

Constants	1	2	3	4
ι	0.7893	-1.298	0.8714	0.2192
ξ	-0.5563	0.9413	-0.6617	0.7731

By the above equations, the relationship of electric power, system efficiency, and heat can be obtained as shown in Figure 3-3. Hence the coupling of power, heat, and hydrogen of CPHH can be determined, more specifically, for each power output value of CPHH, a unique value of hydrogen and heat generation or consumption can be obtained.

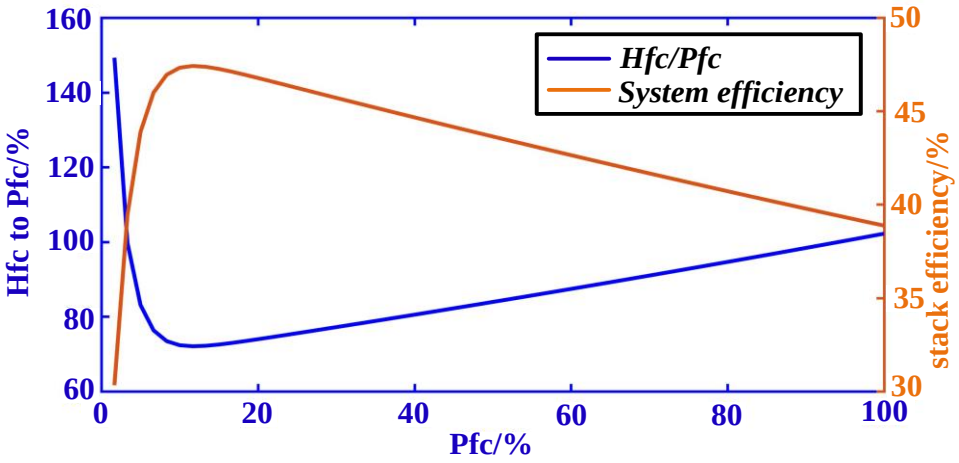

(a) Energy diagram of fuel cell

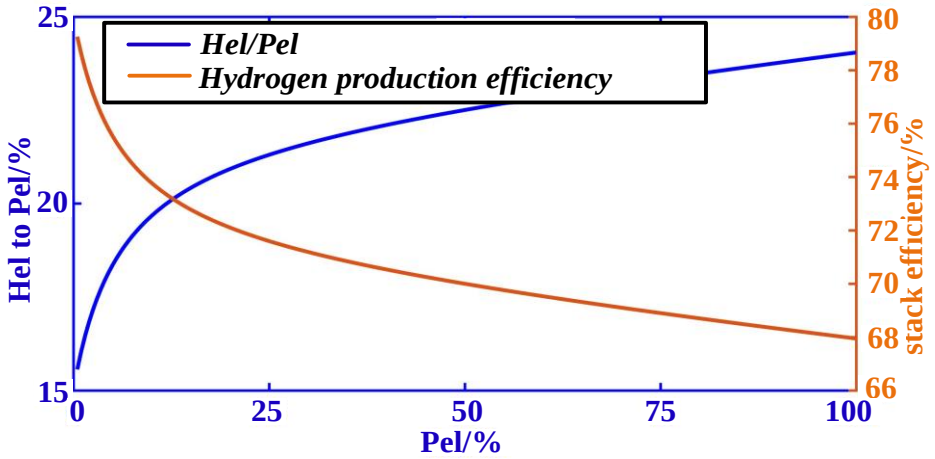

(b) Energy diagram of electrolyzer

Figure. 3- 3 Energy diagram of the CPHH system

The model of a hydrogen tank can be expressed as follows:

$$\begin{cases} C_{\mathrm{H2}} = C_{\mathrm{H2\_re}} + \int_{\Delta t} ((1 - loss_{\mathrm{conv}}) n_{\mathrm{el}} + n_{\mathrm{fc}} - n_{\mathrm{H2HVs}}) dt \\ SOHC = \dfrac{C_{\mathrm{H2}} R T_{\mathrm{H2}}}{V P_{\mathrm{tank\_max}}} \times 100\% \end{cases} \tag{3.18}$$

where $C_{\mathrm{H2\_re}}$ is the existing storage at last time, n_{el} is the hydrogen produced by the electrolyzer, n_{fc} is the hydrogen used by the fuel cell, $loss_{\mathrm{conv}}$ is the hydrogen losses, n_{H2HVs} is the charging rate of HVs, T_{H2} is temperature, V is volume of tank, $P_{\mathrm{tank\_max}}$ is the maximum pressure and $SOHC$ is the storage state of tank, Δt is length of an optimized time slot.

The energy consumption of the compressor is related to the state of gas, thus the power consumption during the operation of the compressor can be written as follows.

$$P_{\mathrm{conv}} = 3.6 w_{\mathrm{comp}} M_{\mathrm{H2}} n_{\mathrm{el}} \tag{3.19}$$

where P_{conv} is the power demands of the compressor, w_{comp} is the energy consumption for compression in kWh/kg, M_{H2} is the molar mass of hydrogen gas.
The calculation of w_{comp} is:

$$w_{\mathrm{comp}} = \frac{w_{\mathrm{h}}}{\eta_{\mathrm{m}}} = \frac{w_{\mathrm{h}}}{f(P_{\mathrm{m}})} \tag{3.20}$$

$$P_{\mathrm{m}} = w_{\mathrm{h}} \dot{m} \tag{3.21}$$

$$f(P_{\mathrm{m}}) = \kappa_1 (\ln P_{\mathrm{m}})^4 + \kappa_2 (\ln P_{\mathrm{m}})^3 + \kappa_3 (\ln P_{\mathrm{m}})^2 + \kappa_4 (\ln P_{\mathrm{m}}) + \kappa_5 \tag{3.22}$$

$$w_{\mathrm{h}} = \sum_{i=1}^{n} w_{\mathrm{h},i} \tag{3.23}$$

$$w_{\mathrm{h},i} = \frac{h_{\mathrm{out},i} - h_{\mathrm{in},i}}{\eta_{\mathrm{comp}}} \tag{3.24}$$

where w_{h} is the power consumption of the compressor in kWh/kg, η_{m} is the efficiency of the motor, Pm is the power of the motor, $\dot{m}$ is the compressor capacity in kg/h, κ_1-κ_5 are the constants for motor efficiency, $w_{\mathrm{h},i}$ is the i-th compression stage in kWh/kg, $h_{\mathrm{out},i}$ is the enthalpy of i-th stage of the output hydrogen in J/kg, $h_{\mathrm{in},i}$ is the enthalpy of i-th stage of the input hydrogen in J/kg, η_{comp} is the efficiency of the compressor of each stage.
The value of the enthalpy of each stage needs to be solved iteratively by partial differential equations, thus Coolprog is applied for the parameter solving, which is an online solver for the enthalpy. Tables 3-3 and 3-4 shows the results of the calculated parameters when the hydrogen needs to be compressed at different pressure.

Table 3- 3 Target of compression

Parameters	value
$T_{\mathrm{in},1}$ /K(℃)	298.15(25)

$T_{out,2+}$ /K(℃)	313.15(40)
p_{in} /bar	3bar
p_{out} /bar	200bar/350bar/700bar
stage	4

Table 3- 4 Value of compression parameters

Pressure	w_h/kWh/kg	m/kg/h	P_m/kW	η_m/%	w_{comp}/kWh/kg
20MPa	2.7373	60	109.492	0.9341	2.9303
35MPa	3.2083	60	109.492	0.9370	3.4240
70MPa	3.8714	60	232.284	0.9401	4.1180

3.2.3. RESs

When the size of the photovoltaic system is determined, its power output depends entirely on the irradiance and temperature:

$$P_{pv} = \frac{Ir_r}{Ir_{STC}} Cap_{pv}\eta_{pv}\eta_{con}[1+\alpha_{pv}(T_m - T_{STC})] \tag{3.25}$$

where P_{PV} is the real-time output power of PV, Ir_t is the instantaneous solar irradiance in kW/m^2 at time t, Ir_{STC} is the solar irradiance at Standard Test Conditions (STC) in kW/m^2, Cap_{pv} is the capacity of PV, η_{pv} is the system derating factor in %, here the value of η_{pv} is 86%, η_{con} is the efficiency of convertor, α_{pv} is the PV cell temperature coefficient of power in %/℃, T_m is the PV cell temperature in ℃.

The temperature of the PV panel can be calculated by:

$$T_m = T_{am,t} + 1000 Ir_t \left(\frac{T_{NOCT} - 20}{800}\right) \tag{3.26}$$

where $T_{am,t}$ is the ambient temperature at time t in ℃, T_{NOCT} is the nominal cell operating temperature.

Note that this model is often applied for large-time scale optimization, the time scale must be up to 5 minutes generally. Otherwise, the transient problem of PV will gradually be revealed with the reduction of the time scale. At this time, a more accurate model should be adopted.

The absorbed wind power of WT is:

$$P_{\text{wind}} = \begin{cases} 0, & v \le v_{\text{ci}} \text{ or } v > v_{\text{co}} \\ \eta_{\text{con}} Cap_{\text{wt}} \dfrac{v - v_{\text{ci}}}{v_{\text{rated}} - v_{\text{ci}}}, & v_{\text{ci}} < v \le v_{\text{rated}} \\ \eta_{\text{con}} Cap_{\text{wt}}, & v_{\text{rated}} < v \le v_{\text{co}} \end{cases} \tag{3.27}$$

where v is wind speed, $Capwt$ is the capacity of wind turbines, v_{ci} is the cut-in wind speed in m/s, v_{co} is the cut-out wind speed, v_{rated} is the rated wind speed.

3.2.4. ESS, TES & EB

ESS includes batteries and converters; the energy conversion can be expressed as follows:

$$\begin{cases} C_{\text{bat}} = C_{\text{bat\_re}} + \int_{\Delta t} (P_{\text{bat\_ch}} \eta_{\text{bat\_ch}} \eta_{\text{con\_bat}} - \dfrac{P_{\text{bat\_dis}}}{\eta_{\text{bat\_dis}} \eta_{\text{con\_bat}}}) \\ SOC = C_{\text{bat}} / C_{\text{bat\_max}} \times 100\% \end{cases} \tag{3.28}$$

where C_{bat} is the current storage, $C_{\text{bat\_re}}$ is the storage of last time, $P_{\text{bat\_ch}}$ and $\eta_{\text{bat\_ch}}$ are the charging power and efficiency, $P_{\text{bat\_dis}}$ and $\eta_{\text{bat\_dis}}$ are the discharging power and efficiency, $\eta_{\text{con\_bat}}$ is the efficiency of converters, SOC is the state of charge, and $C_{\text{bat\_max}}$ is the maximum capacity.

The efficiency of the battery can be linearized by:

$$\eta_{\text{bat\_ch}} = \begin{cases} -0.06 c_{\text{ch}} + 1.011, & c_{\text{ch}} > 0.2 \\ 1, & c_{\text{ch}} \le 0.2 \end{cases} \tag{3.29}$$

$$\eta_{\text{bat\_dis}} = -0.0535 c_{\text{dis}} + 0.999 \tag{3.30}$$

where c_{ch} is the current c-rate during charging, c_{dis} is the current c-rate during discharging.

The modeling of TES is similar to the ESS, which can be expressed by:

$$\begin{cases} C_{\text{t}} = C_{\text{t\_re}} + \int_{\Delta t} (H_{\text{t\_ch}} \eta_{\text{t\_ch}} - H_{\text{t\_dis}} / \eta_{\text{t-dis}}) dt \\ SOHE = C_{\text{t}} / C_{\text{t\_max}} \times 100\% \end{cases} \tag{3.31}$$

where C_{t} is the current storage of TES, $C_{\text{t\_re}}$ is the storage of last time, $H_{\text{t\_ch}}$ and $\eta_{\text{t\_ch}}$ are charging power and efficiency, $H_{\text{t\_dis}}$ and $\eta_{\text{t\_dis}}$ are discharging power and efficiency, $SOHE$ is the storage state of the tank, and $C_{\text{t\_max}}$ is the maximum capacity.

EB converts electrical energy into thermal energy, and the model is related to converters and conversion efficiency:

$$H_{bo} = \eta_{con\_bo}\eta_{e\_h}P_{bo} \tag{3.32}$$

where H_{bo} is the thermal power generated by EB, η_{con_bo} is the efficiency of converters, η_{e_h} is the power to heat efficiency, and P_{bo} is the power flows into EB.

3.2.5. Vehicles & Buildings

As for a residential area, it is necessary to consider the charging of vehicles. In this chapter, the model of EVs is established, and the probability density functions of time of arriving at IES and mileage are shown in eq. (3.33), eq. (3.34) and Figure 3-4. After that, the Monte Carlo method is used to simulate. The calculation of the charging situation is carried out by the simulated results.

$$f_S(t) = \begin{cases} \frac{1}{\sigma_S(2\pi)^{1/2}}\exp[\frac{(t-\mu_S)^2}{2\sigma_S^{\ 2}}], (\mu_S - 12) < t \le 24 \\ \frac{1}{\sigma_S(2\pi)^{1/2}}\exp[\frac{(t+24-\mu_S)^2}{2\sigma_S^{\ 2}}], 0 < t \le (\mu_S - 12) \end{cases} \tag{3.33}$$

$$f_D(L) = \frac{1}{L\sigma_D(2\pi)^{1/2}}\exp[-\frac{(\ln x - \mu_D)^2}{2\sigma_D^{\ 2}}] \tag{3.34}$$

where t and L respectively correspond to the time of arrival and driving mileage, μ_s, μ_D, σ_s, and σ_D are constants, which are related to the mean value of arriving time and driving mileage.

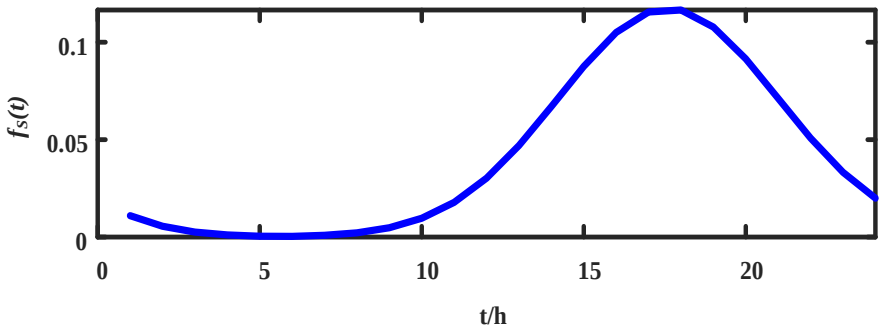

(a)Probability density of the last trip

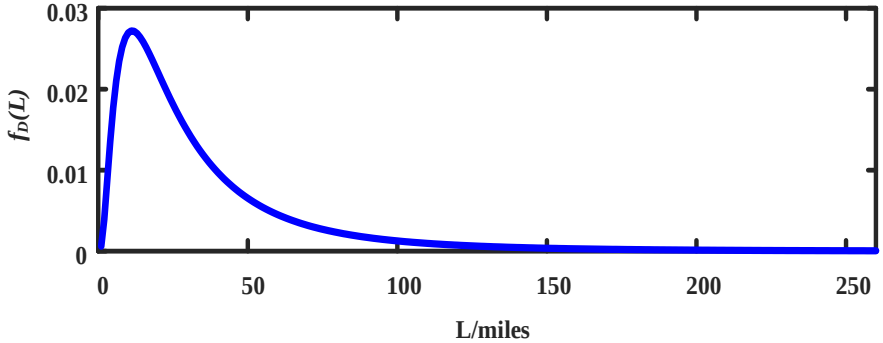

(b)Probability density of driving distance

Fig. 3- 4 Probability density of new energy vehicles

The thermal load established here considers the actual situation of the residential area, which can be written as follows:

$$\rho CV\frac{dT_{\text{indoor}}}{dt}-H_{\text{wall}}-H_{\text{win}}=H_{\text{el}}+H_{\text{fc}}+H_{\text{bo}}+H_{\text{t}} \tag{3.35}$$

$$\begin{cases}H_{\text{win}}=k_{\text{wi}}S_{\text{wi}}(T_{\text{en}}-T_{\text{indoor}})\\H_{\text{wall}}=k_{\text{w}}S_{\text{w}}(T_{\text{en}}-T_{\text{indoor}})\end{cases} \tag{3.36}$$

where ρ the is the air density, C is the specific heat capacity of air, T_{indoor} is the indoor temperature, H_{wall} is the heat conduction of walls, H_{win} is the heat conduction of windows, T_{en} is the outdoor temperature, H_{t} is the heat provided by TES, k_{w} is the heat transfer coefficient of walls, S_{w} is the area of walls, k_{wi} is the heat transfer coefficient of the window, S_{wi} is the area of windows.

3.3. Constraints, scheduling algorithm and linearization

3.3.1. Constraints

The IES established in this chapter includes power bus, thermal bus, and hydrogen pipeline. Therefore, the main balance constraints include electrical, thermal, and hydrogen power flow constraints. The constraints of the hydrogen energy system have been given in the modeling of hydrogen tank. Then the power and heat constraints are:

$$\begin{cases}P_{\text{load}}+P_{\text{bo}}+P_{\text{bat\_ch}}+P_{\text{EVs}}+P_{\text{el}}+P_{\text{conv}}=P_{\text{pv}}+P_{\text{wind}}+P_{\text{fc}}+P_{\text{bat\_dis}}\\H_{\text{load}}+H_{\text{t\_ch}}=H_{\text{fc}}+H_{\text{el}}+H_{\text{bo}}+H_{\text{t\_dis}}\end{cases} \tag{3.37}$$

where P_{load} is electricity demand and P_{EVs} are the power required by EVs, H_{load} is heat demand.

The constraints of EB, ESS, TES, and CPHH are as follows:

$$0\le P_{\text{bo}}\le P_{\text{bomax}} \tag{3.38}$$

$$\begin{cases}-H_{\text{t\_chmax}}\le H_t\le H_{\text{t\_dismax}}\\SOHE_{\min}\le SOHE\le SOHE_{\max}\end{cases} \tag{3.39}$$

$$\begin{cases}-P_{\text{bat\_chmax}}\le P_{\text{bat}}\le P_{\text{bat\_dismax}}\\SOC_{\min}\le SOC\le SOC_{\max}\end{cases} \tag{3.40}$$

$$\begin{cases} P_{\mathrm{hy}} = P_{\mathrm{fc}} + P_{\mathrm{el}} \\ -P_{\mathrm{elmax}} \le P_{\mathrm{hy}} \le -P_{\mathrm{elmin}} \quad ,P_{\mathrm{hy}} < 0 \\ P_{\mathrm{fcmax}} \le P_{\mathrm{hy}} \le -P_{\mathrm{fcmin}} \quad ,P_{\mathrm{hy}} > 0 \\ SOHC_{\min} \le SOHC \le SOHC_{\max} \end{cases} \tag{3.41}$$

where P_{bomax} is the rated power of EB, $P_{\mathrm{bat\_chmax,}}$ and $P_{\mathrm{bat\_dismax}}$ are the maximum charge and discharge power of the battery, $SOC_{\min}$ and $SOC_{\max}$ are the minimum and maximum of SOC, $H_{\mathrm{t\_chmax,}}$ and $H_{\mathrm{t\_dismax}}$ are the maximum endothermic and exothermic power of TES, and $SOHE_{\min}$ and $SOHE_{\max}$ are the upper and lower limits of $SOHE$, P_{hy} represents the power of CPHH, $P_{\mathrm{elmin,}}$ and P_{elmax} are the minimum and maximum power of the electrolyzer, P_{fcmin} and P_{fcmax} represent the minimum and maximum output power of the fuel cell, $SOHC_{\min}$ and $SOHC_{\max}$ are the upper and lower limits of $SOHC$.

In [11], EVs are regarded as ESS, which can be both charged and discharged. But once leaving the parking lot, the SOC of the EV must be charged to a value higher than the SOC when it arrives. In order to eliminate inefficiency caused by frequent charging and discharging, EVs are no longer considered to discharge, but as special DR loads. Thus, when EVs return to IES, the total charging demand is determined according to the mileage. All the vehicles will receive the integrated scheduling of IES. The constraints of EVs are as follows:

$$\begin{cases} {P_{\mathrm{EVs}}}^{\mathrm{t}} = \sum_{1}^{n} \Delta t {P_{\mathrm{EVs},i}}^{t} \\ Q_{\mathrm{EVs},i} = k_{\mathrm{EVs}} L_{\mathrm{EVs},i} = \sum_{t0}^{tm} \int \eta_{\mathrm{EVs}} \Delta t {P_{\mathrm{EVs},i}}^{t} dt \\ 0 \le {P_{\mathrm{EVs},i}}^{t} \le P_{\mathrm{EVsmax}} \end{cases} \tag{3.42}$$

where ${P_{\mathrm{EVs}}}^{t}$ is the total demand of all EVs at time t, ${P_{\mathrm{EVs},i}}^{t}$ is the demand of the i-th EV at time t, n is the number of EV, $Q_{\mathrm{EVs},i}$ is the demand of i- EV, k_{EVs} is the energy consumption coefficient per 100 km, $L_{\mathrm{EVs},i}$ is the driving mileage of the i- EV, η_{EVs} is the charging efficiency of each EVs, P_{EVSmax} is the maximum charging power of EVs.

For HVs, the charging time is short, so it is considered that for any HVs, the charging is completed within a time slot. Therefore, the constraints of HVs are:

$$\begin{cases} {Q_{\mathrm{H2HVs}}}^{t} = \sum_{1}^{m} {Q_{\mathrm{H2HVs},j}}^{t} \\ Q_{\mathrm{H2HVs},j} = {Q_{\mathrm{H2HVs},j}}^{t} = k_{\mathrm{HVs}} L_{\mathrm{HVs},j} \end{cases} \tag{3.43}$$

where Q_{H2HVs}^{t} is the amount of hydrogen required by the HVs at time t, $Q_{H2HVs,j}^{t}$ is the amount of hydrogen required by the *j*-th HV at time *t*, *m* is the number of HVs, $Q_{H2HVs,j}$ is the total amount of hydrogen required by the *j*-th HV, k_{HVs} is the coefficient of hydrogen consumption per 100km of HVs, $L_{HVS,j}$ is the mileage of the *j*-th HV.

3.3.2. Two-stage scheduling

The proposed two-stage IES scheduling method is shown in Fig. 3-5. The scheduling consists of two parts: day-ahead global optimal scheduling and real-time adjustment operation.

In the day-ahead optimization, based on the data of prediction and vehicles, the global optimal scheduling which aims to minimize the operation cost of each hour is carried out.

After receiving the day-ahead results, the MPC runs to minimize the operation errors according to the ultra-short-term prediction and feedback data every 15 minutes.

As DR loads, EVs take part in the daily scheduling of IES flexibly when return to IES.

The day-ahead scheduling steps are as follows:

1) Prediction.

2) Calculate RESs output based on prediction data.

3) Initialization, setting SOC, SOHE, and SOHC initial values.

4) Simulate and input vehicle data.

5) Set the scheduling step length (1h), system constraints, and input objective function. Solve the MILP problem.

6) Output day-ahead optimal scheduling results.

The real-time MPC scheduling steps are as follows:

1) Receive optimization results from stage 1.

2) Set the system status at the initial condition.

3) Set the initial time and step size (15 min).

4) Obtain the feedback data of storage systems, temperature, and charge condition of each EV of the last rolling optimization.

5) Obtain real-time data.

6) Ultra-short-term prediction based on real-time and historical data, with a prediction length of 15min×5.

7) The total length of rolling scheduling is 15min×6, which is composed of real-time values and predicted values. According to the objective function, the MIQP problem is solved by Matlab / Yalmip and Gurobi.

8) Output the real-time optimization results, and update and feedback the data.

9) Judge whether it is the last time interval. If not, go back to step 4, if yes, end the algorithm.

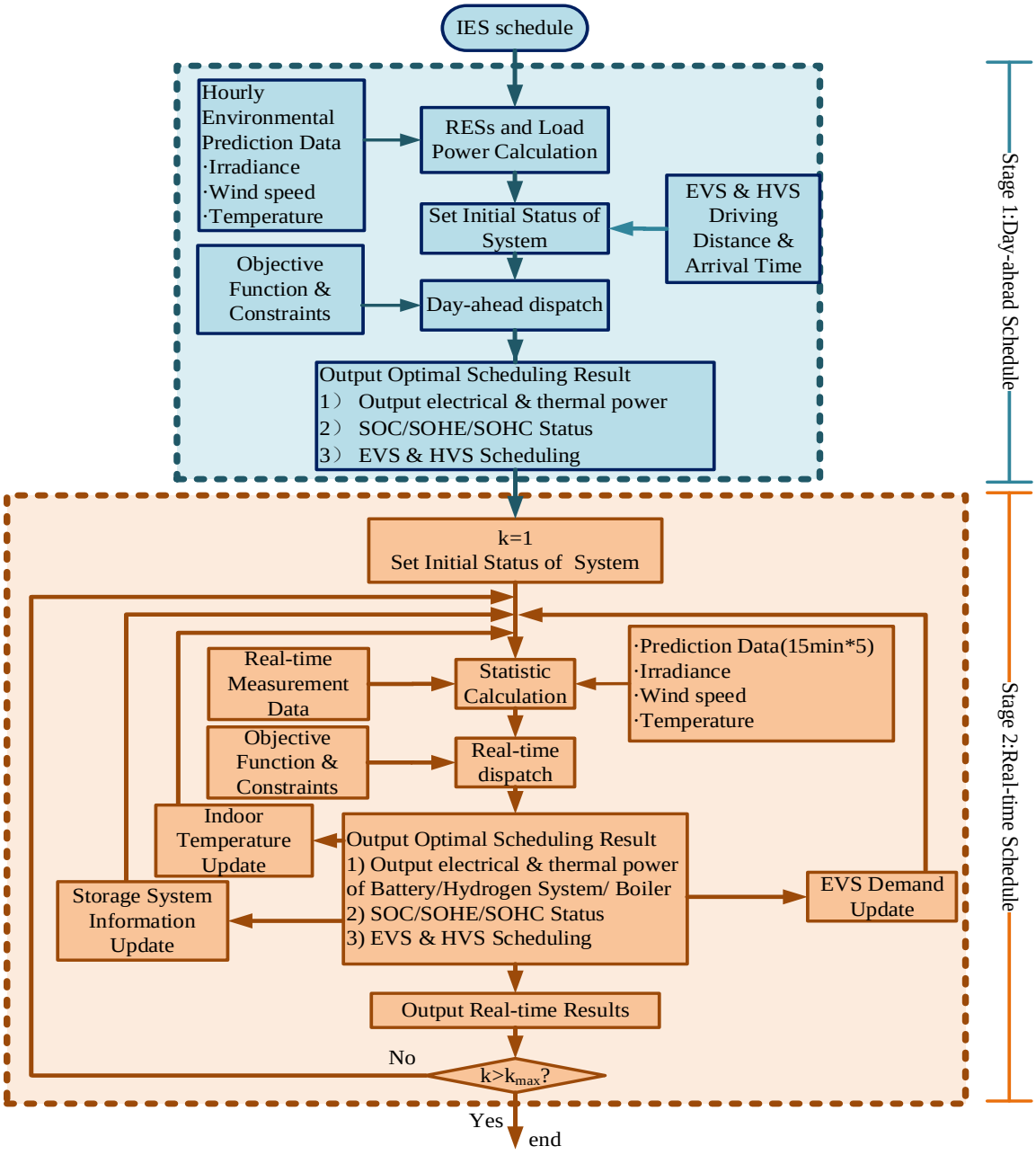

Fig. 3- 5 Scheduling flow chart

The day-ahead scheduling realizes the minimum operation cost of IES, and its cost function contains the cost of each MS which can be expressed as follows:

$$F = \min \sum_{t=0}^{24} \left[C_{\mathrm{RESs},t} + C_{\mathrm{bo},t} + C_{\mathrm{fc},t} + C_{\mathrm{el},t} + C_{\mathrm{bat},t} + C_{\mathrm{h},t} \right] \quad (3.44)$$
$$s.t. (3.1) - (3.24)$$

where $C_{\mathrm{RESs},t}$ is the cost of RESs, $C_{\mathrm{bo},t}$ is the cost of EB, $C_{\mathrm{fc},t}$ is the cost of fuel cell, $C_{\mathrm{el},t}$ is the cost of electrolyzer, $C_{\mathrm{bat},t}$ is the cost of battery, $C_{\mathrm{h},t}$ is the cost of TES.

For each part of the cost function, the specific calculation method can be found in [25].

The purposes of MPC scheduling are to adjust the day-head optimal results in real-time and reduce the economic losses caused by uncertainty. The objective function is as follows:

$$\begin{aligned} &F = \min \sum_{k}^{k+5} \left\{ \alpha_1 \left(P_{\mathrm{MS},t} - P_{\mathrm{MS,tref}} \right)^2 + \alpha_2 (T_{\mathrm{inddor},t} - T_{\mathrm{indoor,tref}})^2 \right\} \\ &s.t. (3.1) - (3.44) \end{aligned} \tag{3.45}$$

where α_1 and α_2 are the weight coefficients, k is the current time slot, $P_{\mathrm{MS},t}$ is the output electric and thermal power of each MS, $P_{\mathrm{MS,tref}}$ is the reference power at time t. $T_{\mathrm{indoor},t}$ is the indoor temperature, $T_{\mathrm{indoor,tref}}$ is the reference value of indoor temperature.

For the scheduling participation of EVs as DR load in this stage, the constraints can be expressed as follows:

$$\begin{cases} Q_{\mathrm{EVs,r}} = \sum_{1}^{6} \Delta t_{\mathrm{s}} \eta_{\mathrm{EVs}} P_{\mathrm{EVs},i}{}^{t_{\mathrm{s}}} \\ 0 \le P_{\mathrm{EVs},i}{}^{t_{\mathrm{s}}} \le P_{\mathrm{EVsmax}} \end{cases} \tag{3.46}$$

where $Q_{\mathrm{EVs,r}}$ is the total demand of all EVs at r-th rolling optimization according to the optimization results in the first stage, Δt_{s} is the time step size of the second stage (15min), and $P_{\mathrm{EVS},i}{}^{t}$ is the power consumption of i-th EVs.

The non-linear relationship of heat production and the electric power of CPHH brings difficulties to the fast solution of scheduling. In this chapter, the piecewise linearization of the CPHH relationship is carried out. Because MILP and MIQP method are used in this chapter, the switch variables can be used to construct the piecewise linear function.

3.3.3. Linearization of CPHH

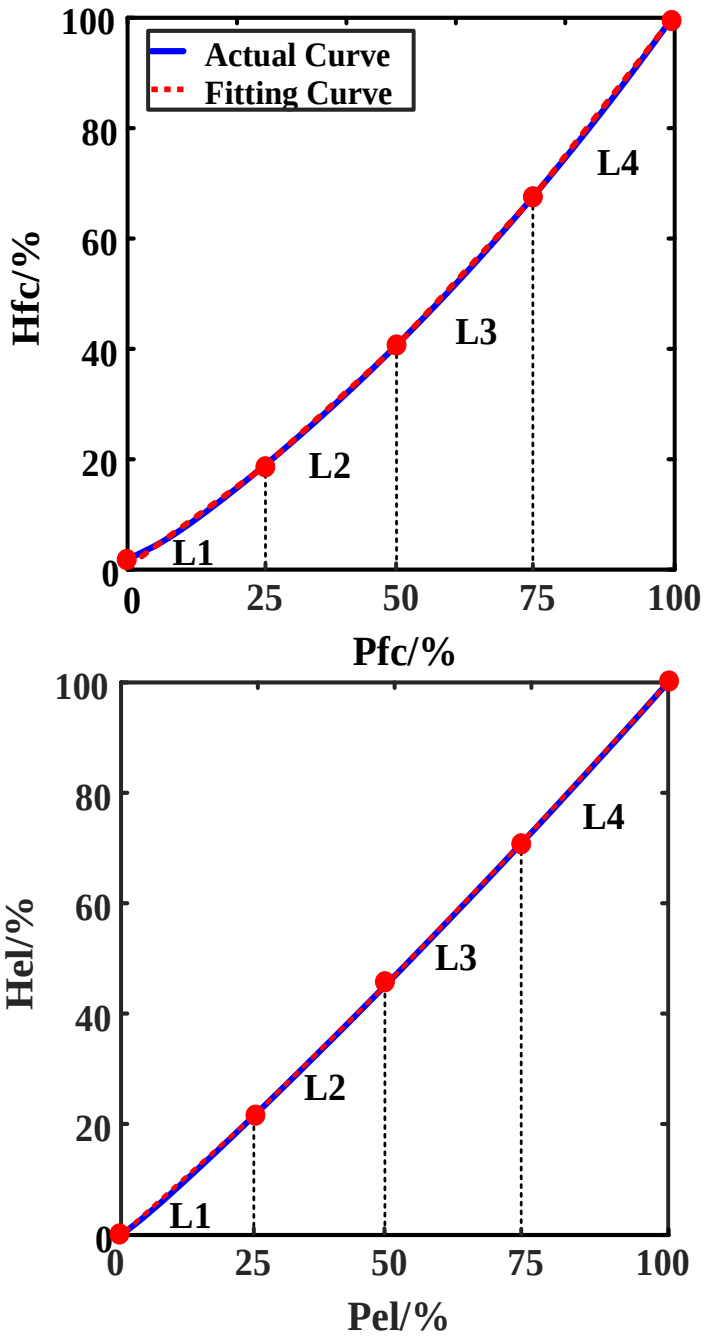

Fig. 3- 6 Fitting curve of CPHH

According to the electric-thermo-hydrogen coupling of the CPHH system described above, the non-linear relationship between heat production and electric power brings great difficulties to the fast solution of scheduling. Thus, the piecewise linearization of the CPHH relationship between the fuel cell and electrolyzer is carried out. Since the mixed integer programming method is used, the switch variable can be used to construct the piecewise linear function:

$$f_{\text{linear}} = \sum_{i=1}^{r} H_i \sigma_i \tag{3.47}$$

$$H_i = k_i P_i + c_i \tag{3.48}$$

$$\sum_{i=1}^{r} \sigma_i = 1 \tag{3.49}$$

where f_{liner} is the constructed piecewise linear function, r is the total number of linear functions, H_i is the ith linear function, k_i and c_i are the parameters of the linear function, and σi is the binary switch variable. In this chapter, the CPHH curve is divided into four sections for fitting. The comparison between the fitting results and the original curve is shown in Figure 3-6. The R^2 regression adjustments of the fitting results of the two curves are both greater than 98%.

3.4. Case study

In order to verify the rationality of the method proposed in this chapter, a typical small-scale residential model in France is set, including several residential buildings.

3.4.1. Parameter settings

The parameter settings are as shown in Tables 3-5 to 3-7.

Table 3- 5 IES Parameters

	Parameter	Value
PV	Rated power per panel	10kw
	Panels number	30
WT	Blade length	3m
	Number	30
Battery	Maximum charge and discharge power	±150kw
	Capacity	1000kwh
EB	Rated power	60kw
	Efficiency	90%
TES	Maximum charge and discharge power	±50kw
	Capacity	1000kwh
Fuel cell	Rated power	60kw
Electrolyzer	Rated power	200kw
Hydrogen tank	Volume	28L
	Maximum pressure	35Mpa

Convertors	Efficiency	95%
EVs	Maximum charge power	3.5kw
	Number	20
HVs	Number	10
Buildings	Walls area	2920m^2
	Windows area	200m^2
	Heat transfer coefficient of wall	0.85
	Heat transfer coefficient of window	2
	Comfortable temperature	18-22℃

Table 3- 6 Building parameters

Items	*Value*
Total building area	*1320m2*
Window area	*2920m2*
Thermal conductivity of wall	*200m2*
Heat transfer coefficient of wall	*0.85*
Heat transfer coefficient of window	*2*
Comfortable temperature	*18-22℃*

Table 3- 7 Vehicle parameters

	EV1	*EV2*	*EV3*	*EV4*	*EV5*	*EV6*
time(h)	*22*	*14*	*18*	*18*	*15*	*19*
mileage(km)	*21.8*	*11.5*	*13.8*	*147*	*31.4*	*32.8*
	EV7	*EV8*	*EV9*	*EV10*	*EV11*	*EV12*
time(h)	*1*	*15*	*19*	*19*	*19*	*18*
mileage(km)	*25.1*	*44.2*	*102*	*3.6*	*40.3*	*17.8*
	EV13	*EV14*	*EV15*	*EV16*	*EV16*	*EV18*
time(h)	*17*	*19*	*23*	*16*	*13*	*18*
mileage(km)	*69.8*	*13.2*	*42.9*	*50.4*	*9.2*	*32.1*
	EV19	*EV20*	*HV1*	*HV2*	*HV3*	*HV4*
time(h)	*17*	*17*	*18*	*17*	*16*	*19*

mileage(km)	*71.9*	*6.6*	*75.4*	*112*	*43.8*	*75.4*
	HV4	*HV5*	*HV6*	*HV8*	*HV9*	*HV10*
time(h)	*15*	*23*	*17*	*13*	*14*	*15*
mileage(km)	*15.4*	*31.8*	*96.4*	*41.3*	*37.2*	*62.8*

3.4.2. Prediction

The historical data of a meteorological station is selected for the simulation. And the data from January 15, 2018, and August 22, 2018, is chosen for prediction. And long short-term memory (LSTM) method is used for prediction. The flowchart of LSTM for day-ahead prediction is shown in Figure 3-7.

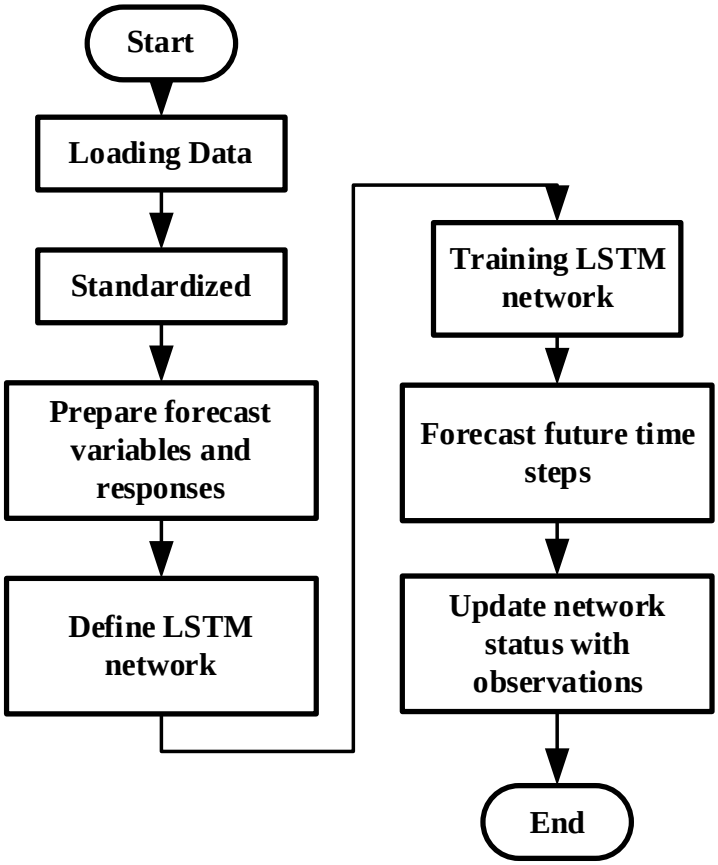

Figure 3- 7 Prediction flowchart of LSTM

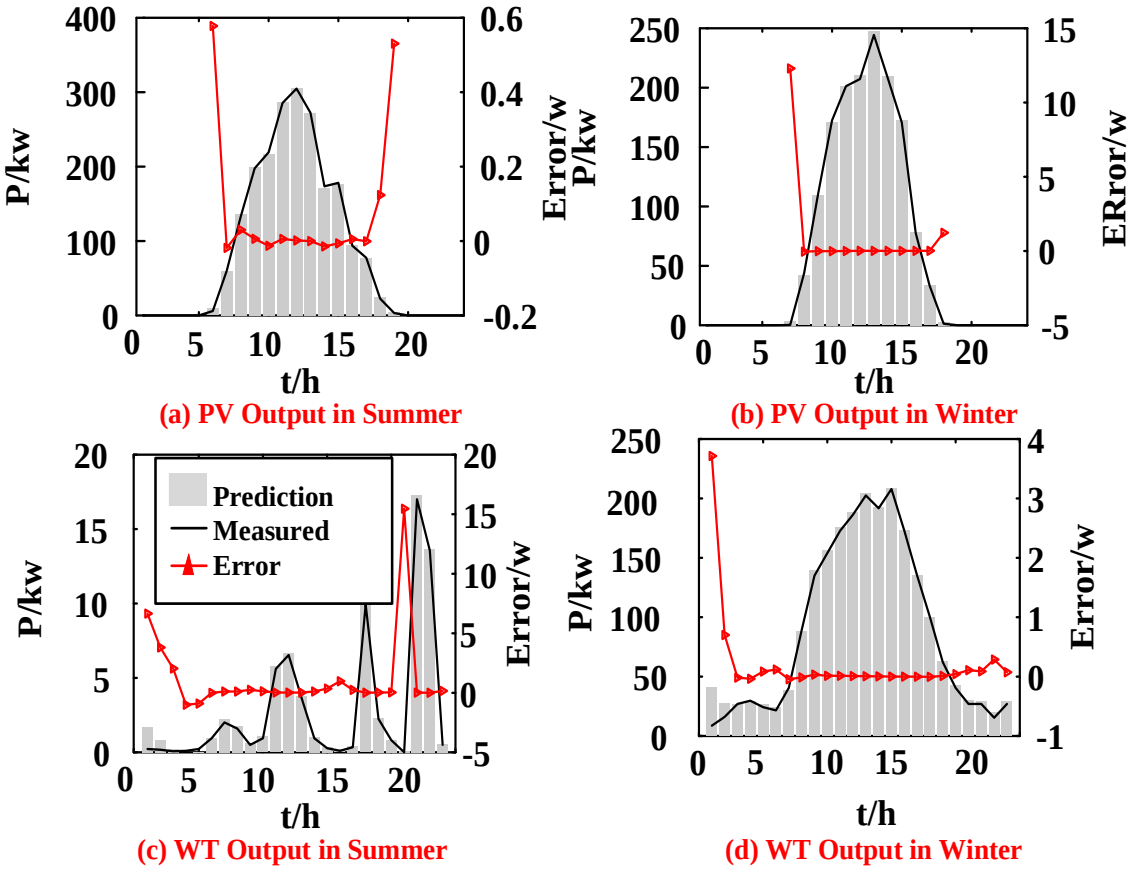

Fig. 3- 8 Prediction results of LSTM

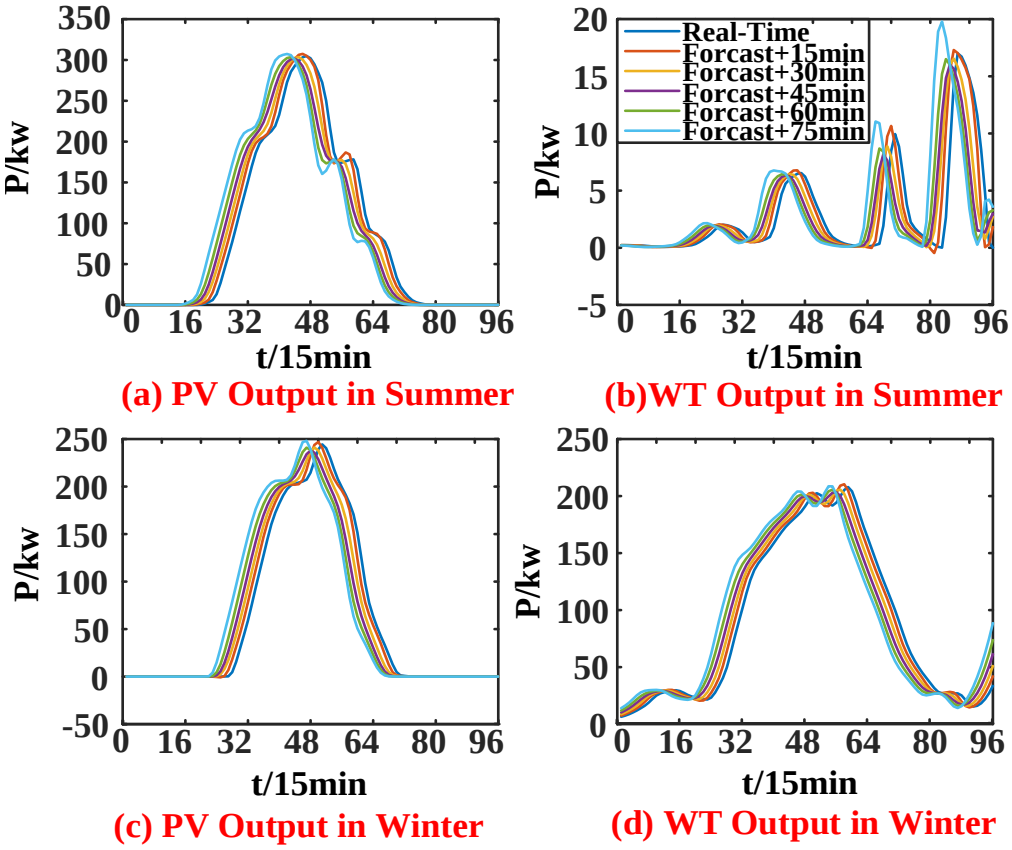

Fig. 3- 9 Prediction results of gray method

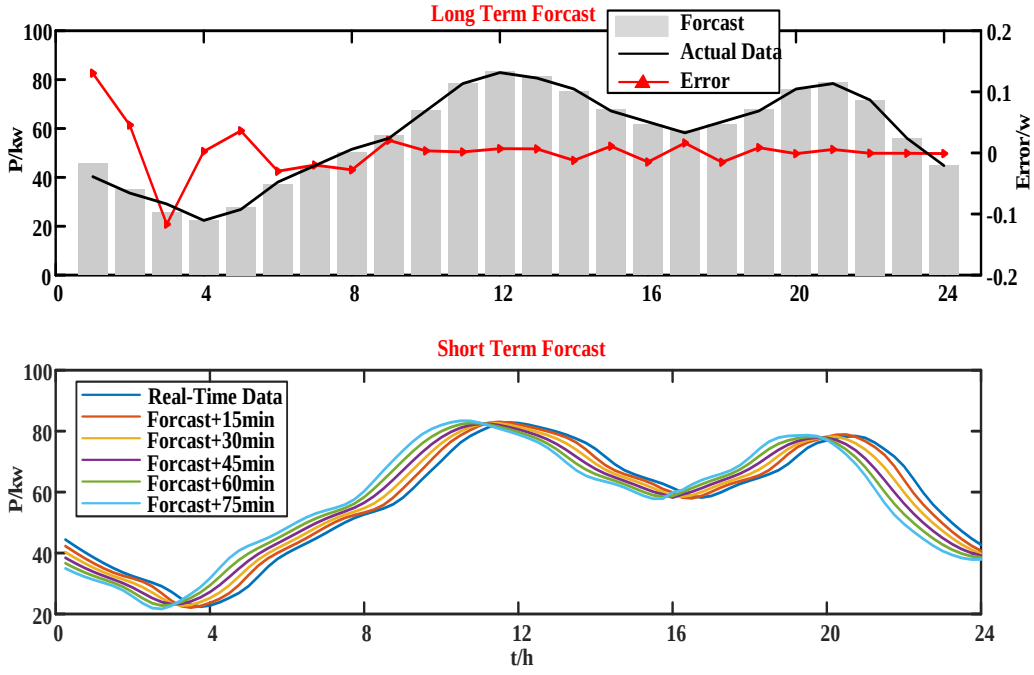

Fig. 3- 10 Electric load prediction results

Then, the data from January 6 to 14 and August 13 to 21 is used for training the neural network. The prediction results of LSTM are shown in Figure 3-8. Besides, the gray method is used to achieve ultra-short-term prediction as shown in Figures 3-9 and 3-10. The RMSE of prediction results is less than 1%.

3.4.3. Results

3.4.3.1. Day-ahead scheduling results

The day-ahead scheduling results are shown in Figure 3-11. The summer day is dominated by sufficient illumination with relatively high outdoor temperatures. At this time, the heat demand is kept at a low level and the working hours of EB and CPHH system are reduced greatly. However, due to the large temperature difference between day and night (for almost 13℃), the TES still works at night to provide heat for users. Meanwhile, to meet the hydrogen demands of HVs, the electrolyzer works to provide enough fuel and releases heat to the heat bus. However, most of the heat generated by CPHH is absorbed by TES to keep the indoor temperature. When the outdoor temperature exceeds 18℃, almost all the heat devices stop working to keep the indoor temperature within the comfortable range. The relatively low demand for heat leads to the inactivity of the CPHH system, thus the ESS works more frequently to provide power. Compared with ESS, the working time of the CPHH system is only half of the ESS.

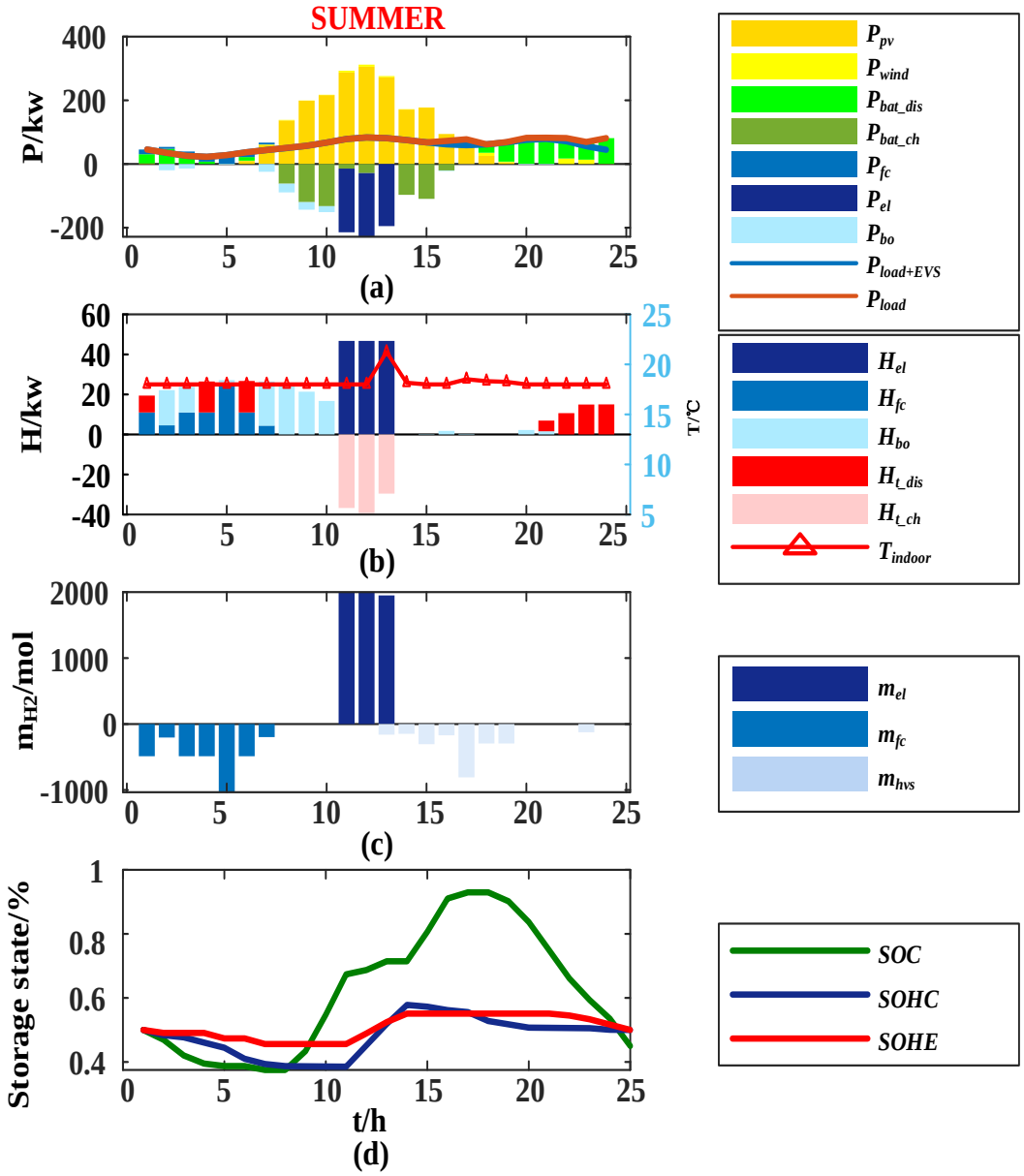

Fig. 3- 11 Day-ahead scheduling result in summer

(a) Power in summer, (b) Heat power in summer, (c) Hydrogen consumption in summer, (d) Storages in summer

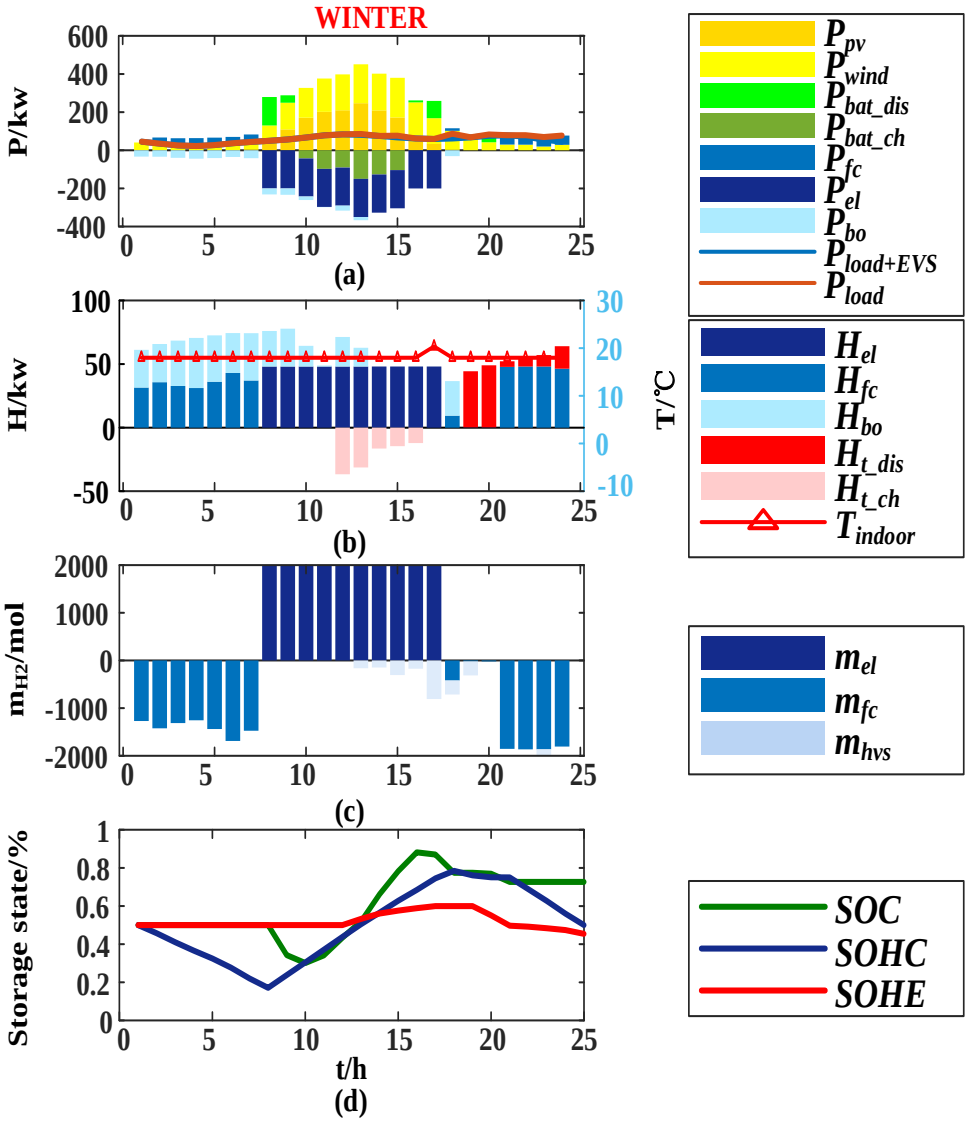

Fig. 3- 12 Day-ahead scheduling result

(a) Power in winter, (b) Heat power in winter, (c) Hydrogen consumption in winter, (d) Storages in winter

As for winter, although the climate still presents a large temperature difference between day and night, due to its continuous low temperature all day, the power transmission of the heat bus increases sharply, and the heat supply devices work almost all day. The irradiance of PV is relatively small compared with the summer day, the strong winds still provide huge amounts of energy for CPHH to produce hydrogen and heat. During the day, the electrolyzer reaches the maximum power limit from the beginning and keeps the power level for 10 hours. From the discharge action of the battery during daytime in Figure 3-11-(a) and (b), when the system needs a large amount of hydrogen and heat, the battery also discharges

to support the CPHH system. Yet, the working time and energy flow of ESS are still within a lower range, and this system mainly focuses on supporting the CPHH system and providing power for users as an auxiliary power source.

In general, no matter in winter or summer, IES meets the power, heat, and hydrogen demands of residents, and the state of energy storage systems is relatively balanced. The charge and discharge of ESS are more frequent in summer, while the working hours of the CPHH system are relatively short in winter, the large demand for heat leads to the increase of output power and working time of the CPHH system, and ESS works as supplementary energy source at the same time.

3.4.3.2 Real-time MPC results

The MPC results are shown in Figure 3-13 and Figure 3-14. The comparison of Figure 3-11 to Figure 3-14 shows that real-time scheduling tracks the results of day-ahead optimization. For the time slot with a small error, the output of each power or heat source changes slightly to remedy the error. For the time slot with large errors, the real-time scheduling no longer operates according to the results of day-ahead optimization, but to meet the residents' demands and prevent increased costs caused by errors. For example, from the 35th time slot to the 39th time slot (8:30-9:45) in summer, according to the day-ahead optimization, there is a shortage of heat and EB should be fully responsible for the supply. However, the fuel cell works to provide heat and power in MPC operation. On the one hand, it increases the supply of power to the EB. On the other hand, the action of fuel cells further overcomes the heat shortage. From 0:00 to 1:00, according to the original plan, the output of the fuel cell leads to a surplus of power. But in real-time operation, EB works to absorb the surplus power and provides heat for residential area. In the two cases, EB as an auxiliary system, plays a great role in reducing the gap between the day-ahead scheduling and the real-time situation. Its output flexibly supplements the heat vacancy and ensures the stable operation of the whole system.

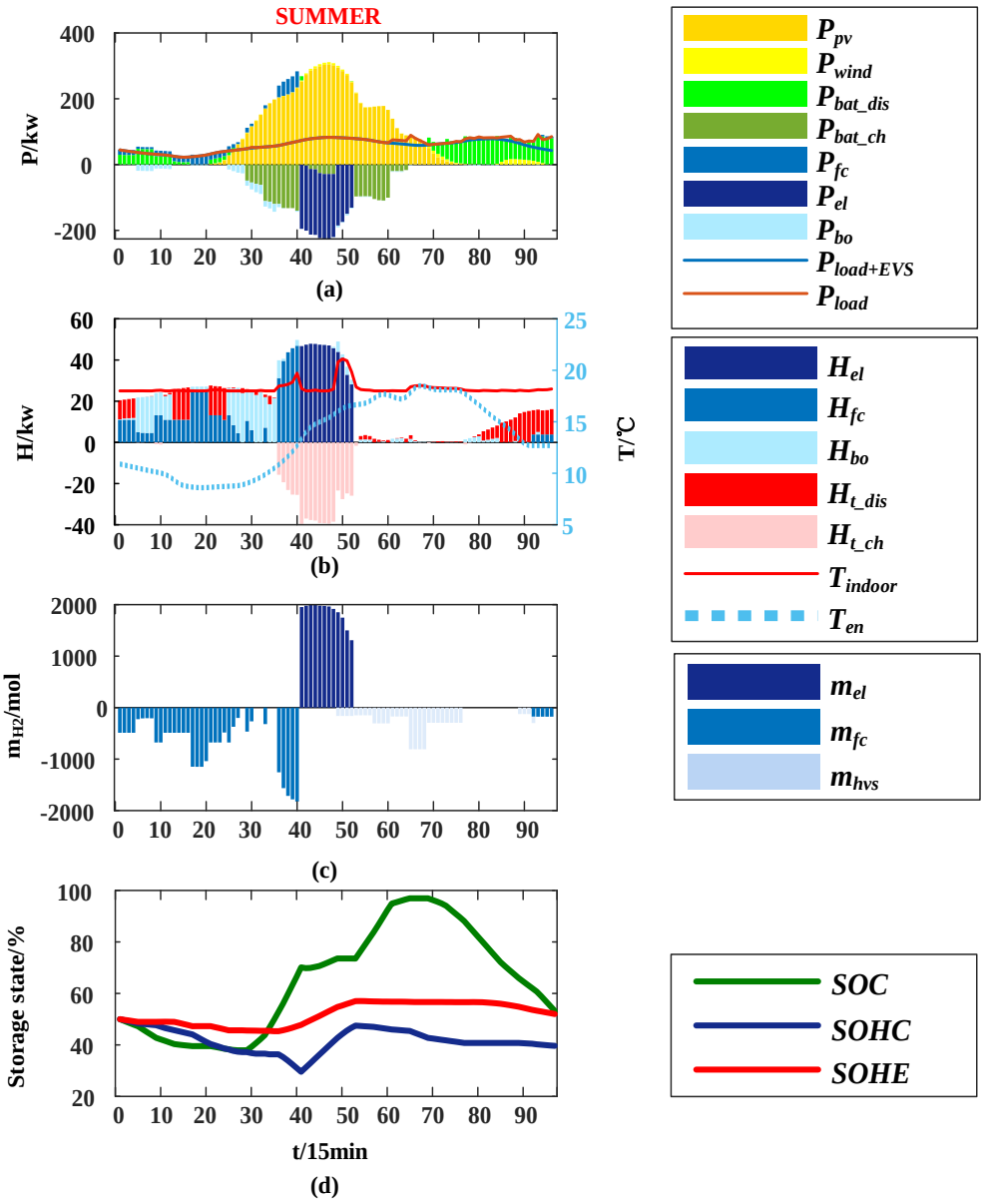

Figure 3- 13 Real-time MPC scheduling results in summer

(a) Power in summer, (b) Heat power in summer, (c) Hydrogen consumption in summer, (d) Storages in summer

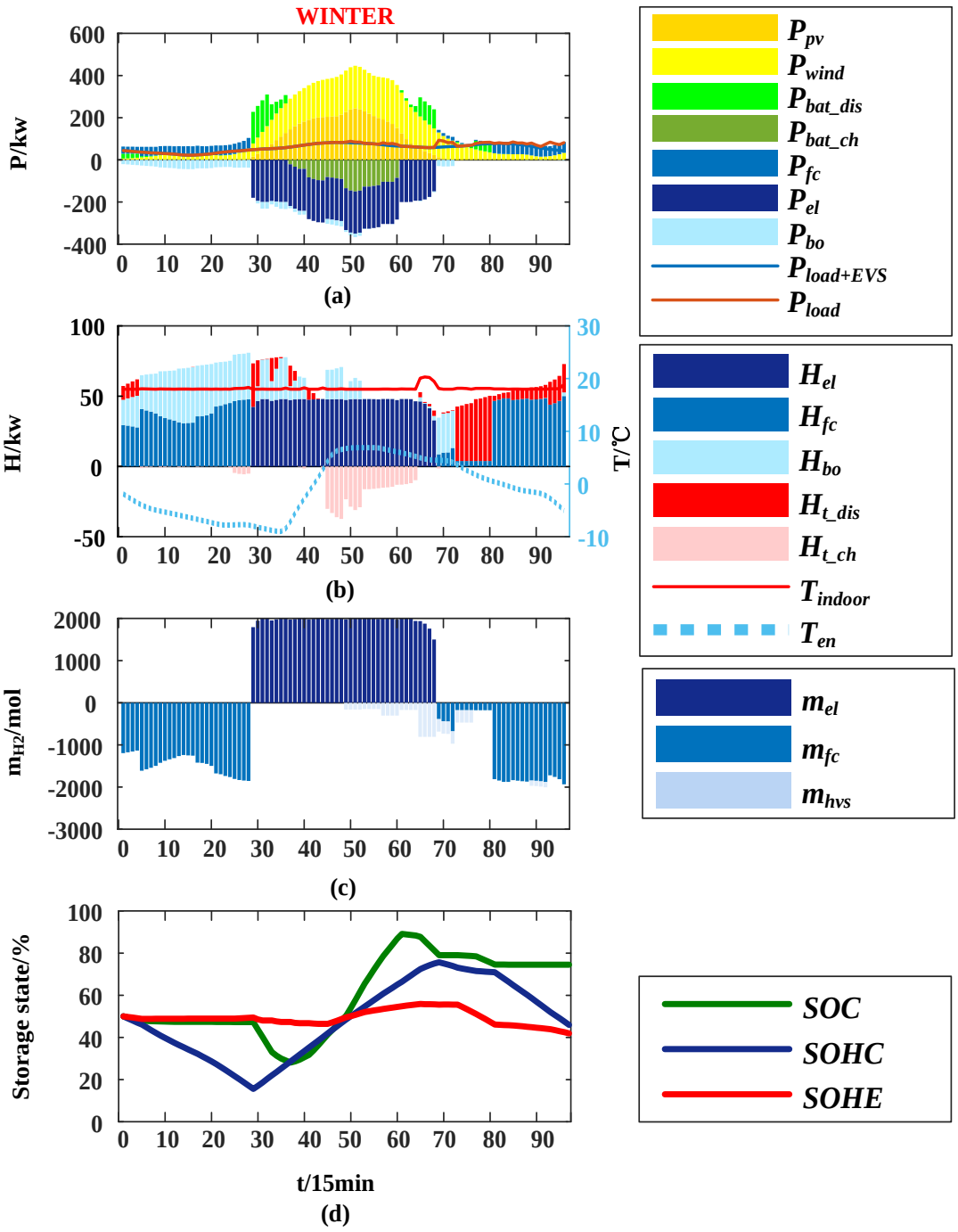

Figure. 3- 14 Real-time MPC scheduling results in winter

(a) Power in winter, (b) Heat power in winter, (c) Hydrogen consumption in winter, (d) Storages in winter

Real-time scheduling realizes the flexible operation of IES by tracking the day-ahead scheduling results. Besides, the temperature is still within the comfortable range with small fluctuations. The states of energy storage system are consistent comparatively with day-ahead scheduling. In summary, this method

can track the optimal results of day-ahead scheduling and realize the coordinate operation of each device, indicating the feasibility of the real-time scheduling, which improves the reliability of IES operation.

2. Analysis

1) System efficiency

The demands of residents include the power, heat, EVs, and HVs, and the power demand of HVs is calculated by the low heat value of hydrogen. The power stack of IES is shown in Figure 3-15.

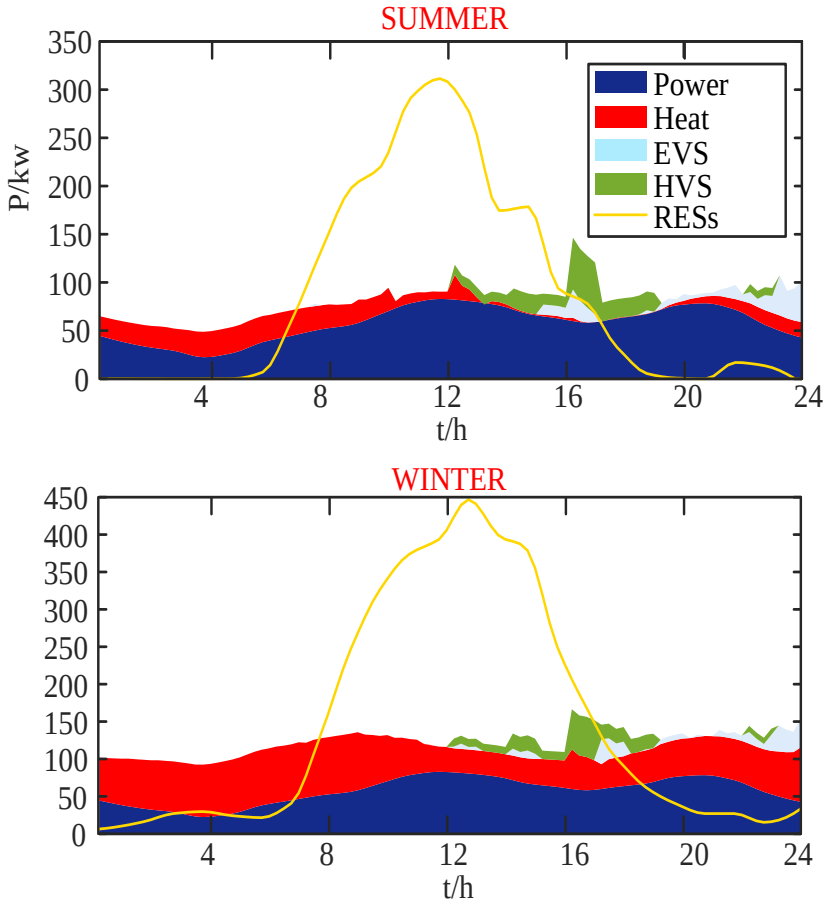

Figure 3- 15 IES power stack

System efficiency is the ratio of the sum of the energy consumed by the loads and the energy stored during 24h by ESS, hydrogen tank, and TES to the energy generated by RES, which can be expressed as follows:

$$\eta_{sys} = \frac{E_{load} + E_{sto}}{E_{RES}} \tag{3.50}$$

$$\begin{cases} E_{\text{load}} = \int (P_{load}^{t} + H_{\text{load}}^{t} + P_{\text{EVs}}^{t} + HHV_{\text{H2}} Q_{\text{H2HVS}}^{t}) dt \\ E_{\text{sto}} = (SOC_{\text{f}} - SOC_{i}) C_{\text{bat\_max}} + \\ \qquad (SOHE_{\text{f}} - SOHE_{i}) C_{\text{t\_max}} + (C_{\text{H2,f}} - C_{\text{H2},i}) HHV_{\text{H2}} \\ E_{\text{RES}} = \int (P_{\text{pv}}^{t} / \eta_{\text{con\_pv}} + P_{\text{wind}}^{t} / \eta_{\text{con\_wind}}) dt \end{cases} \tag{3.51}$$

where E_{load} is the energy demand of load and vehicles, E_{sto} is the surplus energy of storage systems, E_{RES} is the energy produced by RES, $P_{\text{load}}{}^{t}$ is the electricity load at time t, $H_{load}{}^{t}$ is the heat demand at time t, $P_{\text{pv}}{}^{t}$ is the output power of PV at time t, $P_{\text{wind}}{}^{t}$ is the output power of WT at time t, HHV_{H2} is the higher heating value of hydrogen, SOC_{f} is the final value of SOC, SOC_i is the initial value of *SOC*, $SOHE_{\text{f}}$ is the final value of *SOHE*, $SOHE_i$ is the initial value of SOHE, $C_{\text{H2,f}}$ is the final amount of hydrogen stored in the tank, and $C_{\text{H2},i}$ is the initial amount of hydrogen in the tank.

In Table 3-8, the energy proportions are calculated. Due to the high temperature in summer, the heat demand accounts for a relatively small proportion, while the heat consumption in winter is close to the electric power consumption. In terms of total efficiency, due to the inactivity of heat supply devices in summer, the energy loss during transmission is reduced. In addition, because the RESs output in summer is less than that in winter, the power waste is less than that in winter, so the total efficiency of IES in summer is higher.

Table 3- 8 Energy proportions OF IES

	Power	Heat	EVs	HVs	Storage	System Efficiency
Summer	70.18%	16.95%	5.08%	7.83%	-0.04%	88.77%
Winter	45.36%	43.80%	3.28%	5.06%	2.50%	80.34%

2) Economy and storage state

Table 3- 9 Comparison

Method	SUMMER						WINTER					
	Two-stage DR		Single-stage DR		Without DR		Two-stage DR		Single-stage DR		Without DR	
Stage	Stage I	Stage II	Stage I	Stage II	Stage I	Stage II	Stage I	Stage II	Stage I	Stage II	Stage I	Stage II

Cost(RES)/€	83.82	83.30	83.82	83.30	83.82	83.30	199.08	193.86	199.08	193.86	199.08	193.86
Cost(MGs)/ €	195.58	212.47	195.58	290.04	273.72	298.56	349.96	351.46	349.96	369.92	373.52	398.73
Total Cost/€	351.94	295.78	351.94	373.34	357.54	2948.0	549.04	545.32	549.04	563.78	572.60	592.59
SOC/%	50/45.0	50/53.2	50/45.0	50/50	50/45	50/70.4	50/72.6	50/74.5	50/72.6	50/80	50/70	50/76.4
SOHC/%	50/50.1	50/39.6	50/50.1	50/19.2	50/49.7	50/44.3	50/50.0	50/47.6	50/50.0	50/46.6	50/49.8	50/45.6
SOHE/%	50/50.0	50/52.0	50/50.0	50/81	50/51.2	50/42.1	50/45.4	50/45.5	50/45.4	50/22.1	50/50.1	50/46.3

In Figure 3-16, the charging power of EVs in summer and winter after two-stage scheduling is shown. The blue curve is the original power demand of EVs. Since EVs are regarded as special DR loads, the fluctuations of EVs in the scheduling process are all from the compensation of system fluctuations. In order to better verify the advantages of this method, this chapter compares the proposed method with the following methods, and the results are shown in Table 3-9.

This chapter runs a two-stage EVs scheduling method, only a day-ahead EVs scheduling method, and no EVs scheduling method. The costs and system status are shown in Table 3-9. It can be concluded that the scheduling based on two-stage DR is better than the other two methods. The power curve of EVs with two-stage scheduling in Figure 3-16 is quite different from that of EVs with no scheduling, which changes the operation and state of the system greatly and further reduces the operation cost of the system. In addition, real-time scheduling helps to maintain the balance of energy storage state of the system.

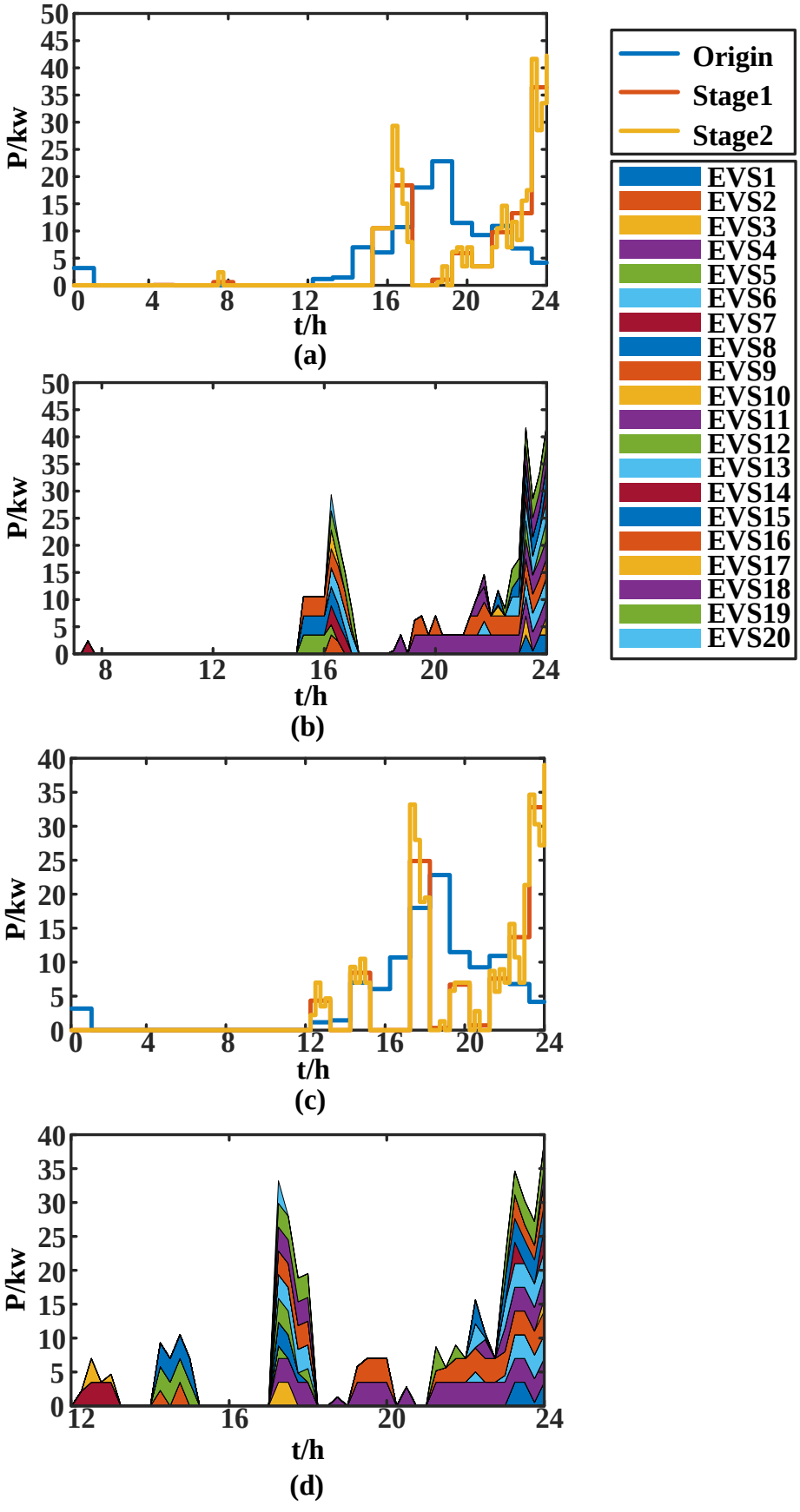

Figure 3- 16 EVs scheduling results

(a) Day-ahead scheduling of EVs in summer, (b) Real-time scheduling of EVs in summer, (c) Day-ahead scheduling of EVs in winter, (d) Real-time scheduling of EVs in winter

There are some alternative structures for island IES. This chapter compares three options including the IES proposed in this chapter, and all these structures are equipped with RESs, ESS, TES, and EB. For PEMFCPP, there is no effective way to provide hydrogen. As for P2HH, it can be discussed as an alternative, which can produce heat and hydrogen by using renewable energy. In terms of the traditional system, the IES with a gas turbine is not suitable for the area, so only EB converts electricity into heat. The cost and efficiency of each model is shown in Figure 3-17.

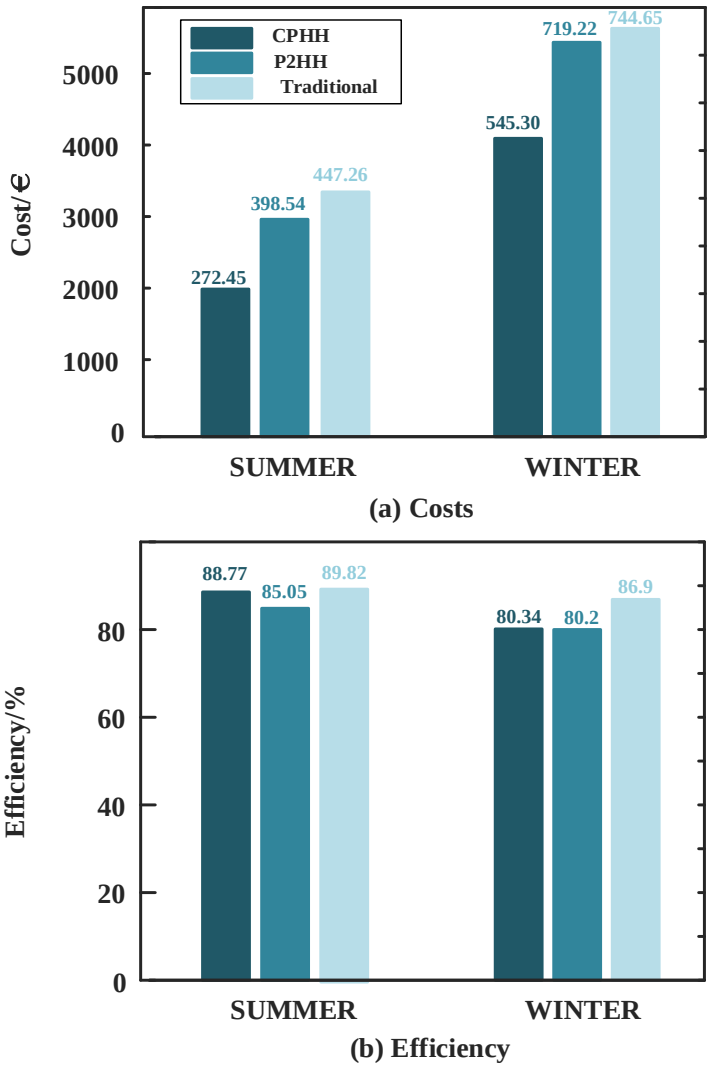

Figure 3- 17 Structures comparison

Figure 3-17(a) shows the operation cost of each structure. It can be concluded that the cost of P2HH is lower than the traditional system, which is also consistent with the conclusion of [26], while the IES

with CPHH further reduces the operation cost. Compared with P2HH, the cost is reduced by 31.6% and 24.2% respectively. Figure 3-17(b) shows the efficiency of three structures. The efficiency of the proposed structure is lower than the traditional structure, while the difference between winter and summer is obviously larger. Similarly, the efficiency difference between the proposed IES and the traditional system is mainly caused by the operation of the CPHH system, and the working time of CPHH in winter is longer, so the efficiency difference between the two systems is greater. Compared with the difference of operation cost, the efficiency difference of each structure is relatively small, hence the IES with CPHH should be the most appropriate choice.

3) Running time

This chapter runs the method with a 2.6GHz i7 CPU and Table IV depicts the results of running time.

According to Table 3-10, as for the first stage of scheduling, the running time in summer and winter is 87.3s and 127.5s respectively and the results indicate that it takes longer to optimize in winter. In the second scheduling stage, the real-time optimization has 96 rolling steps and costs about 1.5 hours in both two cases in total. Furthermore, it costs about 56.6s in summer and 58.5s in winter for each rolling step, the difference between the running time is smaller, and the calculation time of each step is less than 1 min in both cases. Thus, the optimization time is short enough, and this scheduling method is suitable for real-time optimization.

In conclusion, the optimization results of two-stage scheduling and comparative experimental analysis prove the applicability of the structure of island IES, and the two-stage economic scheduling method proposed in this chapter, which provides a basis for the operation of this system.

Table 3- 10 Running time

	Summer Day-ahead	Winter Day-ahead	Summer MPC	Winter MPC
Running Time	87.3s	127.5s	1.51h	1.56h

3.5. Chapter summary

Due to the variety of demands of energy users, a reliable, efficient, and economical IES is needed. Therefore, this chapter proposes the concept of CPHH. Considering the power-heat-hydrogen characteristics of the fuel cell and electrolyzer, the IES with CPHH is built. Then, a two-stage IES

scheduling method is proposed and operated under a typical climate. The first stage completes the global day-ahead optimization by using MILP, while the MPC method is carried out for real-time operation in the second stage. After that, the efficiency, economy, and storage state are discussed in detail which indicates that the proposed method has a lower cost and keeps the storage balance of the storage system. Besides, the scheduling results and analysis indicate that the IES proposed in this chapter is an independent and reliable system. The CPHH system improves the economy of IES with high efficiency compared with other optional structures.

References

[1] J. Yang, N. Zhang, A. Botterud, C. Kang, "On an equivalent representation of the dynamics in district heating networks for combined electricity-heat operation," IEEE T. Power Syst., 35, pp. 560-570, (2020).

[2] Y. Chen, Q. Guo, H. Sun, "Decentralized unit commitment in integrated heat and electricity systems using SDM-GS-ALM," IEEE T. Power Syst., 34, pp. 2322-2333, (2019).

[3] F. M. Benelmir R, "Energy cogeneration systems and energy management strategy," Energ. Convers. Manage., 39, pp. 1791-1802, (1998).

[4] S. Zhou, W. Zhuang, Z. Wu, W. Gu, X. Zhan, Z. Liu, S. Cao, "Optimized Scheduling of Multi-Region Gas and Power Complementary System considering Tiered Gas Tariff, " Energy., https://doi.org /10.1016/j.energy.2019.116677, (2020).

[5] T. O. Jing Yana, "Advanced wind power prediction based on data-driven error correction," Energy Conversion and Management, 180, pp. 302-311, (2019).

[6] Y. Han, N. Wang, M. Ma, H. Zhou, S. Dai, and H. Zhu, "A PV power interval forecasting based on seasonal model and nonparametric estimation algorithm," Sol. Energy, 184, pp. 515-526, (2019).

[7] M. Yang and X. Huang, "Ultra-Short-Term Prediction of Photovoltaic Power Based on Periodic Extraction of PV Energy and LSH Algorithm," IEEE Access, 6, pp. 51200-51205, (2018).

[8] N. Safari, C. Y. Chung and G. C. D. Price, "Novel Multi-Step Short-Term Wind Power Prediction Framework Based on Chaotic Time Series Analysis and Singular Spectrum Analysis," IEEE T. Power Syst., 33, pp. 590-601, (2018).

[9] H. Shuai, J. Fang, X. Ai, W. Yao, J. Wen, and H. He, "On-line energy management of microgrid via parametric cost function approximation," IEEE T. Power Syst., 34, pp. 3300-3302, (2019).

[10] T. Yun, W. Zedi, L. Yan, M. Qian, H. Qian, and L. Shubin, "A multi energy storage system model based on electricity heat and hydrogen coordinated optimization for power grid flexibility," CSEE Journal of Power and Energy Systems, (2019).

[11] X. Jin, J. Wu, Y. Mu, M. Wang, X. Xu, and H. Jia, "Hierarchical microgrid energy management in an office building," Appl. Energ., 208, pp. 480-494, (2017).

[12] J. Vasilj, S. Gros, D. Jakus, and M. Zanon, "Day-Ahead Scheduling and Real-Time Economic MPC of CHP Unit in Microgrid With Smart Buildings," IEEE T. Smart Grid, 10, pp. 1992-2001, (2019).

[13] L. Yang, X. Zhang and P. Gao, "Research on heat and electricity coordinated dispatch model for better integration of wind power based on electric boiler with thermal storage," IET Generation, Transmission & Distribution, 12, pp. 3736-3743, (2018).

[14] M. Tasdighi, H. Ghasemi, A. Rahimi-Kian. "Residential Microgrid Scheduling Based on Smart Meters Data and Temperature Dependent Thermal Load Modeling," IEEE T SMART GRID, 5, pp. 349-57, (2014).

[15] M. Nazari-Heris, B. Mohammadi-Ivatloo, GB. Gharehpetian, M. Shahidehpour. "Robust Short-Term Scheduling of Integrated Heat and Power Microgrids," IEEE SYST J., 13, pp. 3295-303. (2019)

[16] F. Garcia-Torres and C. Bordons, "Optimal Economical Schedule of Hydrogen-Based Microgrids With Hybrid Storage Using Model Predictive Control," IEEE T. Ind. Electron., 62, pp. 5195-5207, (2015).

[17] F. Garcia-Torres, C. Bordons and M. A. Ridao, "Optimal Economic Schedule for a Network of Microgrids With Hybrid Energy Storage System Using Distributed Model Predictive Control," IEEE T. Ind. Electron., 66, pp. 1919-1929, (2019).

[18] W. Gu, Z. Wang, Z. Wu, Z. Luo, Y. Tang, and J. Wang, "An Online Optimal Dispatch Schedule for CCHP Microgrids Based on Model Predictive Control," IEEE T. Smart Grid, 8, pp. 2332-2342, (2017).

[19] GKH. Larsen, ND. van Foreest, JMA. Scherpen, "Distributed MPC Applied to a Network of Households With Micro-CHP and Heat Storage," IEEE T SMART GRID, 5,pp. 2106-14, (2014).

[20] A. Ouammi. "Optimal Power Scheduling for a Cooperative Network of Smart Residential Buildings," IEEE T SUSTAIN ENERG., 7,pp. :1317-26, (2016).

[21] T. Özgür and A. C. Yakaryılmaz, "A review: Exergy analysis of PEM and PEM fuel cell based CHP systems," Int. J. Hydrogen Energ., 43, pp. 17993-18000, (2018).

[22] M. Shahverdi and S. M. Moghaddas-Tafreshi, "Operation optimization of Fuel Cell Power Plant with new method in thermal recovery using particle swarm algorithm,", 2008, pp. 2542-2547.

[23] T. Niknam, A. Kavousi-Fard and A. Ostadi, "Impact of Hydrogen Production and Thermal Energy Recovery of PEMFCPPs on Optimal Management of Renewable Microgrids," IEEE T. Ind. Inform., 11, pp. 1190-1197, (2015).

[24] A. Herrmann, A. Mädlow and H. Krause, "Key performance indicators evaluation of a domestic hydrogen fuel cell CHP," Int. J. Hydrogen Energ., 44, pp. 19061-19066, (2019).

[25] H. Pashaei-Didani, S. Nojavan, R. Nourollahi, and K. Zare, "Optimal economic-emission performance of fuel cell/CHP/storage based microgrid," Int. J. Hydrogen Energ., 44, pp. 6896-6908, (2019).

[26] J. Li, J. Lin, Y. Song, X. Xing, and C. Fu, "Operation Optimization of Power to Hydrogen and Heat (P2HH) in ADN Coordinated With the District Heating Network," IEEE T. Sustain. Energ., 10, pp. 1672-1683, (2019).

[27] S. Zhou, F. Zou, Z. Wu, W. Gu, Q. Hong, C. Booth, "A smart community energy management scheme considering user dominated demand side response and P2P trading, ". Int. J. Ele. Pow. & Energ. Sys., 114. 105378. (2020).

[28] Y. Guo, J. Xiong, S. Xu, and W. Su, "Two-Stage Economic Operation of Microgrid-Like Electric Vehicle Parking Deck," IEEE T. Smart Grid, 7, pp. 1703-1712, (2016).

Chapter 4. Optimal Configuration for Shared Electric-hydrogen Energy Storage for Multiple Integrated Energy Systems with Mobile Hydrogen Transportation

4.1. Introduction

Against the backdrop of energy shortages and increasingly prominent environmental issues, the world is launching the construction of renewable energy and the development of various alternative energy sources. According to IEA estimates, from 2015 to 2022, the installed capacity of photovoltaic will increase by 400% [1], and the installed capacity of renewable energy will continue to increase [2], and multiple energy sources will become more closely linked, forming an energy internet with multiple integrated energy systems (IESs) [3, 4]. However, geographically adjacent IESs have different environmental statuses, power generation, and consumption requirements, resulting in differences in their operational conditions. Hence, IESs can complement and collaborate through information exchange and energy transmission [5].

Energy storage, as a key technology applied in energy production and supply processes, has achieved significant results in enhancing system flexibility and improving renewable energy consumption. With the participation of large-scale energy storage systems, they can not only achieve flexible energy allocation within the IES but also be independent of the IES, utilizing the supply-demand differences of each energy system to provide energy interaction services for them in a region, thereby improving operational independence and efficiency. Under this concept, shared energy storage (SES) has emerged, integrating the supply and demand of various energy systems, participating in energy storage capacity leasing and sharing, and achieving coordinated operation of energy systems within the region [6, 7].

At present, research has mainly focused on battery-based shared energy storage systems, analyzing their configuration and operation issues. An energy-sharing concept for the data center and the sharing energy storage business model is established, and then a multi-objective sizing method is proposed in consideration of battery degradation in [8]. Considering the peak demand reduction and the self-efficiency enhancement, real-time scheduling based on reinforcement learning is provided to share power with the battery, consumer, and power grid in [9]. A stable marriage matching algorithm is applied for the optimal storage resource allocation based on a blockchain-based energy market, and the pricing

of energy storage is designed in this energy trading framework in [10]. To improve the flexibility of coal-fired power plants, a sizing and operation method for a shared energy storage system is proposed in [11]. Aiming at the benefits of different ownership structures, a shared battery sizing method is studied, and three different structures are analyzed in detail under peer-to-peer (P2P) trading mode in [12]. Bi-level programming is applied to fulfill the sizing and operation of the shared energy storage system in the distribution network. Furthermore, the cost and frequency regulation are optimized by applying an energy storage system in [12]. Considering the electricity-oxygen-hydrogen requirements of high-altitude prosumers, energy cooperation with composite energy storage is established, and an asymmetric profit distribution model with the contribution of multiple energy sharing is proposed in [13]. A P2P trading framework is established for the distribution of energy storage sharing, and carbon trading is also considered during the transaction in [14]. For the capacity allocation of sharing energy storage with different renewable energy generations, a planning and scheduling method for shared energy storage systems on the power generation side is proposed, and an evolution algorithm is used for optimal calculation in [15]. Based on the P2P trading, a conditional value at risk-based hybrid optimization method under uncertain conditions is obtained, and the shared energy storage is scheduled based on the economy and stable operation in [16]. A two-stage framework for wind-photovoltaic-shared energy storage based on GIS is proposed, and a fuzzy multi-criteria decision-making method is used for optimal siting in [17]. For the sizing of centralized battery-shared energy storage of residential areas, a virtual power plant-based method for the enhancement of reliability improvement of the distribution network is established in [18]. To facilitate the application of shared energy storage among local integrated energy systems, a two-stage multiple cooperative games-based planning method is proposed in [19].

With the increasing demand for hydrogen and the economic advantages of hydrogen energy storage systems for long-term and cross-season energy storage, hydrogen energy storage is gradually being applied in shared energy storage which contains hydrogen production, storage, and compression equipment. A hydrogen energy storage-based electricity-heat sharing frame is proposed and a distributed robust optimal method is proposed in [20]. An electricity-hydrogen-electricity-based energy-sharing mode is proposed, and a sizing method for hydrogen energy storage is explored in [21]. To analyze the profits of power to hydrogen mode and distribution trading, a shared hydrogen storage-based capacity

planning and scheduling method is considered in [22]. An evolution algorithm-based planning method is studied, and the benefits of sharing hydrogen storage are analyzed in detail in [23].

To sum up, regarding the application of hydrogen energy storage for shared energy storage operation, most of the hydrogen energy system is used as a local energy storage system to achieve large-scale energy storage while the energy sharing is mainly achieved by the electric-hydrogen-electric (E-H-E) process via electrolyzers and fuel cells. However, the E-H-E process will reduce the energy utilization efficiency since the energy utilization of electrolyzer and fuel cells is relatively low when ignoring the heat recovery of the hydrogen energy system. Thus, it is necessary to further explore the transportation and sharing modes of hydrogen energy. In addition, applying game theories is the main concept for the optimization operation of shared energy storage generally, and the solving of the operation mainly relies on genetic algorithms. When configuring the capacity of shared energy storage, considering the optimization of multiple typical days or seasons, an optimization model based on a multi-layer genetic algorithm will be formed, resulting in a significant increase in solution time.

To address these issues, this chapter proposes a transportation-based electric-hydrogen hybrid shared energy storage system and its operator. The SESO can not only provide battery capacity for IESs but also electricity and hydrogen sharing. The electricity and battery capacity sharing can be accomplished by power lines, while the hydrogen sharing is realized by centralized hydrogen storage and the hydrogen trailers via a transportation network. Then, a two-level configuration method is developed for SESO configuration and the transactions between SESO and IESs. For the upper level, an improved grey wolf method is proposed for optimal configuration, for the bottom level, a Stackelberg-based game is established, and a bisection method is provided for fast solving of the optimal trading and operation scheme. Finally, a case study is implemented to analyze the economy and the performance of the proposed SESO and the method. The main works and contributions of this chapter are, firstly, considering both electricity and hydrogen sharing, a hybrid shared energy storage system is established, and a life-cycle cost (LCC) diagram for SESO is established, then, a Stackelberg game is applied to forming the regional trading market for SESO and IESs, and a transportation network is established by roadmap. For hydrogen trading, the trailers are regarded as mobile hydrogen tanks that can not only deliver but also store hydrogen with IESs, finally, to improve the calculation efficiency and accuracy

during configuration, a two-level GWO-bi-sectional method is proposed for SESO sizing and operation based on typical day selection.

4.2. Structure and modeling of SESO and IESs

4.2.1. Topology of the regional energy system

Figure 4-1 describes the topology of the regional energy system. In this region, SESO IESs, and the upper energy market can transport energy to each other. The IESs aim to operate their local system economically and efficiently. Under the various energy production and demand situations, IESs can trade with SESO. The SESO's target is to gain high benefits and increase the energy utilization efficiency within this region, and it can rent battery capacity, and share electricity and hydrogen with IESs, also, SESO can trade with the upper energy market.

Regarding IES, every IES contains various kinds of energy generation, transmission, storage, and consumption facilities. The main energy resources are renewable energy generation, which includes PV and WT. The main energy demanders are the local electric-heat users and also the EVs and fuel cell vehicles (FCVs). Also, the electric energy storage system and hydrogen storage system are established. The hydrogen storage system contains FC, EL, hydrogen tanks, and auxiliary equipment, the hydrogen system can not only provide electricity, but also hydrogen and heat. Also, the heat boiler and air conditioner are modeled for flexible operation. The SESO contains centralized electric energy storage and a hydrogen tank, also, several hydrogen trailers are prepared for energy sharing.

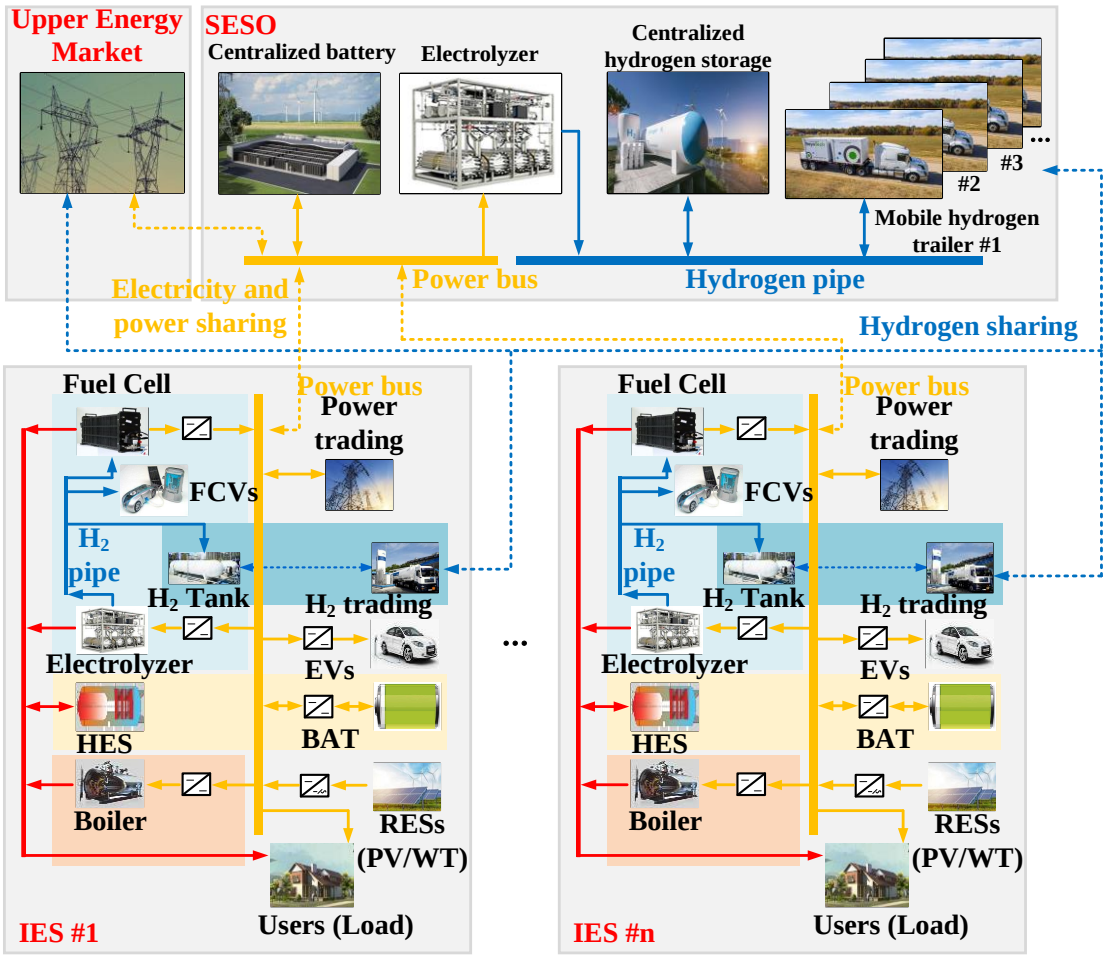

Fig. 4- 1 Topology of the regional energy system

4.2.2. Modeling of IESs

In our previous work in chapter 3, and also my published works in references [24] and [25], the detailed model of IESs is provided, hence this chapter introduce the energy trading part of the IESs.

Since the IES can rent capacity from ESSO, the rented battery and its constraints can be written as follows:

$$0 \le C_{\mathrm{SESO},i,t} \le C_{\mathrm{SESO,rated}} \tag{4.1}$$

$$0 \le C_{\mathrm{SESO},i,t} \le C_{\mathrm{SESO,rated}} \tag{4.2}$$

$$-\mu C_{\mathrm{SESO},i,t} \le P_{\mathrm{SESO},i,t} \le \mu C_{\mathrm{SESO},i,t} \tag{4.3}$$

$$P_{\mathrm{SESO},i,t} = \delta_{\mathrm{cha},i,t} P_{\mathrm{SESO\_cha},i,t} + \delta_{\mathrm{dis},i,t} P_{\mathrm{SESO\_dis},i,t} \tag{4.4}$$

$$\delta_{\mathrm{cha},i,t} + \delta_{\mathrm{dis},i,t} = 1 \tag{4.5}$$

$$soc_{\text{ESSO},i,t} = soc_{\text{ESSO},i,t} + \frac{\sum_{t=1}(P_{\text{SESO\_cha},i,t}\eta_{\text{cha}}\eta_{\text{conv}}\eta_{\text{loss}} + \frac{P_{\text{SESO\_dis},i,t}}{\eta_{\text{dis}}\eta_{\text{conv}}\eta_{\text{loss}}})}{C_{\text{SESO},i,t}} \tag{4.6}$$

$$soc_{\min} \le soc_{\text{ESSO},i,t} \le soc_{\max} \tag{4.7}$$

$$soc_{\text{ESSO},i,t} = soc_{\text{ESSO},i,0} \tag{4.8}$$

where $soc_{\text{ESSO},i,0}$ is the initial value of soc, $C_{\text{seso},i,t}$ is the rent capacity of battery from SESO of ith IES at time slot t, $C_{\text{seso,rated}}$ is the maximum rentable capacity regulated by SESO, μ is the charge-discharge coefficient of shared capacity, $P_{\text{seso},i,t}$ is the power of rent battery, $P_{\text{seso\_cha},i,t}$ and $P_{\text{seso\_dis},i,t}$ are the charging and discharging power of rent battery at time t, this chapter defines the value of $P_{\text{seso\_cha},i,t}$ is positive while the $P_{\text{seso\_dis},i,t}$ is a negative value, $\delta_{\text{seso\_cha},i,t}$ and $\delta_{\text{seso\_dis},i,t}$ are binary variables for indicating the working status of battery, η_{cha} and η_{dis} are the charging and discharging efficiency of battery, and η_{conv} is the efficiency of battery converters, η_{loss} is the losses caused by the transmission by power lines, $soc_{\text{ESSO},i,t}$ is the current state of charge of the rented capacity, $soc_{\min}$ and $soc_{\max}$ is the limits of soc, note that since the capacity is rent from SESO, when the capacity is returned to SESO, the value of soc should be equal with the initial value of soc.

When IES has a surplus or shortage of electricity, IES can sell and purchase electricity through SESO, which can be expressed as:

$$-P_{\text{sell,max}} \le P_{\text{tr},i,t} \le P_{\text{buy,max}} \tag{4.9}$$

$$P_{\text{tr},i,t} = \delta_{\text{buy},i,t}P_{\text{tr\_buy},i,t} + \delta_{\text{sell},i,t}P_{\text{tr\_sell},i,t} \tag{4.10}$$

$$\delta_{\text{buy},i,t} + \delta_{\text{sell},i,t} = 1 \tag{4.11}$$

where $P_{\text{tr},i,t}$ is the value of traded power, $P_{\text{sell,max}}$ and $P_{\text{buy,max}}$ are the maximum value of trade power, $P_{\text{tr\_sell},i,t}$ and $P_{\text{tr\_buy},i,t}$ are the traded electricity at time t, this chapter defines the value of $P_{\text{tr\_buy},i,t}$ is positive while the $P_{\text{tr\_sell},i,t}$ is a negative value, $\delta_{\text{buy},i,t}$ and $\delta_{\text{sell},i,t}$ are binary variables for indicating the trading status.

Since the power traded by IESs and also the power from rent capacity is all transmitted through power lines, the following constraints are set for the operation of SESO and IESs:

$$0 \le \left| P_{\text{tr},i,t} + P_{\text{SESO},i,t} \right| \le C_{\text{lines},i} \tag{4.12}$$

$$\begin{cases} \delta_{\text{buy},i,t} + \delta_{\text{dis},i,t} \le 1 \\ \delta_{\text{sell},i,t} + \delta_{\text{cha},i,t} \le 1 \end{cases} \tag{4.13}$$

where $C_{\text{lines},i}$ is the capacity of the power lines between ith IES and SESO. Eq. (4.12) is to regulate the threshold of total transmitted power, eq. (4.13) is to avoid the IES output and input power with SESO at the same time.

The IESs can also trade hydrogen with SESO through the transportation network. Because the IESs don't have any hydrogen carriers, IESs can send their hydrogen trading request to SESO, which can be obtained as:

$$-m_{\text{sell,max}} \le m_{\text{tr},i,t} \le m_{\text{buy,max}} \tag{4.14}$$

$$m_{\text{tr},i,t} = \delta_{\text{buy\_hy},i,t} m_{\text{tr\_buy},i,t} + \delta_{\text{sell\_hy},i,t} m_{\text{tr\_sell},i,t} \tag{4.15}$$

$$\delta_{\text{buy\_hy},i,t} + \delta_{\text{sell\_hy},i,t} = 1 \tag{4.16}$$

where $m_{\text{tr},i,t}$ is the value of shared hydrogen, $m_{\text{sell,max}}$ and $m_{\text{buy,max}}$ are the maximum value of shared hydrogen, $m_{\text{tr\_sell},i,t}$ and $m_{\text{tr\_buy},i,t}$ are the selling and buying hydrogen at time t, $\delta_{\text{buy\_hy},i,t}$ and $\delta_{\text{sell\_hy},i,t}$ are binary variables for indicating the hydrogen sharing status.

4.2.3. Modeling of SESO

SESO includes centralized electrical and hydrogen storage, mobile hydrogen trailers, and electrolyzers to effectively supplement hydrogen energy. The detailed modeling of the SESO is introduced as follows.

The centralized electric energy storage system is to provide capacity and electricity for IESs and electrolyzers, that is, SESO can provide storage for the flexible operation of IESs and also purchase or sell electricity with IESs to increase the benefits. The capacity of the centralized battery of SESO can be expressed as:

$$0 \le C_{\text{SESO},t} \le C_{\text{SESO}} \tag{4.17}$$

$$C_{\text{SESO},t} = \sum_{i=1}^{n} C_{\text{SESO},i,t} \tag{4.18}$$

where $C_{\text{SESO},t}$ is the total value of rented capacity, C_{SESO} is the capacity of the battery, and n is the number of IESs.

Also, the centralized electric energy storage can charge or discharge power for the flexible scheduling of SESO, which can be expressed as:

$$-\mu(C_{\mathrm{SESO}}-C_{\mathrm{SESO},t})\le P_t\le \mu(C_{\mathrm{SESO}}-C_{\mathrm{SESO},t}) \tag{4.19}$$

$$P_t=\delta_{\mathrm{cha},t}P_{\mathrm{cha},i,t}+\delta_{\mathrm{dis},t}P_{\mathrm{dis},i,t} \tag{4.20}$$

$$\delta_{\mathrm{cha},t}+\delta_{\mathrm{dis},t}=1 \tag{4.21}$$

$$soc_t=soc_{\mathrm{ini}}+\frac{\sum_{t=1}(P_{\mathrm{cha},t}\eta_{\mathrm{cha}}\eta_{\mathrm{conv}}+\frac{P_{\mathrm{dis},t}}{\eta_{\mathrm{dis}}\eta_{\mathrm{conv}}})}{C_{\mathrm{SESO}}-C_{\mathrm{SESO},t}} \tag{4.22}$$

$$soc_{\min}\le soc_t\le soc_{\max} \tag{4.23}$$

where soc_{ini} is the initial value of soc, P_t is the power of battery, $P_{\mathrm{cha},t}$ and $P_{\mathrm{dis},t}$ are the charging and discharging power of the battery at time t, $\delta_{\mathrm{cha},t}$ and $\delta_{\mathrm{dis},t}$ are binary variables for indicating the working status of the battery, soc_t is the current state of charge of the battery.

The power balance of the SESO can be written as:

$$P_t+P_{\mathrm{MAR\_buy},t}+P_{\mathrm{MAR\_sell},t}=\sum_{i=1}^{n}P_{\mathrm{tr},i,t}+P_{\mathrm{el},t} \tag{4.24}$$

where $P_{\mathrm{MAR\_buy},t}$ and $P_{\mathrm{MAR\_sell},t}$ are the purchasing and selling power with upper energy market, $P_{\mathrm{el},t}$ is the power consumption of the electrolyzer.

The shared hydrogen energy storage part includes the centralized hydrogen tank, electrolyzer, and mobile hydrogen trailers. The trailer can be considered as an independent hydrogen tank, which can store or output hydrogen to IESs, the energy market, and SESO. The centralized hydrogen tank can be written as:

$$sohc_t=sohc_{\mathrm{ini}}+\frac{\sum_{t=1}(m_{\mathrm{el},t}-m_{\mathrm{trans},t})}{C_{\mathrm{tank}}} \tag{4.25}$$

$$m_{\mathrm{trans},t}=\sum_{k=1}m_{\mathrm{SESO},k,t} \tag{4.26}$$

$$sohc_{\min}\le sohc_t\le sohc_{\max} \tag{4.27}$$

where $sohc_t$ is the hydrogen storage status of the centralized tank at time t, $sohc_{\mathrm{ini}}$ is the initial value of hydrogen storage, $m_{\mathrm{el},t}$ is the hydrogen production by electrolyzer in kg, $m_{\mathrm{trans},t}$ is the carried hydrogen

by mobile hydrogen trailers, $m_{\mathrm{SESO},k,t}$ is the hydrogen loaded or unloaded with kth mobile hydrogen storage, C_{tank} is the capacity of the tank, $sohc_{\min}$ and $sohc_{\max}$ are the thresholds of $sohc$.

The mobile hydrogen storage system consists of several hydrogen trailers, and its main goal is to achieve hydrogen energy sharing among various energy systems in the region based on transportation networks. When IESs wish to conduct hydrogen trading with SESO, mobile hydrogen storage is dispatched by SESO to load or unload the hydrogen that needs to be traded in IESs. At the same time, mobile hydrogen storage can also be used for hydrogen trading with the upper energy market. It should be noted that traditional delivery of goods using transportation networks usually starts from the manufacturer and loads several goods, distributing them to various destinations along the way. The total amount of goods loaded decreases until all customer needs are met. Unlike the traditional problem of transportation through transportation networks, the mobile hydrogen storage system used in this article can achieve energy storage, rather than just delivering goods through transportation networks. To address this issue, this chapter establishes a mobile hydrogen energy-sharing model as shown below.

A single mobile hydrogen storage can be presented as:

$$sohc_{k,t} = sohc_{\mathrm{ini},k} + \frac{m_{k,t}}{C_{\mathrm{h}}} \tag{4.28}$$

$$0 \le sohc_{k,t} \le 100\% \tag{4.29}$$

where $sohc_{k,t}$ is the $sohc$ of kth mobile hydrogen storage at time t, $sohc_{\mathrm{ini},k}$ is the initial value of $sohc$, $m_{k,t}$ is the loaded or unloaded hydrogen at time t, C_{h} is the maximum capacity of hydrogen storage.

Thus, the delivery of hydrogen can be written as:

$$\sum_{t} m_{k,t} = m_{\mathrm{SESO},k,t} - \sum_{i=1} m_{\mathrm{tr},i,t} \tag{4.30}$$

$$-m_{\max} \sum_{j} \iota_{k,0,j} \le m_{\mathrm{trans},k} \le m_{\max} \sum_{j} \iota_{k,0,j} \tag{4.31}$$

$$-m_{\max} \sum_{j} \iota_{k,0,j} \le m_{k,i} \le m_{\max} \sum_{j} \iota_{k,0,j} \tag{4.32}$$

where $\iota_{k,i,j}$ is the possible route for ith destination to jth destination, $m_{\max}$ is the maximum value a mobile hydrogen storage can load or unload, $m_{k,i}$ is the delivered amount of the hydrogen to ith participator. Note that the location of SESO is set as i=0.

The delivery status of mobile hydrogen storage can be expressed as:

$$T_{\text{truck},i,j} = d_{i,j} / s_{\text{h}} + t_{\text{op}} \tag{4.33}$$

$$\tau_{k,i} = \sum_{j} T_{\text{truck},i,j} \iota_{k,i,j} \tag{4.34}$$

$$m_{k,i} = \sum_{t=1} m_{\text{SESO},k,t} - \sum_{i=1}^{i-1} m_{k,i} \sum_{j} \iota_{k,j,i} \tag{4.35}$$

$$\sum_{i} \iota_{k,i,j} \leq 1 \tag{4.36}$$

$$\sum_{j} \iota_{k,i,j} \leq 1 \tag{4.37}$$

$$\sum_{i} \iota_{k,i,j} = \sum_{j} \iota_{k,i,j} \tag{4.38}$$

$$\iota_{k,i,i} = 0 \tag{4.39}$$

$$\iota_{k,i,j} + \iota_{k,j,i} \leq 1 \tag{4.40}$$

where d_{ij} is the distance of the available path between i and j, v_{truck} is the speed of the trailers, and t_{load} is the loading or unloading time during the hydrogen delivery. $T_{\text{truck},i,j}$ is the minimum time cost from i to j, $\tau_{k,i}$ is the time cost after the mobile hydrogen storage accomplishes its delivery at i. Eq. (4.36)-(4.40) is to regulate the transportation path during operation, the detailed definition can be found in [26].

4.3. Life-cycle cost-based optimal configuration

4.3.1. Life cycle cost of SESO

The configuration aims to achieve the economic construction and operation of SESO. Thus, the investment, operation, and transaction costs need to be included.

$$F_{\text{SESO}} = F_{\text{inv}} + F_{\text{o\&m}} + F_{\text{tra}} \tag{4.41}$$

where F_{SESO} is the total cost of SESO, F_{inv} is the investment cost, $F_{\text{o\&m}}$ is the operation and maintenance cost of SESO, and F_{tra} is the trading cost, which includes the trade cost with the upper energy market and IESs.

The investment cost can be written as follows:

$$F_{\text{inv}} = F_{\text{bat}} + F_{\text{el}} + F_{\text{tank}} + F_{\text{h}} \tag{4.42}$$

$$\begin{cases} F_{\text{bat}} = \lambda C_{\text{SESO}} F_{\text{inv\_bat}} \\ F_{\text{el}} = \lambda C_{\text{el}} F_{\text{inv\_el}} \\ F_{\text{tank}} = \lambda C_{\text{tank}} F_{\text{inv\_h}} \\ F_{\text{h}} = \lambda n_{\text{h}} F_{\text{inv\_bat}} \end{cases} \tag{4.43}$$

$$\lambda = \frac{r(1+r)^{life}}{(1+r)^{life} - 1} \tag{4.44}$$

where F_{bat}, F_{el}, F_{tank}, F_{h} are the annualized investment costs of centralized electric energy storage, electrolyzer, hydrogen tank, and mobile hydrogen storage, λ is the capital recovery factor, C_{el} is the capacity of electrolyzer, n_{h} is the number of mobile hydrogen storage, $F_{\text{inv\_bat}}$, $F_{\text{inv\_el}}$, $F_{\text{inv\_tank}}$, $F_{\text{inv\_h}}$ are the investment costs of centralized electric energy storage, electrolyzer, hydrogen tank, and mobile hydrogen storage, r is the discount rate, life is the service life of SESO.

Since the calculations of the life cycle of the battery and hydrogen energy system are different, for the battery, the life cycle is estimated by cycling life while the life of the electrolyzer is accounted for by operation time. The operation and maintenance cost of SESO can be expressed as:

$$F_{\text{o\&m}} = \sum_{q=1}^{Q} \left\{ n_q \left(\sum_{t=1} \left(F_{\text{op\_bat},t} + F_{\text{op\_el},t} + F_{\text{op\_tank},t} \right) + F_{\text{op\_h}} \right) \right\} \tag{4.45}$$

$$\begin{cases} F_{\text{op\_bat},t} = \dfrac{C_{\text{SESO}} \left| P_t \right|}{L_{\text{SESO}}} \\ F_{\text{op\_el},t} = \delta_{\text{el},t} \left(\dfrac{C_{\text{el}}}{L_{\text{el}}} + C_{\text{m\_el}} \right) \\ F_{\text{op\_tank},t} = \dfrac{C_{\text{tank}} \left| m_{\text{el},t} - m_{\text{trans},t} \right|}{L_{\text{tank}}} \\ F_{\text{op\_h}} = \sum_{k} \left(F_{\text{trans}} \sum_{i} \sum_{j} \iota_{k,i,j} d_{i,j} + F_{\text{del}} \sum_{i} \iota_{k,i,j} \right) \end{cases} \tag{4.46}$$

where q indicates the number of the typical days, Q is the total number of typical days, n_q is the total number of days represented by the qth typical day, $F_{\text{op\_bat},t}$, $F_{\text{op\_el},t}$, $F_{\text{op\_tank},t}$, $F_{\text{op\_h}}$ is the operation and maintenance costs of centralized electric energy storage, electrolyzer, hydrogen tank and mobile hydrogen storage separately, L_{SESO}, L_{el} and L_{tank} is the life of centralized battery, electrolyzer and tank. $\delta_{\text{el},t}$ is the binary variable indicating the working status of the electrolyzer, $C_{\text{m\_el}}$ is the maintenance cost

of the electrolyzer, F_{trans} is the transportation cost per km, F_{del} is the departure cost, note that for the mobile hydrogen storage, the operation cost is related to the travel distances, not the time.

The energy and capacity transactions of SESO include the trade with IES and the upper energy market, which can be written as:

$$F_{\text{tra}} = \sum_{q=1}^{Q} \left\{ n_q \sum_{t=1} \left(\sum_{i=1} F_{\text{IES},i,t} + F_{\text{MAR},t} \right) \right\} \tag{4.47}$$

$$F_{\text{IES},i,t} = -c_{\text{ESSO},t} C_{\text{SESO},i,t} + c_{\text{buy\_e},t} P_{\text{tr\_sell},i,t} + c_{\text{sell\_e},t} P_{\text{tr\_buy},i,t} + c_{\text{buy\_h},t} m_{\text{tr\_sell},i,t} + c_{\text{sell\_h},t} m_{\text{tr\_buy},i,t} \tag{4.48}$$

$$F_{\text{MAR},t} = c_{\text{MARsell\_e},t} P_{\text{MAR\_sell},t} + c_{\text{MARbuy\_e},t} P_{\text{MAR\_buy},t} + c_{\text{MARsell\_h},t} m_{\text{MAR\_sell},t} + c_{\text{MARbuy\_h},t} m_{\text{tr\_buy},t} \tag{4.49}$$

where $c_{\text{ESSO},t}$, $c_{\text{sell\_e},t}$, $c_{\text{buy\_e},t}$, $c_{\text{sell\_h},t}$, $c_{\text{buy\_h},t}$ are the capacity renting cost, electricity selling cost, electricity purchasing cost, hydrogen selling cost, and buying cost separately, $c_{\text{MARsell\_e},t}$, $c_{\text{MARbuy\_e},t}$, $c_{\text{MARsell\_h},t}$, $c_{\text{MARbuy\_h},t}$ are the electricity selling cost, electricity purchasing cost, hydrogen selling cost and buying cost with upper energy market separately, $m_{\text{MARsell},t}$ and $m_{\text{MARbuy},t}$ are the selling and purchasing amount of hydrogen from energy market.

4.3.2. Stackelberg game-based optimal operation

The energy market in this region mainly includes IESs as prosumers, as well as SESO which connects with IESs and higher-level energy markets. SESO is the only channel for the region to connect with the upper energy market. Each IES can interact with SESO for energy and also lease energy storage capacity from SESO to achieve system optimization operation. SESO earns profits by leasing energy storage capacity from IESs and trading with IESs and the energy market, where electricity can be transmitted and traded through power lines, while hydrogen can be shared through mobile hydrogen storage. Therefore, the energy trading problem in a region can form a Stackelberg game problem, where SESO acts as a leader to set energy prices in the regional energy market, while IESs participate in energy trading based on the prices set by SESO, assuming their own optimal operation.

The operation in a day of the SESO under a determined capacity is to maximize its benefits after receiving the strategies of IESs:

$$f_{\mathrm{SESO}} = \min\left(\sum_{t=1}\left(F_{\mathrm{op\_bat},t} + F_{\mathrm{op\_el},t} + F_{\mathrm{op\_tank},t} + \sum_{i=1}\left(F_{\mathrm{IES},i,t} + F_{\mathrm{MAR},t} \right) \right) + F_{\mathrm{op\_h}} \right) \tag{4.50}$$

where f_{ESSO} is the operation cost within a day.

While the target of the IES is to lower its operation cost by receiving the price information from SESO and thereby renewing its trading strategy. The cost function of the IES is written as:

$$f_{\mathrm{IES},i} = \min\left(\sum_{t=1}\left(F_{\mathrm{IES\_op},i,t} - F_{\mathrm{IES},i,t} \right) \right) \tag{4.51}$$

where $f_{\mathrm{IES},i}$ is the total cost of ith IES in a day, $f_{\mathrm{IES\_op},i,t}$ is the operation cost of the IES, which can be calculated by [27].

4.3.3. Two-level optimal configuration method

In order to ensure maximum profit for SESO during operation, its lifecycle cost should be optimal. Therefore, the problem can be decomposed into two parts: optimizing its daily operating costs and optimizing the entire lifecycle cost based on the daily operating results. In the configuration process, alternative SESO configuration schemes are obtained through the set algorithm. Under this configuration scheme, SESO optimization scheduling is carried out for regional energy market optimization problems considering different typical days. Then, the daily operating cost and system configuration cost are added up to obtain the system's life cycle cost. Mostly, the daily operation based on Stackelberg game theory is accomplished by an evolution approach when the operation status of several typical days is required. However, once a two-layer genetic algorithm is deployed, the calculation time for optimizing a complex energy system is long, and the performance of the method is hard to guarantee. Therefore, this chapter adopts a genetic algorithm based on GWO-SCA and a daily operation optimization method based on fast bi-sectional optimization to implement optimized configuration.

In this configuration method, GWO-SCA is the upper-level algorithm, whose main purpose is to find the optimal configuration solution within the set capacity range. During the optimization process, the upper-level method transfers alternative solutions to the lower level for solution. The lower-level solution is a bi-sectional method based on Stackelberg game theory. Under the determined capacity

scheme, considering the energy trading strategy of SESO and IESs, the daily operation optimization of SESO is achieved, and the daily operation cost is returned to the upper-level algorithm. Then, the upper-level algorithm calculates the entire lifecycle cost of SESO and compares it with other optional solutions, to find optimized configuration solutions through multiple iterations.

1. Upper-level algorithm

The upper level adopts an improved grey wolf algorithm for capacity allocation to find the optimal configuration scheme for the capacities of centralized electric energy storage, centralized hydrogen storage, electrolyzer, and the number of mobile hydrogen storage. Thus, the set of schemes can be expressed as:

$$\mathbf{S} = \left[\mathbf{C}_{\mathrm{SESO}}, \mathbf{C}_{\mathrm{tank}}, \mathbf{C}_{\mathrm{el}}, \mathbf{n}_{\mathrm{h}}\right] \tag{4.52}$$

And the process of the optimal configuration can be shown as follows:

1) Get the environment data and local loads of different IESs and calculate the power generation and consumption of each IES in a whole year.

2) Typical days selection by using the self-organized map (SOM) method [28].

3) Initialize the number of populations θ, maximum iterations n_{maxit}, and the thresholds of the configuration. Thus, the **S** can be formed as a $\theta \times 4 \times n_{\mathrm{maxit}}$ matrix.

4) Randomly generate sizing schemes **S**.

5) Input the generated schemes of the **S** into the lower level of the bi-sectional algorithm to solve the scheduling problem and get the operation and trading cost of the SESO under different typical days.

6) Calculate the life cycle cost and compare it with the existing optimal results F_α, F_β and F_γ, (note that $F_\alpha < F_\beta < F_\gamma$, and the values α, β and γ indicate the position of the optimal solution in current iterations). If the result is better than one of these results, replace the results with the current solution and update the position of **S**.

7) Update indicator v, this indicator marks the process of the iterations, which can be expressed as:

$$\nu=\begin{cases}2-\sin\left(\dfrac{\pi}{2}\dfrac{n_{\max it}}{n_{\max it}}\right) & 0<\dfrac{n_{\max it}}{n_{\max it}}\le 0.5\\ 1+\cos\left(\dfrac{\pi n_{\max it}}{n_{\max it}}\right) & 0.5<\dfrac{n_{\max it}}{n_{\max it}}\le 1\end{cases} \tag{4.53}$$

where $n_{\max it}$ is the maximum iteration set in the algorithm, n_{it} is the number of current iterations.

8) Generate a set of 3×2 0~1 random matrix $\boldsymbol{\Xi}$.

9) Update the position of **S**. The update method is:

$$\begin{aligned}&S_{n_{it}+1,p,q}=S_{n_{it},p,q}+\frac{s_{1,p,q}+s_{2,p,q}+s_{3,p,q}}{3}\\&\text{s.t.}\quad 1\le p\le\theta \qquad 1\le p\le 4\end{aligned} \tag{4.54}$$

$$\begin{cases}s_{1,p,q}=S_{n_{it},\alpha,q}-\nu(2\boldsymbol{\Xi}_{1,1}-1)\left|2\boldsymbol{\Xi}_{1,2}S_{n_{it},\alpha,q}-S_{n_{it},p,q}\right|\\ s_{2,p,q}=S_{n_{it},\beta,q}-\nu(2\boldsymbol{\Xi}_{2,1}-1)\left|2\boldsymbol{\Xi}_{2,2}S_{n_{it},\beta,q}-S_{n_{it},p,q}\right|\\ s_{3,p,q}=S_{n_{it},\gamma,q}-\nu(2\boldsymbol{\Xi}_{3,1}-1)\left|2\boldsymbol{\Xi}_{3,2}S_{n_{it},\gamma,q}-S_{n_{it},p,q}\right|\end{cases} \tag{4.55}$$

where $S_{n_{it}+1,p,q}$ is the updated elements of **S**, $S_{n_{it},p,q}$ is the configuration scheme of the current iteration, $s_{1,p,q}$, $s_{2,p,q}$, $s_{3,p,q}$ are the updated indicators related to the current position of three optimal solutions, $S_{n_{it}+1,\alpha,q}$, $S_{n_{it}+1,\beta,q}$ and $S_{n_{it}+1,\gamma,q}$ are the optimal position of the qth elements.

10) Repeat steps 5)-9) until the maximum iteration is reached.

2. Lower-level algorithm

In the lower level of the method, a Stackelberg game is processed after receiving the configuration scheme. In this game, IESs submit energy-sharing strategies to SESO based on their own operating conditions and energy-sharing prices. After receiving the strategies, SESO reformulates energy sharing prices to maximize its own interests. After multiple iterations, SESO's pricing and IESs' strategy set will gradually converge and achieve transaction agreements. Then, SESO delivers energy to IESs according to the agreed energy-sharing strategy, and IESs trade at the prices set by SESO. In general, this type of game problem can be solved through genetic algorithms or using KKT conditions. However, for the KKT condition, due to the presence of binary variables, it is difficult to transform the two-layer problem

into a single-layer problem [29]. In addition, due to the use of data from multiple typical days for separate solutions during system optimization configuration, using genetic algorithms will greatly increase calculation time. Thus, this chapter proposes a bi-sectional pricing algorithm for fast solving. The steps of the algorithm are:

1) Get the configuration scheme and the data of typical days from the upper level.

2) Initialize the tolerance and iteration number, the set of energy prices **Φ**, and the thresholds of the prices **Ψ**.

$$\mathbf{\Phi}_t = \left[c_{\mathrm{ESSO},t} \;\; c_{\mathrm{buy\_e},t} \;\; c_{\mathrm{sell\_e},t} \;\; c_{\mathrm{buy\_h},t} \;\; c_{\mathrm{sell\_h},t} \right] \tag{4.56}$$

$$\mathbf{\Psi} = \begin{bmatrix} \overline{c}_{\mathrm{ESSO},t} & \overline{c}_{\mathrm{buy\_e},t} & \overline{c}_{\mathrm{sell\_e},t} & \overline{c}_{\mathrm{buy\_h},t} & \overline{c}_{\mathrm{sell\_h},t} \\ \underline{c}_{\mathrm{ESSO},t} & \underline{c}_{\mathrm{buy\_e},t} & \underline{c}_{\mathrm{sell\_e},t} & \underline{c}_{\mathrm{buy\_h},t} & \underline{c}_{\mathrm{sell\_h},t} \end{bmatrix} \tag{4.57}$$

$$\begin{cases} \underline{c}_{\mathrm{ESSO},t} \le c_{\mathrm{ESSO},t} \le \overline{c}_{\mathrm{ESSO},t} \\ \underline{c}_{\mathrm{buy\_e},t} \le c_{\mathrm{buy\_e},t} \le \overline{c}_{\mathrm{buy\_e},t} \\ \underline{c}_{\mathrm{sell\_e},t} \le c_{\mathrm{sell\_e},t} \le \overline{c}_{\mathrm{sell\_e},t} \\ \underline{c}_{\mathrm{buy\_h},t} \le c_{\mathrm{buy\_h},t} \le \overline{c}_{\mathrm{buy\_h},t} \\ \underline{c}_{\mathrm{sell\_h},t} \le c_{\mathrm{sell\_h},t} \le \overline{c}_{\mathrm{sell\_h},t} \end{cases} \tag{4.58}$$

where $\overline{c}_{\mathrm{ESSO},t}$, $\overline{c}_{\mathrm{buy\_e},t}$, $\overline{c}_{\mathrm{sell\_e},t}$, $\overline{c}_{\mathrm{buy\_h},t}$, $\overline{c}_{\mathrm{sell\_h},t}$ are the upper limits of the energy prices, $\underline{c}_{\mathrm{ESSO},t}$, $\underline{c}_{\mathrm{buy\_e},t}$, $\underline{c}_{\mathrm{sell\_e},t}$, $\underline{c}_{\mathrm{buy\_h},t}$, $\underline{c}_{\mathrm{sell\_h},t}$ are the lower limits of the energy prices.

3) Based on the price set **Φ** and the data of typical days, IESs calculate their strategy set **X** by eq. (4.50) by MILP solver.

$$\mathbf{X}_{i,t} = [C_{\mathrm{SESO},i,t}, P_{\mathrm{tr\_sell},i,t}, P_{\mathrm{tr\_buy},i,t}, m_{\mathrm{tr\_sell},i,t}, m_{\mathrm{tr\_buy},i,t}] \tag{4.59}$$

4) Based on the strategy, SESO updates **Φ** by eq. (4.56) by solving a MILP problem.

5) Calculate the price tolerance of the two iterations, if the tolerance meets the requirement, end the algorithm and send the cost of SESO to the upper level.

6) Update the thresholds of the energy prices.

7) Repeat steps 3)-6) until the tolerance is small enough.

The detailed flowchart of the method is shown in Figure 4-2 and the calculations of the thresholds of the energy prices are introduced in this figure.

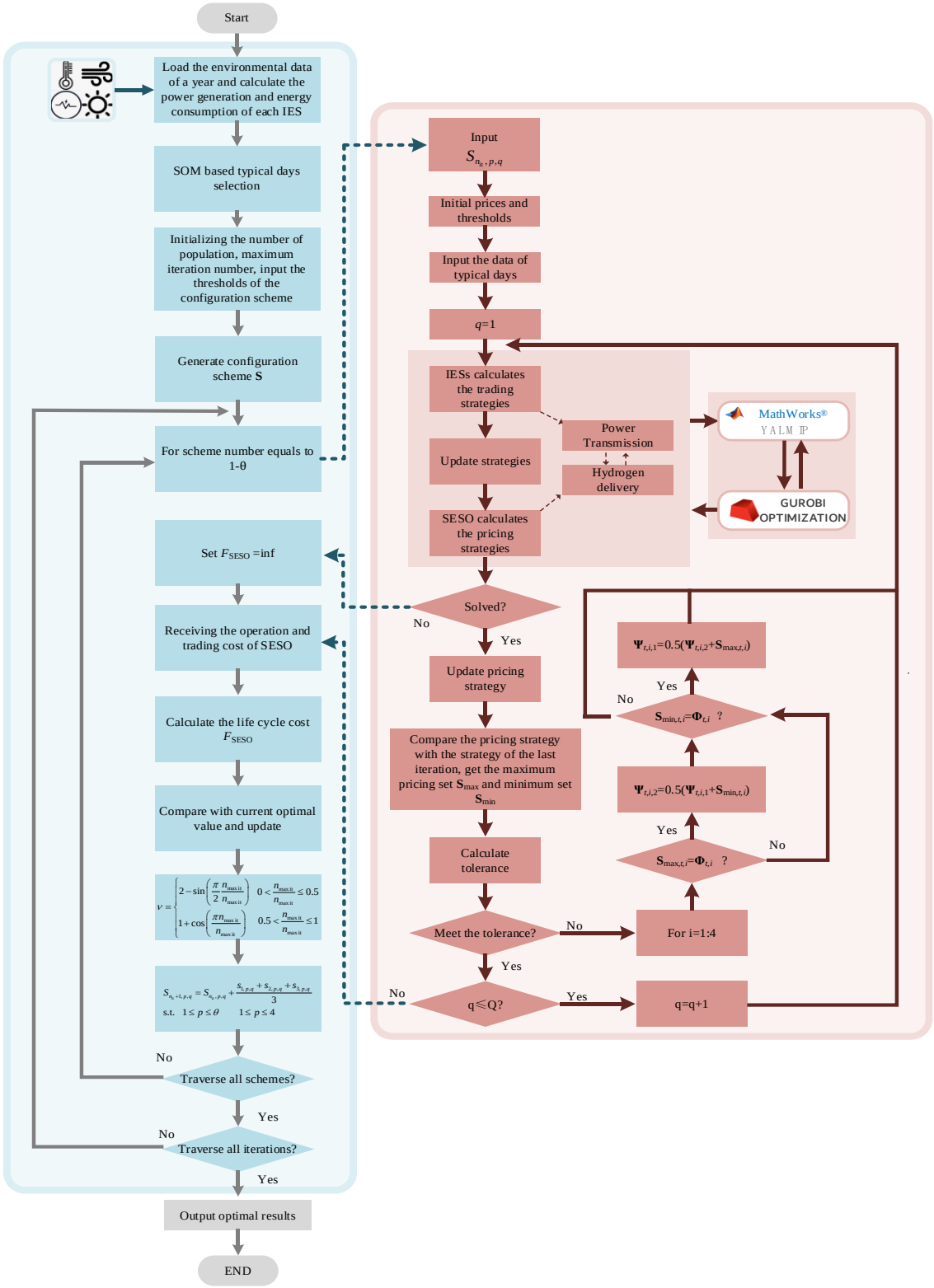

Figure 4- 2 Flowchart of the two-level optimal configuration method

4.4. Case study

A region located in eastern France is used for the configuration of the SESO. Note that the hydrogen energy is shared by the mobile hydrogen storages, which can load and unload hydrogen for every energy system via road. For the two-level method proposed in this chapter, the programming is based on Matlab, and the solving of the MILP problem when IESs and SESO update their strategies is accomplished by Yalmip/Gurobi software, and this case is run by a laptop with intel i7 core with 16 GB RAM. By using the SOM method for typical days selection, four days are selected for the optimal configuration. And the output power of PV, WT, the demands of local loads and the EVs, the ambient temperature, and the hydrogen demand of FCVs of each IES are shown in Figure 4-3. Note that the heat demand of local users is calculated by the temperature and the data of the area, thus this chapter didn't provide the detailed curves in the figure. Table 4-1 shows the economic parameters used in the SESO configuration, and the capacity of the mobile hydrogen storage is set to 300kg, and the moving speed is 60km/h. The geographical data of the IESs and SESO is shown in Figure 4-4.

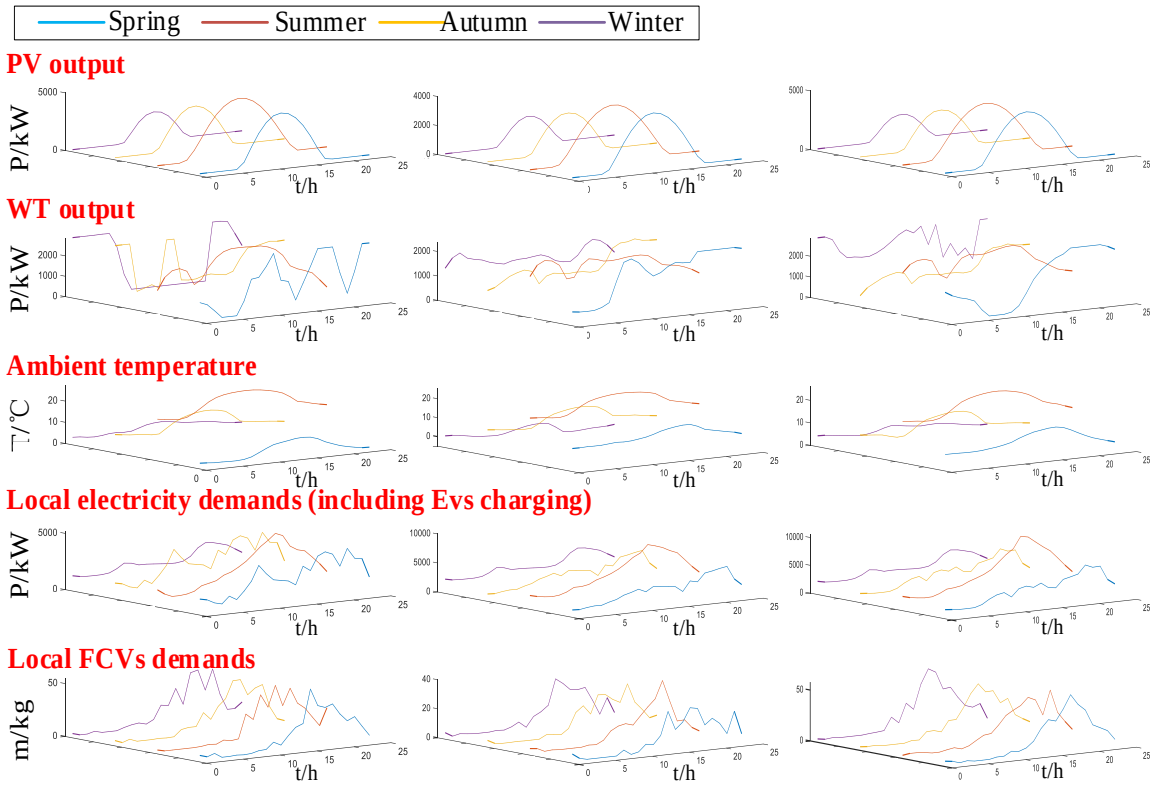

(1) Typical days of IES Besançon

(2) Typical days of IES Dijon

(3) Typical days of IES Langres

Fig. 4- 3 Data of typical days

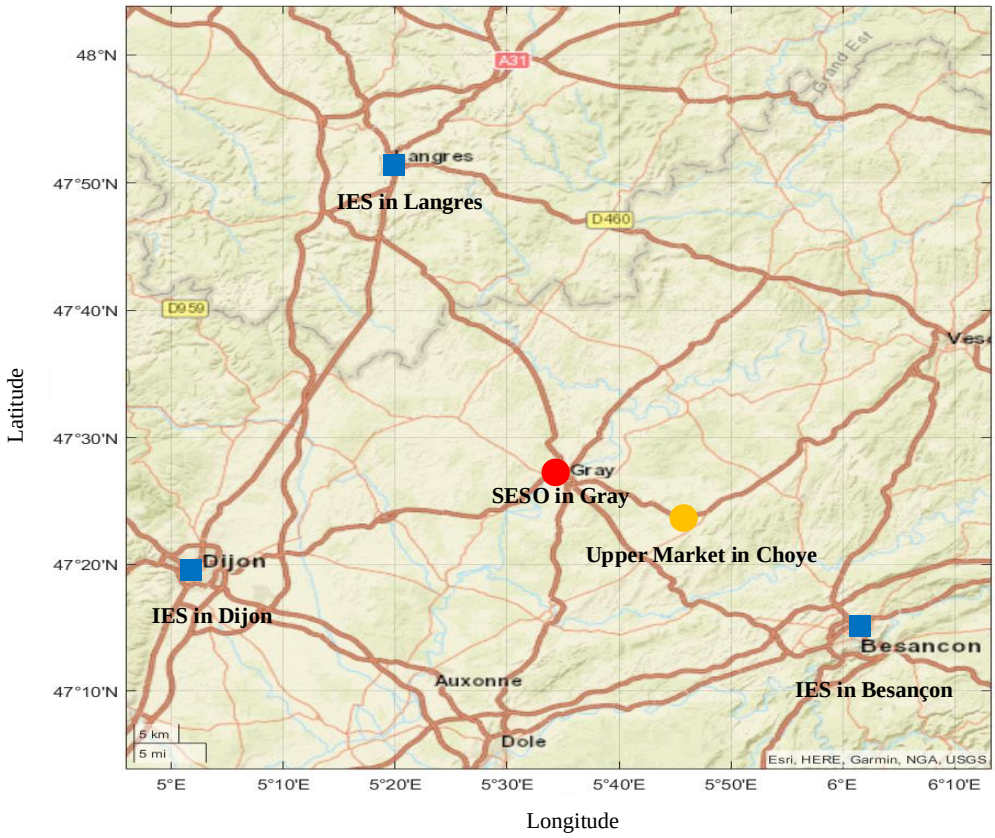

Figure 4- 4 Location of the studied energy systems

Table 4- 1 SESO parameter settings

Parameters	Value	Parameters	Value
F_{inv_bat}(€/kWh)	140.74	F_{inv_tank}(€/Nm^3)	38.15
F_{inv_el}(€/kW)	1222.08	F_{inv_h}(€/vehicle)	38734.67
r	0.067%	$life$ (yr)	20

4.4.1. Configuration and operation results

After obtaining the renewable energy generation power and load demands by SOM of each IES and the geographical location of IESs, SESO, and the upper energy market by the geographic information system (GIS), the proposed GWO-SCA-bi-sectional method is used to solve the capacity of each part of SESO, and the optimized configuration results are shown in Table 4-2.

Table 4- 2 Configuration results of SESO

Parameters	Capacity

C_{SESO}(kWh)	6000.59
C_{el}(kW)	2850.00
C_{tank}(Nm^3)	7802.67
n_h	4

To further analyze the operation of multiple energy systems in this region, Figures 4-5 to 4-9 depict the mobile hydrogen storages operation of SESO, the energy storage rental capacity and charging and discharging power of each IES, as well as the electricity trading and balance status of SESO.

Figure 4-5 illustrates the operation results of mobile hydrogen storage under four typical days. The left side of each subgraph shows the routes of mobile hydrogen storage in the transportation network and the loading and unloading status of hydrogen, while the right side shows the specific time for loading and unloading hydrogen and the hydrogen storage capacity of each mobile hydrogen storage.

From Figure 4-5(a), there are three mobile hydrogen storage units participating in hydrogen energy sharing. According to Figure 4-5, each mobile hydrogen storage unit is loaded with hydrogen produced by the electrolyzer of SESO when departing from SESO, which is sold to IESs and energy markets to earn profits. On this typical day, only IES Besançon requires a hydrogen energy supply, which is caused by the low renewable power generation in spring and relatively high hydrogen and electricity demand. From the perspective of hydrogen energy demand, IES Besançon obtained 97.11kg of hydrogen, IES Dijon sold 312.69kg of hydrogen, and IES Langres sold 11.39kg of hydrogen.

Figure 4-5(b) shows the operation of the mobile hydrogen storage on typical summer days. According to Figure 4-3, the local load of each IES further increases in summer, and due to the insufficient renewable power generation of IES Langres, the mobile hydrogen storages deliver 575.27kg of hydrogen to Langres. IES Dijon also has a large demand for hydrogen due to the lack of wind power generation in summer, and a total of 284.54kg of hydrogen is obtained from mobile hydrogen storage. However, the increase in photovoltaic power generation of IES Dijon guarantees its energy demand, and surplus hydrogen with a total of 48.58kg is sold to support the energy supply of other energy systems. But still, the insufficient hydrogen production of SESO causes a 143.27kg order of hydrogen from the upper market. In the summer, all four mobile hydrogen storage systems are in operation because of the massive demand and production of hydrogen. Figure 4-5(c) shows the operation of autumn day. During

this typical day, IES Dijon has no demand from outside for hydrogen energy due to its relatively balanced energy production and demand. At the same time, due to the decrease in renewable power generation, the other two IESs have a certain demand for hydrogen. With SESO's hydrogen production and a small number of market hydrogen purchases, the hydrogen energy demand in the entire region is met, and only one mobile hydrogen storage is needed for operation.

Figure 4-5(d) shows the operation of mobile hydrogen storage on typical winter days. On this typical day, due to the abundant wind power resources, IES Langres produced additional hydrogen while meeting the system's own energy needs and shared it through a mobile hydrogen storage system. IES Dijon and IES Besançon have a hydrogen demand of 230.23kg and 162.22kg. Currently, SESO is still producing hydrogen during the low electricity price period to achieve hydrogen energy supply in the region and selling a small amount of surplus hydrogen to the upper energy market. In total, through the effective planning of four shared hydrogen energy storage systems, hydrogen energy sharing among various energy systems can be achieved, improving the flexible operation of IESs.

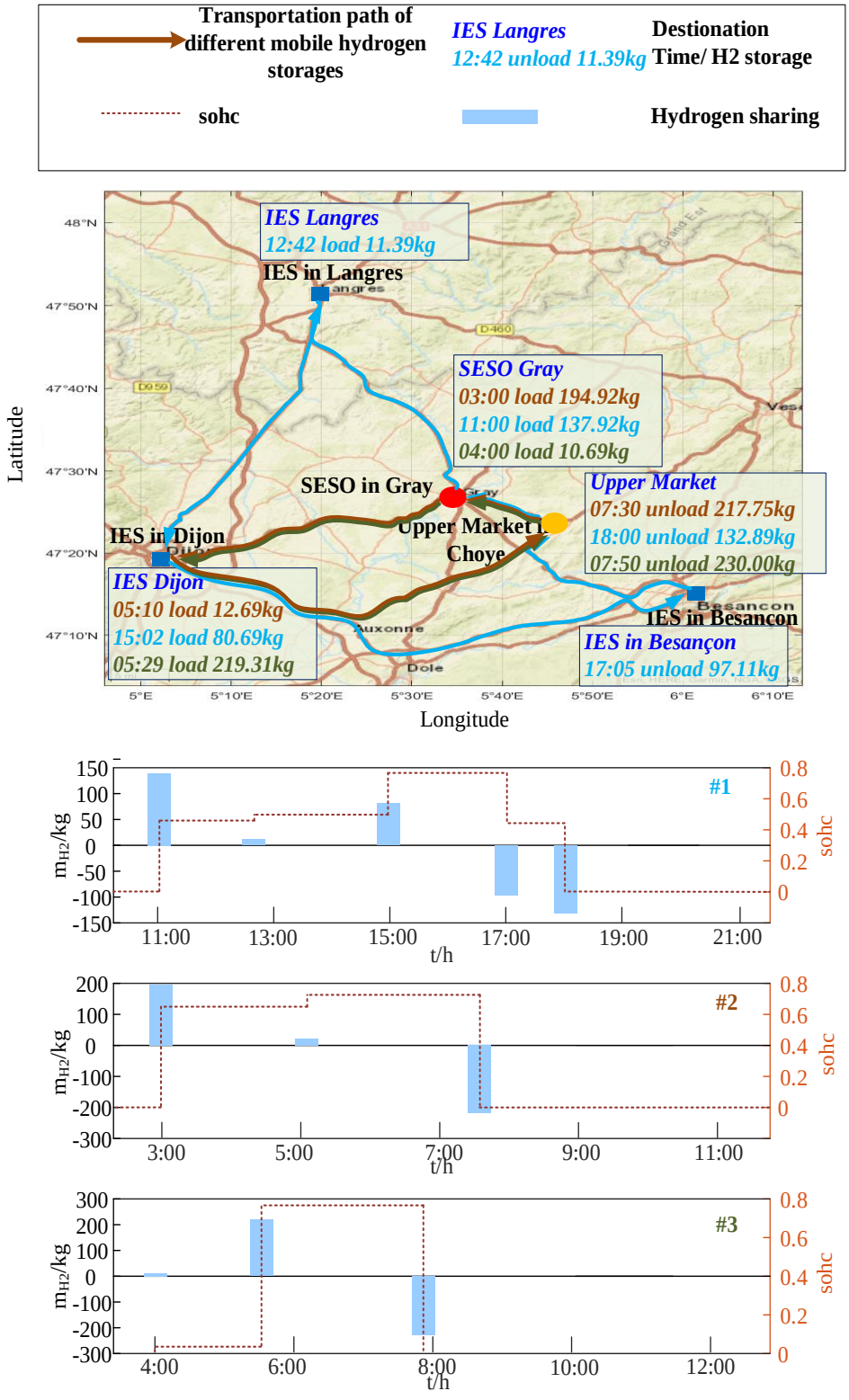

(a) Mobile hydrogen sharing in spring

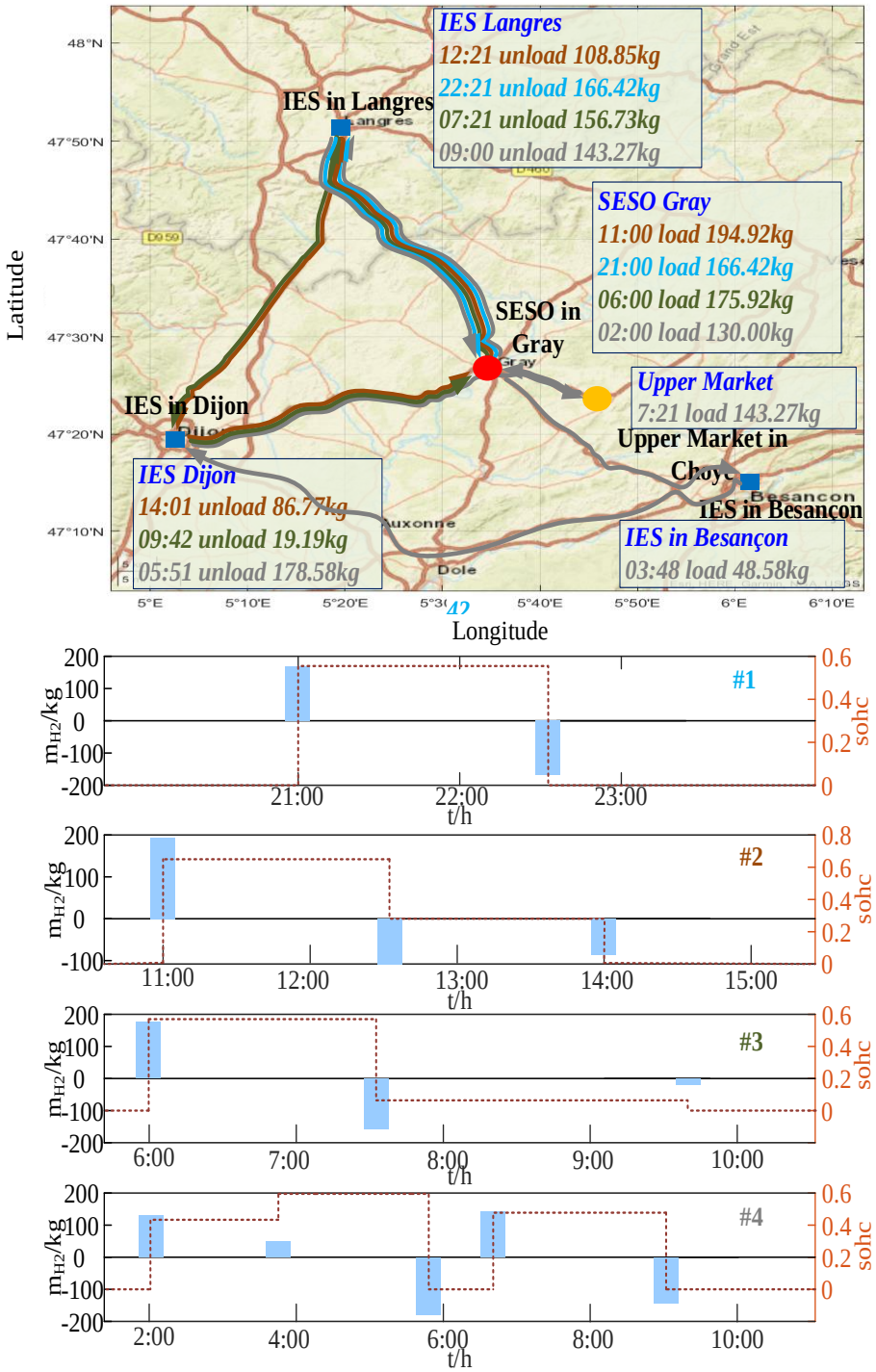

(b) Mobile hydrogen sharing in summer

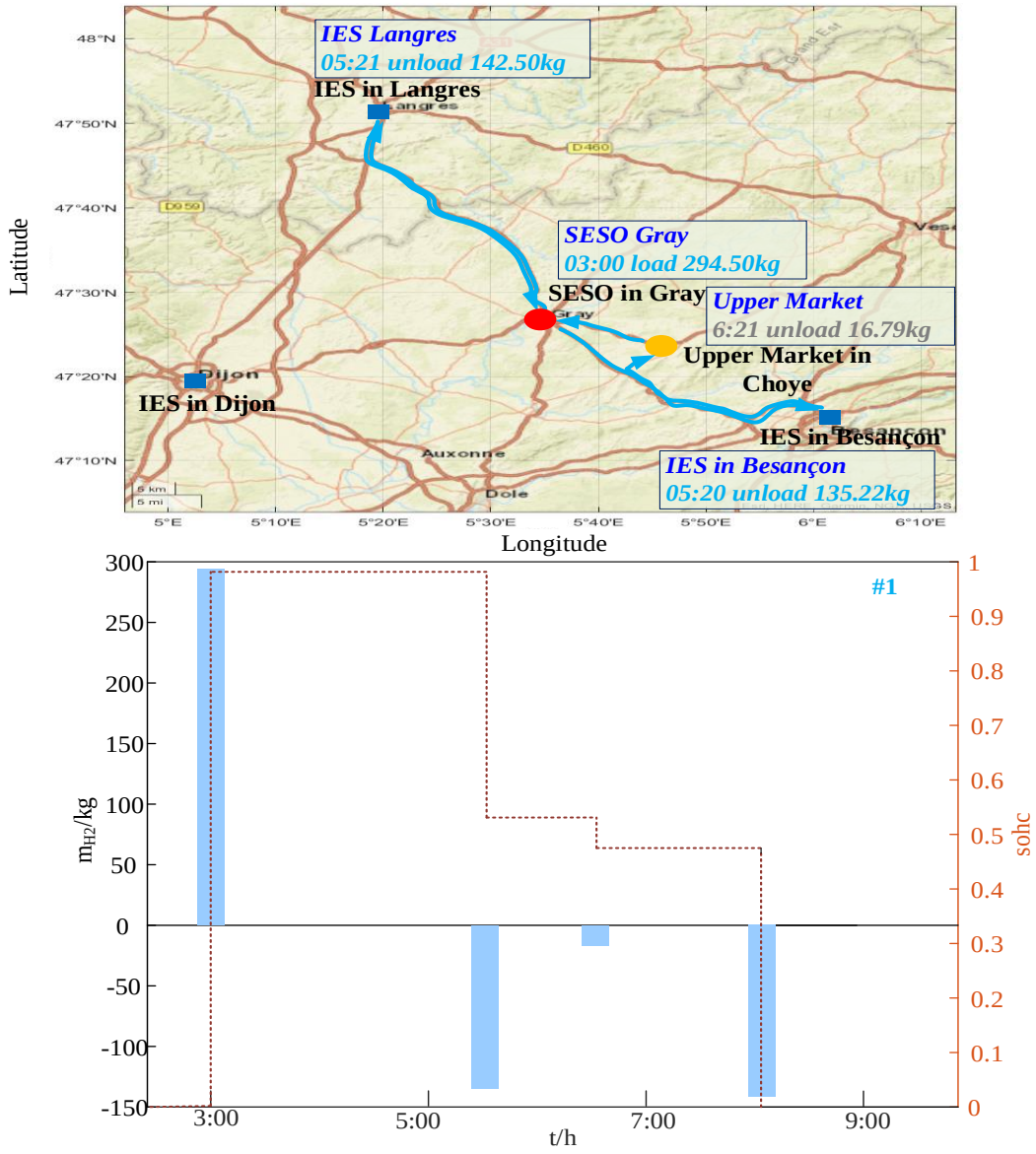

(c) Mobile hydrogen sharing in autumn

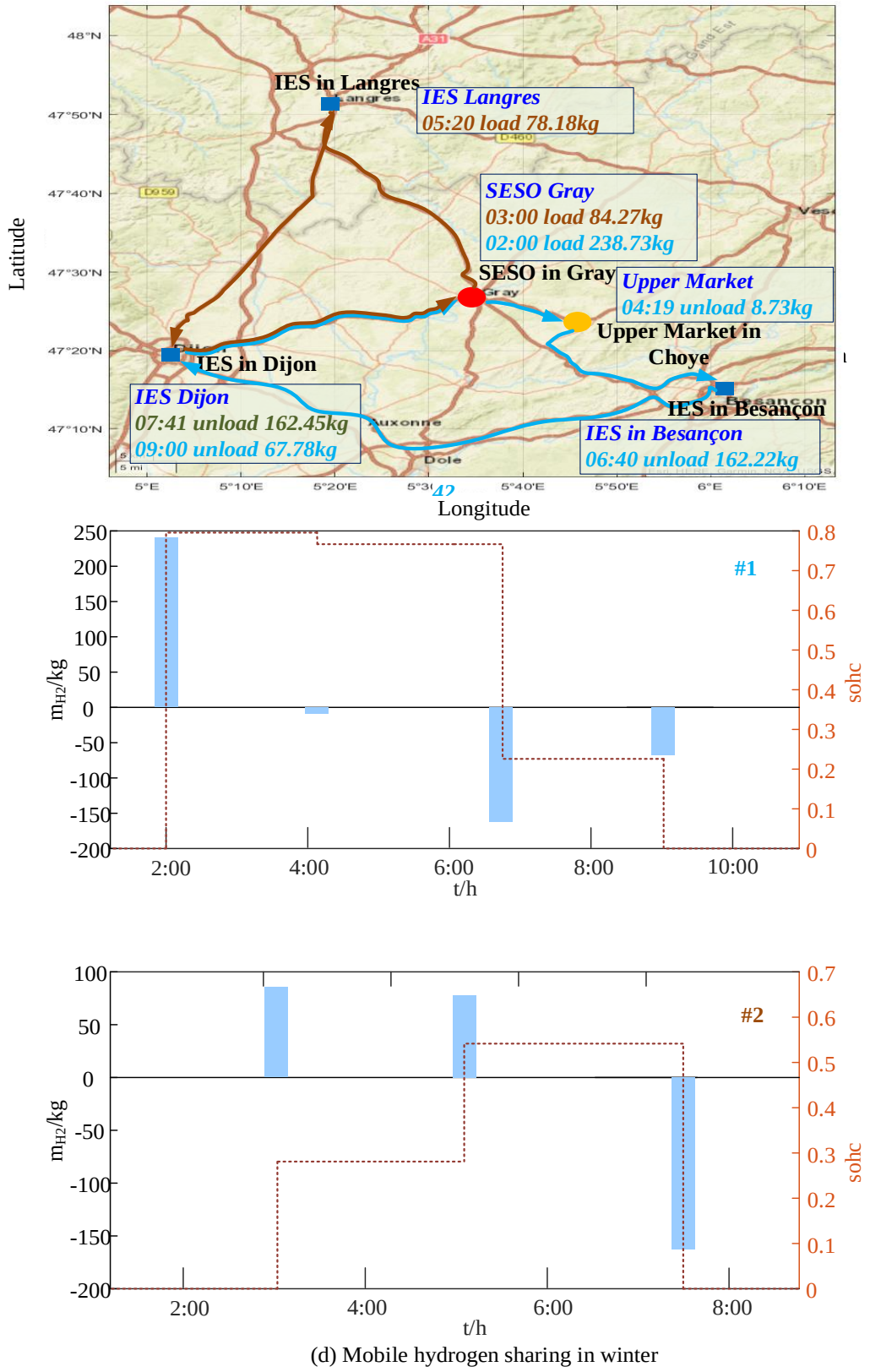

(d) Mobile hydrogen sharing in winter

Figure 4- 5 Operation of mobile hydrogen storages.

Figures 4-6 to 4-8 show the centralized energy storage capacity leasing situation and the charging and discharging power of shared capacity for each IES on typical days and IESs renting energy storage based

on its own needs during various typical days. Figure 4-6 shows the shared energy storage usage of IES Besançon. It is known that IES Besançon only rented capacity in autumn and winter. In autumn, IES Besançon uses shared energy storage charging during the day to absorb excess renewable energy generation, while discharging at night to support power load demand. In winter, the storage rented by IES Besançon is more flexible.

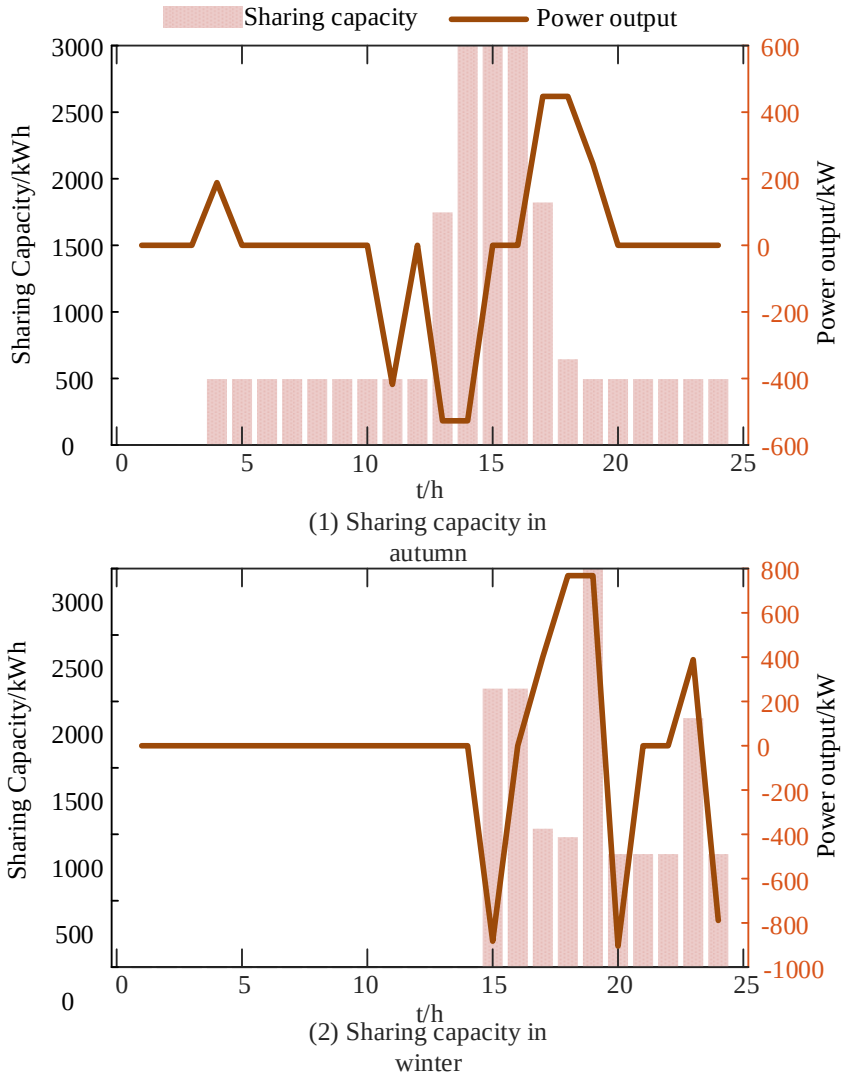

Figure 4- 6 Capacity sharing for IES Besançon

Figure 4-7 shows the capacity and operating results of IES Dijon's leased shared energy storage. In summer, the shared energy storage of IES Dijon mainly charges from 14:00 to 16:00 and discharges from 17:00 to 24:00 to achieve flexible operation of the system. In typical autumn days, shared energy storage operates more frequently at night to balance wind power fluctuations.

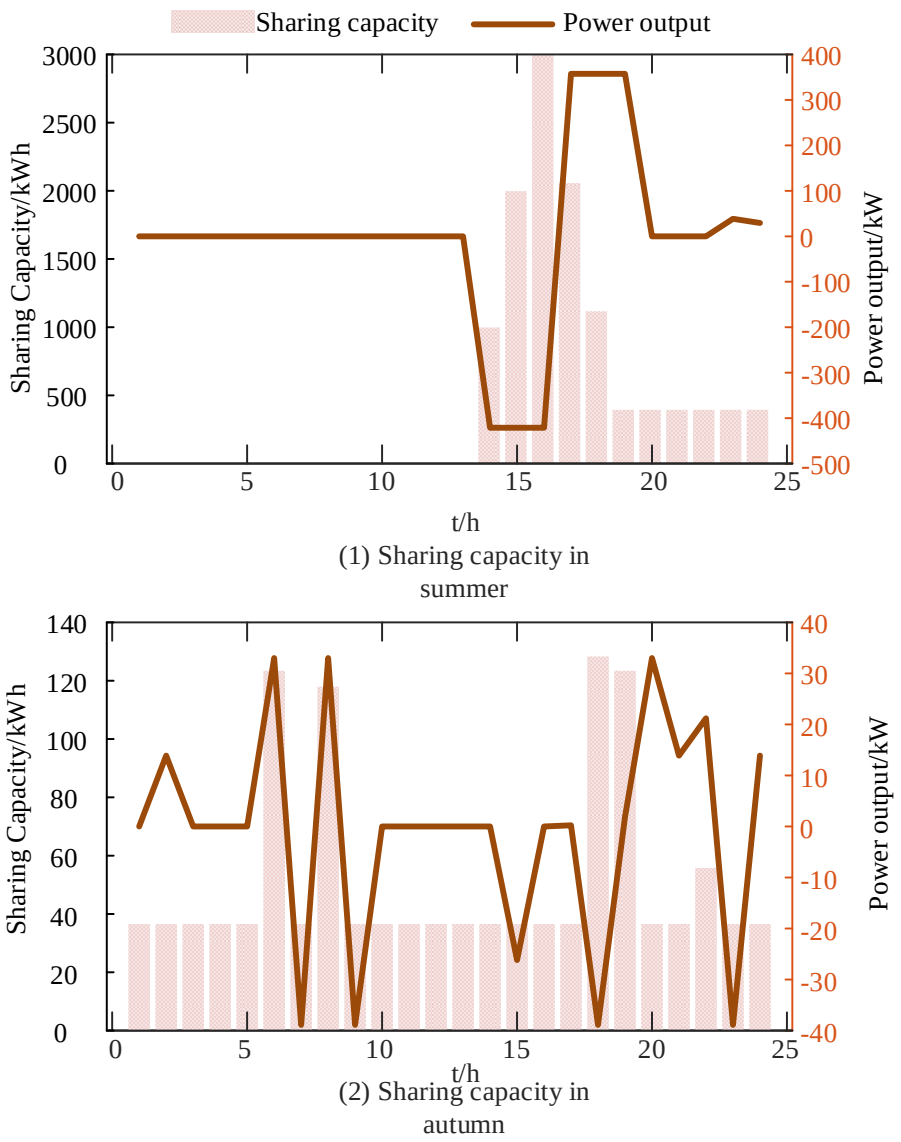

Figure 4- 7 Capacity sharing for IES Dijon

Figure 4-8 shows the shared energy storage operation results of IES Langres. In typical summer days, due to the high demand for load at night, IES Langres stores energy during the day and meets the electricity load demand at night. In winter, due to the increase in wind power generation, shared energy storage mainly aims to suppress fluctuations in wind power generation power.

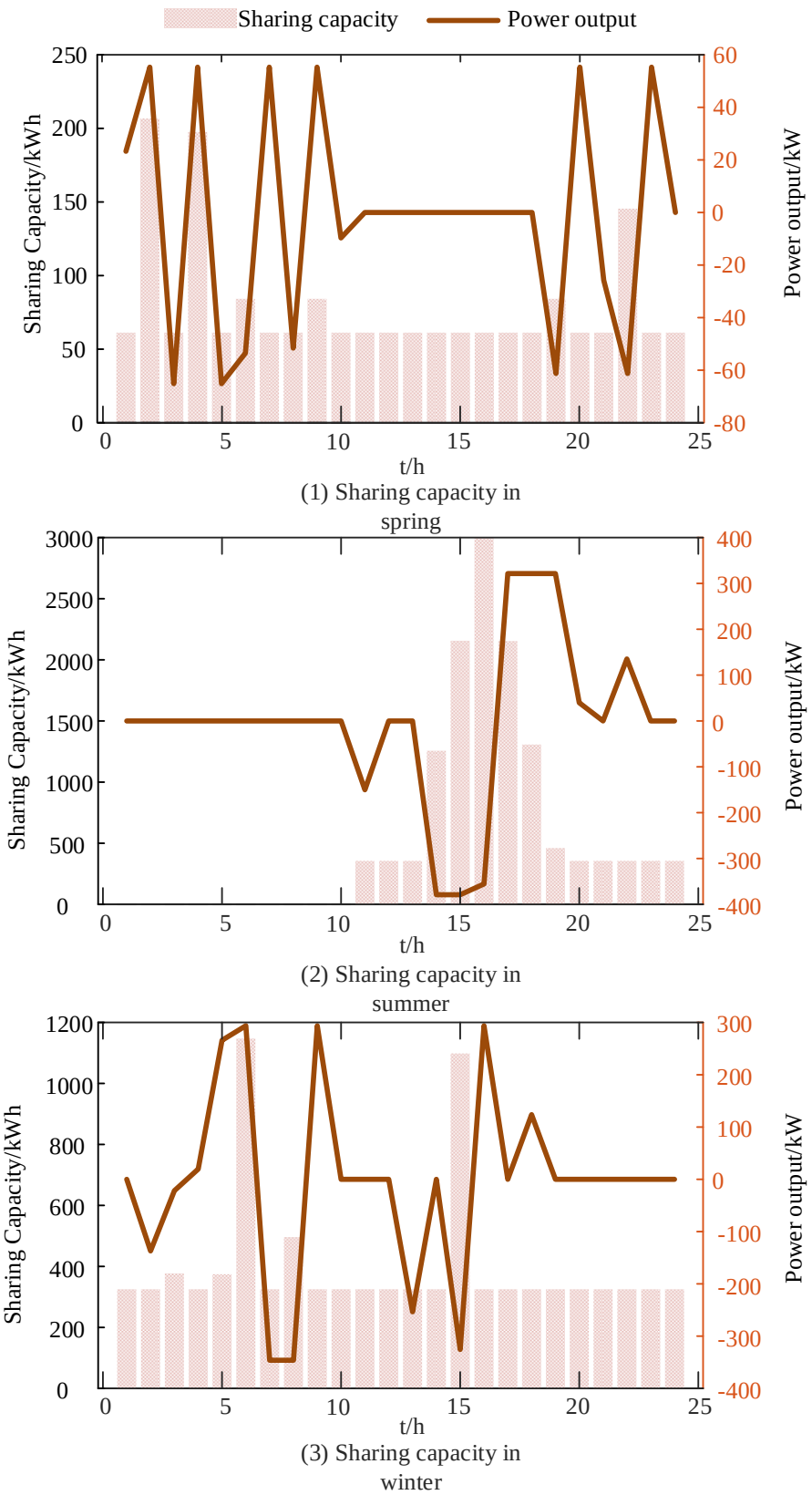

Figure 4- 8 Capacity sharing for IES Langres

Figure 4-9 shows the power balance curves of SESO. During the four typical days, SESO purchased a large amount of electricity from the upper energy market to produce hydrogen when the electricity price

is low at night and also met its energy needs by interacting with the electricity of other IES. In summer, due to the increasing demand for hydrogen energy, the working time of the electrolytic cell is longer, and the consumption power of the electrolyzer is higher.

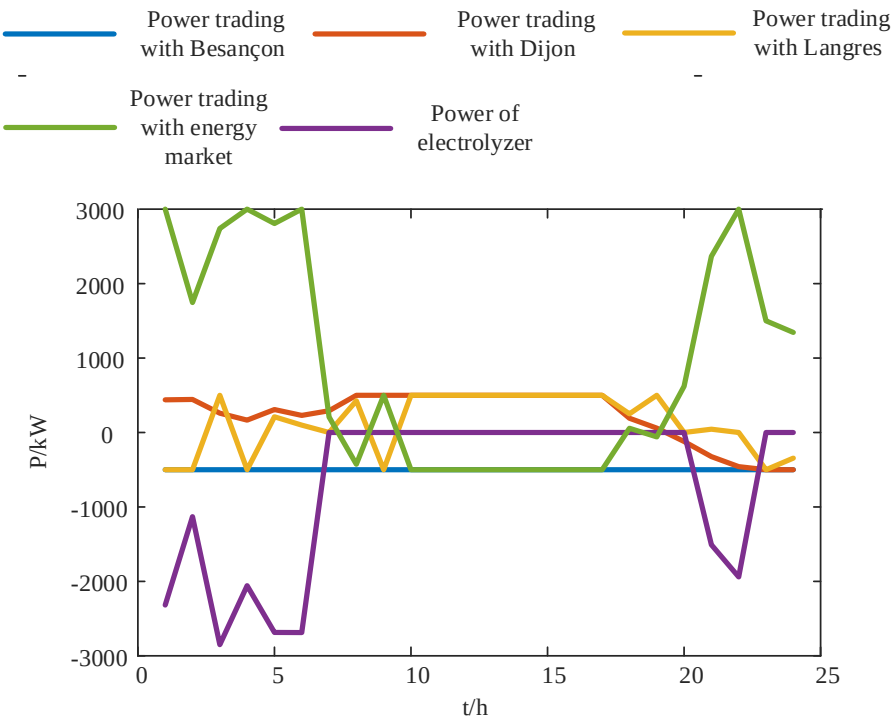

(a) Spring

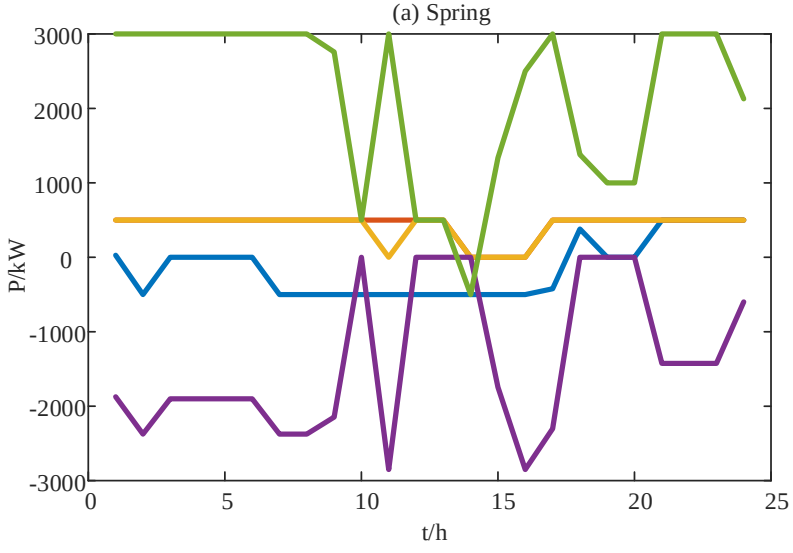

(b) Summer

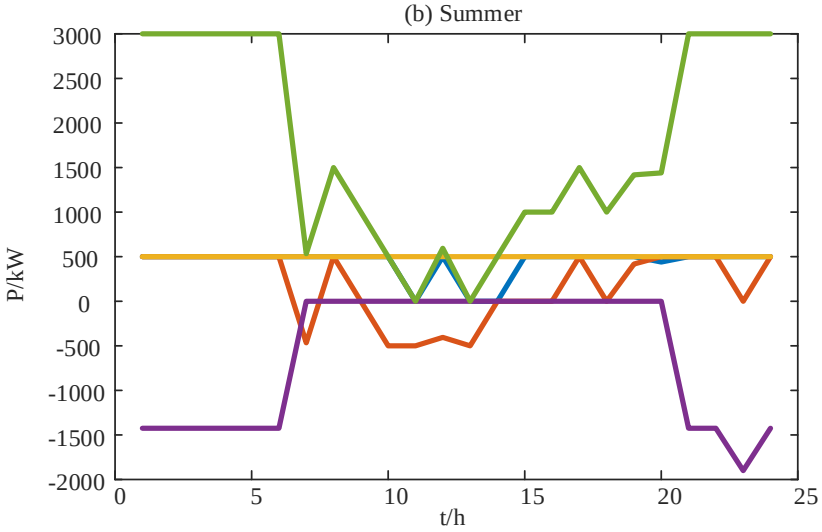

(c) Autumn

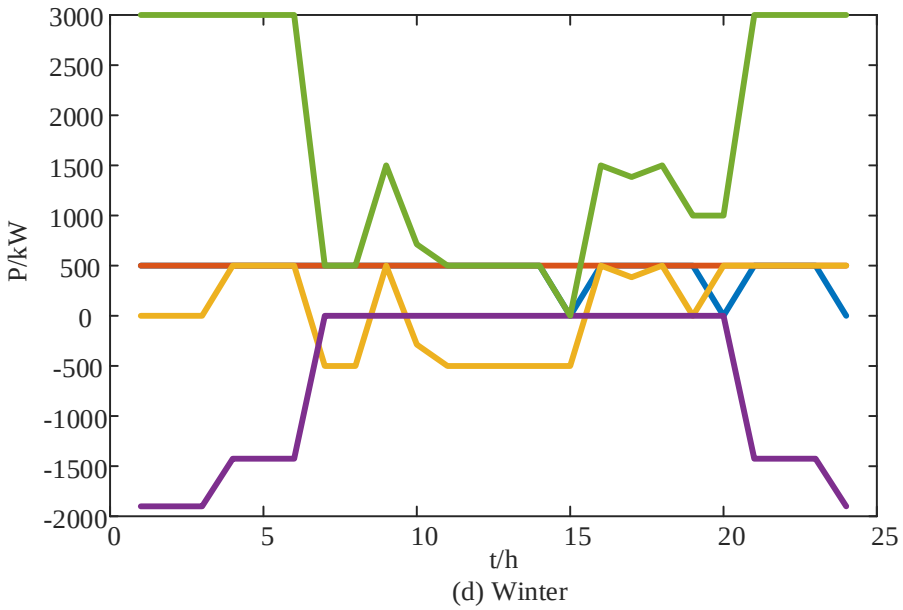

Figure 4- 9 Power trading of IESs

Based on the operation results provided above, in the regional energy sharing model established in this chapter, IES Besançon, IES Dijon, and IES Langres contribute hydrogen energy to other energy systems in the region in summer, spring, and winter, respectively. Each IES produces hydrogen energy when there is a high amount of photovoltaic power generation during the day. Due to the different characteristics of hydrogen energy supply and demand, the three IESs achieved effective coordinated supply of hydrogen energy with the participation of SESO, thereby achieving flexible and coordinated operation of energy systems within the region.

4.4.2. Comparisons and analysis

Table 4-3 shows the lifecycle cost of SESO, of which the annualized purchase cost of the system is 91647.94 euros, accounting for 65% of total expenses, and the operation and maintenance cost is 48317.82 euros, accounting for 35% of total expenses. The total revenue of SESO in sharing energy is 261431.1 euros, allowing SESO's construction to generate significant profits.

Table 4- 3 Life-cycle cost of SESO

		Cost/€
Investment	F_{bat}	77857.37
	F_{el}	321126.00
	F_{tank}	297671.86
	F_{h}	14285.35

Operation	*Spring*	84145.28
	Summer	139194.63
	Autumn	64780.01
	Winter	86695.91
Trading	*Spring*	-231542.97
	Summer	-917742.62
	Autumn	-366160.01
	Winter	-512553.88
Total	F_{SESO}	-942243

To further verify the economic feasibility of SESO, this article compares and analyzes the economic benefits of energy-sharing modes based on shared electric energy storage and shared hydrogen storage, without changing the structure of each system. The settings of scenarios are shown in Table 4-4. Scenario 4 does not have the SESO, and each IES is an independent individual that can only purchase and sell energy from the upper market to meet the daily demands. Scenario 3 establishes a separate shared electric energy storage, and each IES can interact with the shared energy storage. Scenario 2 establishes a shared hydrogen storage system. The shared energy storage station in Scenario 1 includes centralized electric energy storage and hydrogen storage, which can achieve resource complementarity by both electricity and hydrogen energy.

According to the comparative analysis of the operating costs of shared energy storage operators in four scenarios, compared to the operating model that can only purchase and sell electricity from the shared energy operator, adopting the SESO energy sharing model proposed in this chapter can increase annual profits by 587402 euros, an increase of 265%, and the energy utilization rate in the region has increased by 9.3%. Compared to the operation mode of only using shared hydrogen energy, the annual profits of the SESO can increase by 467134 euros, and the energy utilization efficiency has also been improved. Compared to the scenario where no shared energy storage mode is adopted, the mode proposed in this chapter can improve energy utilization by 11.4%. From the above results, it can be seen that although using only electricity storage sharing or hydrogen storage sharing can achieve an improvement in regional energy utilization efficiency, the multi energy sharing of electricity and hydrogen in scenario 1 can realize the optimal coordinated operation within the regional energy systems, and its economy is also better than other scenarios.

Table 4- 4 Comparison with other sharing modes

Mode	Sharing strategy	Annual cost/€	Regional energy utilization ratio

	Capacity sharing	Mobile hydrogen sharing		
1	Yes	Yes	-942243	92.7%
2	Yes	No	-354841	83.4%
3	No	Yes	-475109	86.8%
4	No	No	0	81.3%

To verify the performance of the two-level optimization configuration method proposed in this chapter, this chapter conducts comparative experiments on the upper-level optimization algorithm and the lower-level algorithm, as shown in Table 4-5.

Table 4- 5 Performance of the proposed method

Upper-level method	Average iterations	Optimal results	Lower-level method	Average iterations	Average time costs
Proposed method	52	-942243	*Proposed method*	11	312s
PSO	98	-876518	*PSO*	56	1648s
GWO	77	-931458	*GWO-SCA*	48	1575s

For the upper-level optimization algorithm, this chapter compares the GWO-SCA algorithm used in this chapter with traditional PSO and GWO algorithms. The results show that using the improved algorithm proposed in this chapter requires fewer average iterations and yields better optimization results. In the performance verification of the lower-level algorithms, this chapter compares two genetic algorithms with the bi-sectional algorithm proposed in this chapter. The results showed that the algorithm proposed in this chapter can obtain optimized running results in fewer iterations, and its required time is 1336 seconds shorter than the PSO algorithm and 1263 seconds shorter than the GWO-SCA method. Although the GWO-SCA algorithm is suitable for the upper-level capacity configuration, the proposed bi-sectional algorithm gains calculation advantages when solving the lower-level energy sharing problem because all the genetic algorithms require numbers of iteration for negotiation while the bi-sectional algorithm can solve the problem faster by speeding the processes of pricing. Therefore, based on the verification results of the two-level algorithms, adopting the method proposed in this chapter can significantly reduce calculation time and improve calculation accuracy.

4.5. Chapter summary

To analyze the economy of SESO in a region from whole sides, this chapter proposes a structure of SESO with both electric and hydrogen sharing functions. The capacity and electricity sharing are realized by power lines, while the hydrogen sharing is accomplished by mobile hydrogen storage. Then

a life cycle cost scheme is proposed, and a two-level configuration method is provided. Finally, the results are analyzed in detail. In this chapter, the proposed mobile hydrogen storage can effectively achieve hydrogen energy sharing between energy systems in a region through transportation systems, thereby effectively connecting geographically isolated energy systems through transportation networks. And the proposed framework for sharing two types of energy, electric and hydrogen, effectively improves the utilization rate of energy in the region and maximizes the operational economy of energy-sharing operators, the energy utilization ratio of the whole region is increased by 14.02% compared with the energy market without hydrogen sharing. Also, the proposed two-level optimal configuration method is tested, and the case study shows that both of the GWO-SCA and the bi-sectional algorithm applied in the upper and lower level can achieve the fast solving of the problem, and the calculation speed has increased by 32.5%. .

References

[1] I. E. Agency, "Net Zero Roadmap: A Global Pathway to Keep the 1.5℃ Goal in Reach,", 2023.

[2] A. Bouakkaz, A. J. G. Mena, S. Haddad, and M. L. Ferrari, "Efficient energy scheduling considering cost reduction and energy saving in hybrid energy system with energy storage," J. Energy Storage, 33, p. 101887, (2021).

[3] M. A. Bagherian and K. Mehranzamir, "A comprehensive review on renewable energy integration for combined heat and power production," Energy Conv. Manag., 224, p. 113454, (2020).

[4] M. Farrokhifar, Y. Nie and D. Pozo, "Energy systems planning: A survey on models for integrated power and natural gas networks coordination," Appl. Energy, 262, p. 114567, (2020).

[5] S. Zhang, Y. Li, E. Du, C. Fan, Z. Wu, Y. Yao, L. Liu, and N. Zhang, "A review and outlook on cloud energy storage: An aggregated and shared utilizing method of energy storage system," Renewable and Sustainable Energy Reviews, 185, p. 113606, (2023).

[6] B. Chreim, M. Esseghir and L. Merghem-Boulahia, "Recent sizing, placement, and management techniques for individual and shared battery energy storage systems in residential areas: A review," Energy Rep., 11, pp. 250-260, (2024).

[7] Z. Guo, W. Wei, L. Chen, X. Zhang, and S. Mei, "Equilibrium model of a regional hydrogen market with renewable energy based suppliers and transportation costs," Energy, 220, p. 119608, (2021).

[8] Y. Bian, L. Xie, J. Ye, and L. Ma, "A new shared energy storage business model for data center clusters considering energy storage degradation," Renew. Energy, 225, p. 120283, (2024).

[9] H. Kang, S. Jung, H. Kim, J. Hong, J. Jeoung, and T. Hong, "Multi-objective sizing and real-time scheduling of battery energy storage in energy-sharing community based on reinforcement learning," Renewable and Sustainable Energy Reviews, 185, p. 113655, (2023).

[10] L. Guanjie, M. Zeng, Z. Shan, K. Wu, G. Wang, and K. Lei, "Blockchain-based cooperative game bilateral matching architecture for shared storage," Future Generation Computer Systems, (2024).

[11] R. Tian, F. Li, W. Xie, and D. Ma, "Optimization of configuration and operation of shared energy storage facilities invested by conventional coal-fired power plants," J. Energy Storage, 84, p. 110905, (2024).

[12] D. L. Rodrigues, X. Ye, X. Xia, and B. Zhu, "Battery energy storage sizing optimisation for different ownership structures in a peer-to-peer energy sharing community," Appl. Energy, 262, p. 114498, (2020).

[13] S. Cui, J. Wu, Y. Gao, and R. Zhu, "A high altitude prosumer energy cooperation framework considering composite energy storage sharing and electric-oxygen-hydrogen flexible supply," Appl. Energy, 349, p. 121601, (2023).

[14] Y. He, H. Wu, A. Y. Wu, P. Li, and M. Ding, "Optimized shared energy storage in a peer-to-peer energy trading market: Two-stage strategic model regards bargaining and evolutionary game theory," Renew. Energy, 224, p. 120190, (2024).

[15] X. Song, H. Zhang, L. Fan, Z. Zhang, and F. Peña-Mora, "Planning shared energy storage systems for the spatio-temporal coordination of multi-site renewable energy sources on the power generation side," Energy, 282, p. 128976, (2023).

[16] W. Qiu and Y. Yang, "Impact assessment of shared storage and peer-to-peer trading on industrial buildings in the presence of electric vehicle parking lots: A hybrid robust-CVaR analysis," Energy Build., 304, p. 113847, (2024).

[17] J. Gao, Y. Wang, N. Huang, L. Wei, and Z. Zhang, "Optimal site selection study of wind-photovoltaic-shared energy storage power stations based on GIS and multi-criteria decision making: A two-stage framework," Renew. Energy, 201, pp. 1139-1162, (2022).

[18] R. V. Morcilla and N. H. Enano, "Sizing of community centralized battery energy storage system and aggregated residential solar PV system as virtual power plant to support electrical distribution network reliability improvement," Renew. Energy Focus, 46, pp. 27-38, (2023).

[19] C. Chen, Y. Zhu, T. Zhang, Q. Li, Z. Li, H. Liang, C. Liu, Y. Ma, Z. Lin, and L. Yang, "Two-stage multiple cooperative games-based joint planning for shared energy storage provider and local integrated energy systems," Energy, 284, p. 129114, (2023).

[20] Y. Li, W. Hu, F. Zhang, and Y. Li, "Collaborative operational model for shared hydrogen energy storage and park cluster: A multiple values assessment," J. Energy Storage, 82, p. 110507, (2024).

[21] C. Xu, X. Wu, Z. Shan, Q. Zhang, B. Dang, Y. Wang, F. Wang, X. Jiang, Y. Xue, and C. Shi, "Bi-level configuration and operation collaborative optimization of shared hydrogen energy storage system for a wind farm cluster," J. Energy Storage, 86, p. 111107, (2024).

[22] M. Shi, Y. Huang and H. Lin, "Research on power to hydrogen optimization and profit distribution of microgrid cluster considering shared hydrogen storage," Energy, 264, p. 126113, (2023).

[23] X. Li, L. Chen, Y. Hao, Z. Wang, Y. Changxing, and S. Mei, "Sharing hydrogen storage capacity planning for multi-microgrid investors with limited rationality: A differential evolution game approach," J. Clean. Prod., 417, p. 138100, (2023).

[24] S. Luo, Q. Li, Y. Pu, X. Xiao, W. Chen, S. Liu, and X. Mao, "A carbon trading approach for heat-power-hydrogen integrated energy systems based on a Vickrey auction strategy," J. Energy Storage, 72, p. 108613, (2023).

[25] P. Y., L. Q., Q. Y., Z. X., and C. W., "Two-stage scheduling for island CPHH IES considering plateau climate," CSEE J. Power Energy Syst., pp. 1-10, (2020).

[26] Y. Pu, Q. Li, S. Luo, W. Chen, E. Breaz, and F. Gao, "Peer-to-peer Electricity-hydrogen Trading Among Integrated Energy Systems Considering Hydrogen Delivery and Transportation," IEEE Trans. Power Syst., pp. 1-16.

[27] Y. Pu, Q. Li, Y. Qiu, X. Zou, and W. Chen, "Two-stage scheduling for island CPHH IES considering plateau climate," CSEE J. Power Energy Syst., (2020).

[28] L. Xu, T. W. Chow and E. W. Ma, "Topology-based clustering using polar self-organizing map," IEEE Trans. Neural Netw. Learn. Syst., 26, pp. 798-807, (2015).

[29] C. Wang, X. Zhang, Y. Wang, H. Xiong, X. Ding, and C. Guo, "Pricing method of electric-thermal heterogeneous shared energy storage service," Energy, 281, p. 128275, (2023).

Chapter 5. Conclusion

5.1. Summary of the research works

This thesis mainly focuses on the application of hydrogen energy systems in microgrids and energy systems, and studies the optimization operation of microgrids containing hydrogen energy storage, comprehensive energy systems considering electric and hydrogen coupling, and the electricity hydrogen regional energy market to ensure the stability and economy of the system operation. In addition, it mainly studies hierarchical energy management, two-stage integrated energy system optimization operation method based on mixed integer optimization, and energy sharing based on multi energy systems.

Firstly, the research background, the application of hydrogen energy and the current development status of corresponding technologies, the energy management of microgrids and the optimization operation status of integrated energy systems, as well as the optimization operation status of the energy market are presented. Then, a hierarchical energy management strategy considering economy was proposed for DC microgrids containing hydrogen energy storage, and fair comparison with other strategies has been done. Subsequently, a two-stage optimization operation method for a comprehensive energy system considering cogeneration was proposed to address the electrical thermal hydrogen coupling relationship between fuel cells and electrolytic cells in hydrogen energy systems, and its economic feasibility was analyzed in detail. Finally, considering the participation of multiple integrated energy systems and shared energy storage operators in the regional energy sharing market, a shared energy storage optimization method is proposed. The collinearity and innovation of this thesis work are as follows:

Proposed a hierarchical state machine energy management control based on the minimum utilization cost. In this method, the cost of energy storage system is reduced. At the same time, the energy storage level is maintained by adding the state machine control strategy. The proposed control method is divided into two layers. At the bottom layer, the control of each device is realized separately, and the data from each power system is sent to the top layer which greatly assists the top layer control system. As for the top layer, by analyzing data collected by bottom layer, this layer can obtain the best working mode for each power system. By the coordination work of two control layer, the power of the electric-hydrogen energy storage system is allocated reasonably in the case of the surplus and absence power of the microgrid, which realize the optimal control of the cost and the energy storage level of the system.

Proposed a two-stage optimal scheduling method for CPHH-IES. Due to the variety demands of energy users, a reliable, efficient and economic IES is needed. Therefore, the concept of CPHH has been proposed. Considering the power-heat-hydrogen characteristics of fuel cell and electrolyzer, the IES with CPHH is built. Then, a two-stage IES scheduling method is proposed and operated under a typical climate. The first stage completes the global day-ahead optimization by using MILP, while the MPC method is carried out for real-time operation in the second stage. After that, the efficiency, economy and storage state are discussed in detail which indicate that the proposed method has a lower cost and keep the storage balance of storage system. Besides, the scheduling results and analysis indicate that the IES proposed in this chapter is an independent and reliable system. The CPHH system improves the economy of IES with high efficiency compared with other optional structures.

Proposed a structure and capacity allocation method for SESO on the consideration of the optimal operation of regional energy market. A SESO operator with both electric and hydrogen sharing functions is proposed. The capacity and electricity sharing are realized by power lines, while the hydrogen sharing is accomplished by mobile hydrogen storage. Then a life cycle cost scheme is proposed, and a two-level configuration method by using GWO-SCA and the bi-sectional algorithm is provided. Finally, the results are analyzed in detail.

5.2. Future research directions

This thesis mainly studies the optimization operation methods of hydrogen energy in different energy systems. Although corresponding research has been carried out on simulation and semi physical platforms, and certain research results have been achieved, the research content of this thesis can still be further improved. Specifically, future work will mainly focus on the following areas:

1) In this thesis, the energy management of the microgrid studied in semi physical simulation was modeled as a system mainly based on electricity, and the electrical thermal hydrogen coupling characteristics of fuel cells and electrolytic cells were not validated in Simulink and semi physical platforms. In the future, multi energy coupling work of hydrogen energy systems can be carried out through experiments, and a control method considering waste heat recovery of electrolytic cells and fuel cells can be proposed.

2) In recent years, with the continuous development of machine learning methods, more and more powerful algorithms with better optimization effects are emerging. Some studies have applied it to the

operation of energy systems to optimize system power allocation, and the results are satisfactory. Therefore, in the future, I plan to conduct research on optimal operation based on machine learning methods.

3) Although this thesis constructs the electricity hydrogen multi energy market and optimizes the operation of regional energy markets by considering the sharing of multiple energy sources, the hydrogen transportation links considered are mainly based on an ideal transportation network, ignoring the impact of vehicle flow on hydrogen transportation in actual situations. Therefore, in future research, more detailed research will be conducted on the modeling of traffic flow.

List of figures

List of tables